Available online at www.sciencedirect.com
SCIENCE DIRECT®
Journal of Human Evolution 50 (2006) 36–77

Description, new reconstruction, comparative anatomy, and classification of the Sterkfontein Stw 53 cranium, with discussions about the taxonomy of other southern African early *Homo* remains

Darren Curnoe [a,b,*], Phillip V. Tobias [b]

[a] *Department of Anatomy, School of Medical Sciences, Faculty of Medicine, University of New South Wales, Sydney NSW 2052, Australia*
[b] *Sterkfontein Research Unit, School of Anatomical Sciences, University of the Witwatersrand Medical School, 7 York Road, Parktown 2193, South Africa*

Received 7 November 2002; accepted 15 July 2005

Abstract

Specimen Stw 53 was recovered in 1976 from Member 5 of the Sterkfontein Formation. Since its incomplete initial description and comparison, the partial cranium has figured prominently in discussions about the systematics of early *Homo*. Despite publication of a preliminary reconstruction in 1985, Stw 53 has yet to be compared comprehensively to other Plio-Pleistocene fossils or assessed systematically. In this paper, we report on a new reconstruction of this specimen and provide a detailed description and comparison of its morphology. Our reconstruction differs in important respects from the earlier one, especially in terms of neurocranial length, breadth, and height. However, given that Stw 53 exhibits extensive damage, these dimensions are most likely prone to much error in reconstruction. In areas of well-preserved bone, Stw 53 shares many cranial features with *Homo habilis*, and we propose retaining it within this species.

We also consider the affinities of dental remains from Sterkfontein Member 5, along with those from Swartkrans and Drimolen previously assigned to *Homo*. We find evidence for sympatry of *H. habilis* and *Australopithecus robustus* and possibly Plio-Pleistocene *Homo sapiens* sensu lato in Sterkfontein Member 5. At Swartkrans and Drimolen, we find evidence of *H. habilis*. We also compare the morphologies of Stw 53 and SK 847 and find compelling evidence to assign the latter specimen to *H. habilis*, as has been proposed.

Keywords: *Homo*; Sterkfontein; Fossil reconstruction; Anatomy; Systematics; Swartkrans; Drimolen

Introduction

In August 1976, the late Alun Hughes recovered a fragmented cranium from the Sterkfontein Cave. Designated Stw 53, it was found partly in decalcified deposit within a mokondo (sinkhole), partly in situ within the surrounding calcified wall formed in breccia attributed to Member 5 of the Sterkfontein Formation (Partridge, 1978). Tobias (1978) provided a detailed account of the discovery and excavation of Stw 53.

Until the recovery of this cranium, controversy surrounded the presence of *Homo* at Sterkfontein. During the 1957–58 excavations, several isolated teeth were recovered from Member 5 (SE 255, 1508, 1579, 1937, 2396, and 2398). Robinson (1958, 1962) considered them to represent *Australopithecus* (although he seems to have had doubts about the classification of one specimen—see Tobias, 1965, 1978). After examining these teeth in 1958, Leakey (cited by Tobias, 1978) challenged Robinson's classification and suggested that they may represent *Telanthropus*. Tobias (1965) described resemblances that the SE series bore to *Homo habilis*, leading him to suggest that they might belong to early *Homo*. Thus, until the discovery of *Australopithecus robustus* in Member 5 after 1991 (Kuman and Clarke, 2000), the only hominid fossils recovered from Member 5 were those that were thought to resemble *H. habilis*.

* Corresponding author. Department of Anatomy, School of Medical Sciences, Faculty of Medicine, University of New South Wales, Sydney NSW 2052, Australia.
E-mail addresses: d.curnoe@unsw.edu.au (D. Curnoe), tobiaspv@anatomy.wits.ac.za (P.V. Tobias).

0047-2484/$ - see front matter © 2005 Elsevier Ltd. All rights reserved.
doi:10.1016/j.jhevol.2005.07.008

In the announcement of its discovery, Stw 53 was classified as *Homo* aff. *H. habilis* (Hughes and Tobias, 1977). Following "preliminary reconstruction," Clarke (1985: 175) concluded that "it looked almost identical to the cranium O.H. 24," an Olduvai specimen referred to *H. habilis* (Leakey et al., 1971). Tobias (1991) later referred Stw 53 to *H. habilis*. Other workers have reaffirmed affinity of this cranium to *Homo*, but opinions have differed about its specific designation; Kimbel et al. (1997) supported its assignment to *H. habilis*, while Chamberlain (1987), Grine et al. (1996), Grine (2001), and Curnoe (1999) suggested that it sampled a novel species of *Homo* in southern Africa.

The case for placing Stw 53 in *Homo* has been questioned. Wolpoff (1996) regarded this specimen to be evolved *Australopithecus africanus*. In a recent change of mind, Clarke (Kuman and Clarke, 2000) agreed with this classification of Stw 53. However, Curnoe (2002) questioned this assessment. Wood and Collard (1999) argued that *H. habilis* sensu lato (i.e., *H. habilis* sensu stricto plus *Homo rudolfensis*) should be removed from *Homo* and be reclassified as *Australopithecus*. Thus, Stw 53 would be classified as either *Australopithecus habilis* or *A. africanus* under such a scheme.

In this paper, we provide a description and comparison of the anatomy of Stw 53 based on a revised restoration. We extend previous descriptions of this specimen, such as those provided by Hughes and Tobias (1977), Tobias (1978), Clarke (1985), and Schwartz and Tattersall (2003). We also outline a new reconstruction of this cranium, highlighting important sources of error in interpretations of its morphology. In comparing Stw 53 to other fossils from Sterkfontein Member 5, we provide new craniometric and odontometric data and reconsider the taxonomy of all these specimens. Furthermore, we compare the Sterkfontein remains with some early *Homo* remains from Swartkrans and Drimolen, and in doing so, reconsider the classification of these fossils.

Preservation

There is much variation in the use of anatomical terms in the anthropological literature, which can lead to confusion. The problem can largely be avoided by using a standard set of internationally agreed upon terms. Here we use the official *Terminologia Anatomica* published by the Federative Committee on Anatomical Terminology (FCAT, 1998). However, as no official terminology exists yet for anthropology, we mainly use the terminology of Tobias (1991).

The maxilla of Stw 53 (Stw 53a and f; Fig. 1) is represented by much of the anterior part of its body (left and right sides), frontal process, piriform aperture, part of the infraorbital and subnasal regions, much of the alveolar processes, maxillary dental arcade, and palate. Parts of the left and right zygomatic bones are attached to the maxilla.

The upper facial skeleton of Stw 53 (Fig. 1) retains most of the frontal process of the maxilla, much of the paired nasal bones, and an almost complete piriform aperture (a small fragment of bone is missing from the left inferolateral margin). The medial third of the left infraorbital part is preserved,

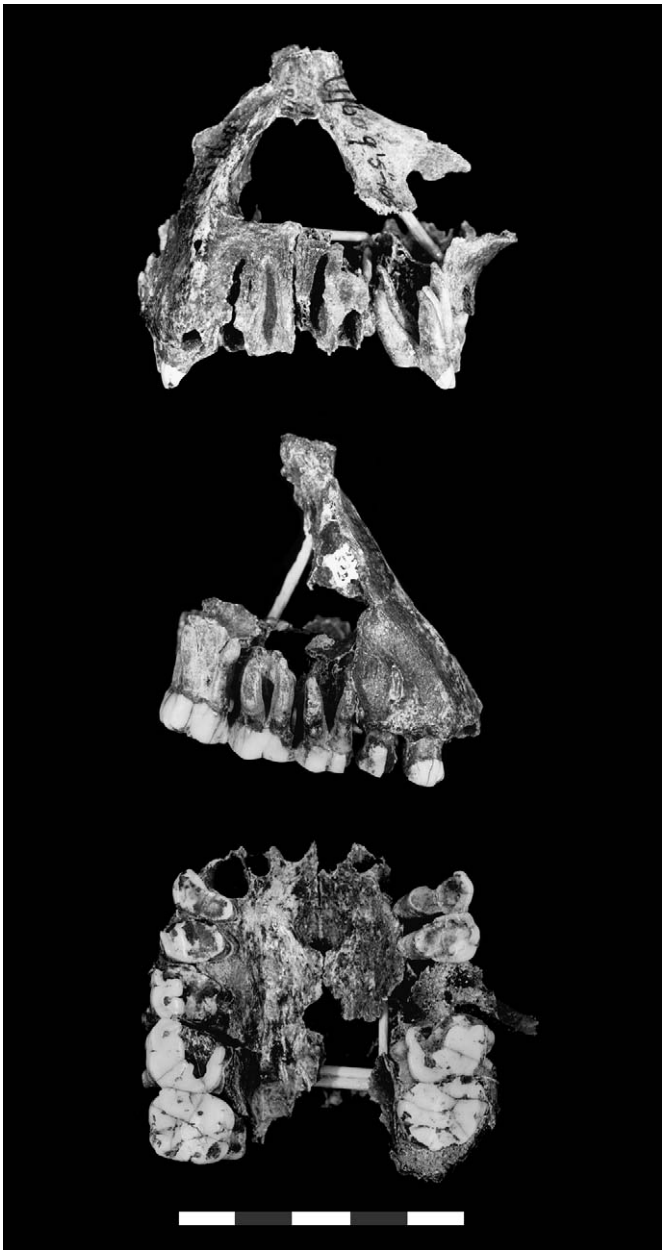

Fig. 1. Maxilla of Stw 53: anterior aspect (top), right lateral aspect (middle), and inferior aspect (bottom). Taken prior to new restoration. Scale bar = 5 cm.

including the superior margin of the infraorbital foramen and zygomatic root. The right infraorbital part is missing, except for a small section superior and lateral to the piriform aperture, and the right zygomatic, including most of its root (Fig. 1). The subnasal region is largely intact, although some of the external table is missing along the nasoalveolar clivus. Partial left and nearly complete right anterior borders of the zygomatic bones are preserved. A well-preserved, delicate and sharp, downward projecting spine marks the most inferior part of the nasal bones (rhinion). It forms a well-preserved long and sharp crest marking the articulation with the anterosuperior edge of the perpendicular plate of the ethmoid. The left zygomatic process is preserved (Fig. 1), and its position can be reconstructed on the right side (Fig. 2).

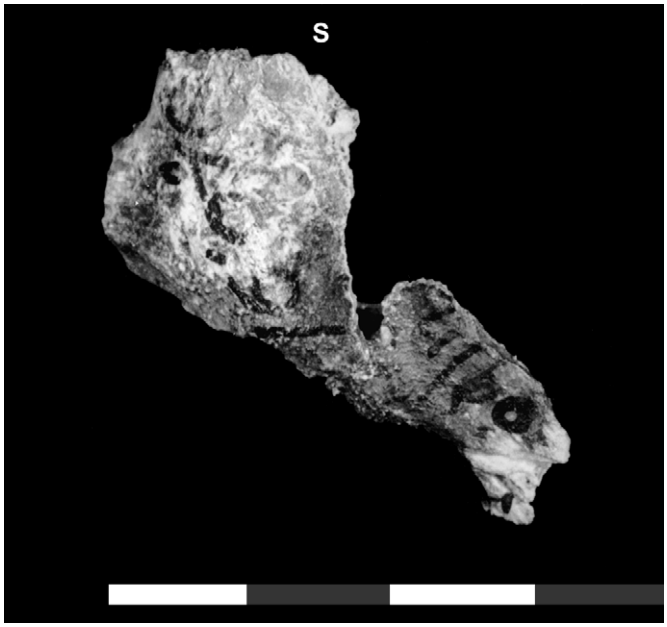

Fig. 2. Right zygomatic fragment of Stw 53 in anterior aspect. Divisions of scale bar = 10 mm each. S = superior.

Two small foramina are present symmetrically on the left and right nasal bones about halfway along their superoinferior extent. A foramen is visible near the most superolateral part of the piriform aperture. A large, nearly complete infraorbital foramen is preserved on the left side. A small part of the superior wall and most of the floor of the left maxillary sinus are preserved. The superior and inferior walls of the anterior part of the right maxillary sinus are also preserved.

The alveolar process, upper dental arcade, and palate preserve much of the borders of the left I^1, I^2, and M^{1-3} tooth sockets, right I^1–P^4 sockets, most of the medial aspect of the right M^1 socket, the complete anterior part of the palate with incisive fossa, the palatine process of the palatine bone, the left greater palatine foramen, a small part of the right pterygoid plate, and part of the left maxillary tuberosity (Fig. 1). The external border of the alveolar process of the maxilla is missing on the left side from the canine to M^1, but part of the superior portion of the canine alveolus and the lateral margin of the alveolar process at M^{2-3} are retained. On the right side, the lateral alveolar surface is missing completely from P^4 posteriorly. The left lateral alveolar surface is missing at all tooth positions, save M^3. The medial alveolar surface on this side is present at I^1–P^4 and M^3 positions (Fig. 1).

The complete right P^3–M^3 and left P^{3-4} and M^{2-3} were recovered from the decalcified matrix (Fig. 1). The anterior cheek teeth (P^3–M^1) are heavily worn, with extensive lingual occlusal attrition and dentine exposure. Enamel is preserved on both lingual and buccal crown faces of P^{3-4}, allowing us to determine mesiodistal (MD) and buccolingual (BL) crown diameters. However, BL diameters should be treated as estimates because they were reconstructed by estimating the thickness of the missing enamel from enamel remaining on the buccal face of the crowns. The posterior cheek teeth (M^{2-3}) show varying degrees of wear, with the M^3s predictably the least worn of all the teeth.

The anterior surface of the right zygomatic (Fig. 2) records its articulation with the zygomatic process of the maxilla. The angles formed by the frontal and temporal processes of the zygomatic bone are preserved, as is its inferolateral corner, which features a crest for the landmark zygomaxillare. Immediately superior are closely positioned zygomaticofacial foramina. With the aid of a low power microscope, several tiny foramina can be seen pitting the surface of the zygomatic bone and along the surface of the masseter muscle attachment.

The frontal bone (Stw 53b; Fig. 3) has an intact right supraorbital margin and zygomatic process and about two-thirds

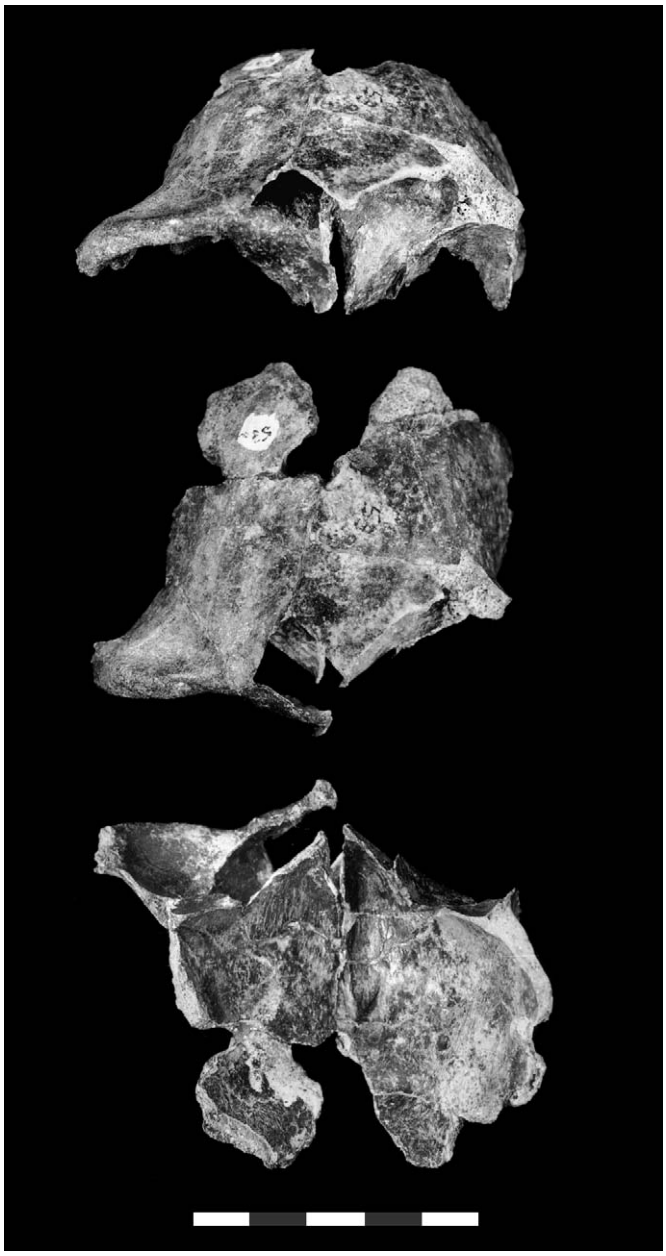

Fig. 3. Frontal bone of Stw 53: anterior aspect (top), superior aspect (middle), and inferior aspect showing endocranial surface (bottom). Scale bar = 5 cm.

of the frontal squama. The right supraorbital region is well preserved, retaining both its superciliary and supraorbital parts. It has a broad supraorbital notch and supraorbital foramen superolateral to the notch. The bone is missing from glabella, but the general size and shape of this part of the frontal bone are discernible. The frontal sinus is exposed, being extensive anteroposteriorly and mediolaterally and extending inferiorly into the nasal part of the frontal bone. The right orbit retains only parts of the superior and posterior orbital plates of the frontal. Left and right lacrimal grooves are preserved; these are wide, and a long and wide right nasolacrimal canal can be seen. The preserved nasal process of the frontal includes a small lateral section of the frontomaxillary suture and approximately the lateral half of the most superior portion of the right nasal bone. A small foramen can be discerned just lateral to the frontomaxillary suture. On the right nasal part, numerous tiny foramina are discernible with the aid of a low power microscope; these are not confluent and their appearance is not vermiculate.

The squamous part of the frontal bone (Fig. 3) is complete anteriorly, but bone is missing laterally, behind the orbits. Sufficient bone remains to provide an estimate of minimum frontal breadth (see below). Most of the medial portion of the squama is missing. The ectocranial surface of the frontal squama is uneven and rough, being rugose in parts. The internal table (Fig. 3) preserves the frontal crest, most of which has been broken away, save for about two-thirds of the anteroposterior ridge joining the crest with the sulcus for the sagittal sinus. Also preserved are complete left and partial right ethmoidal notches, anterior ethmoidal air-cells exposed through broken bone covering the frontal sinus, and impressions of the gyri, sulci, and blood vessels from the surface of the frontal lobes of the cerebrum.

The parietal bones of Stw 53 were recovered separately as right (Stw 53d; Fig. 4) and left (Stw 53e; Fig. 5) fragments from calcified breccia and decalcified sediment, respectively. The right parietal comprises a number of fragments that have been badly fractured and distorted. The ectocranial surface of the right parietal bone possesses a parietal tuberosity. Two moderately large fragments represent the left parietal bone from the medial part, posteriorly, to its articulation with the occipital bone.

Most of the squamous part of the occipital was found as two pieces, the left preserving a section of the lambdoidal suture along its superolateral corner (Stw 53d, e, and h; Fig. 5). A large parietal fragment articulates along this section of suture (Fig. 5). The occipital plane is partially preserved on the right side (Fig. 4). From the area of the asymmetrical external occipital protuberance (Fig. 5), the nuchal crest is traceable laterally (on left and right; Figs. 4, 5). Most of the mastoid angle is retained. The bone has been subjected to severe plastic deformation along its mediolateral axis. Slightly less than half of the left border of the foramen magnum and the nearly complete lateral part, including the left occipital condyle, are preserved as a separate fragment (Fig. 6). The basilar (pre-condylar) part of the occipital is missing.

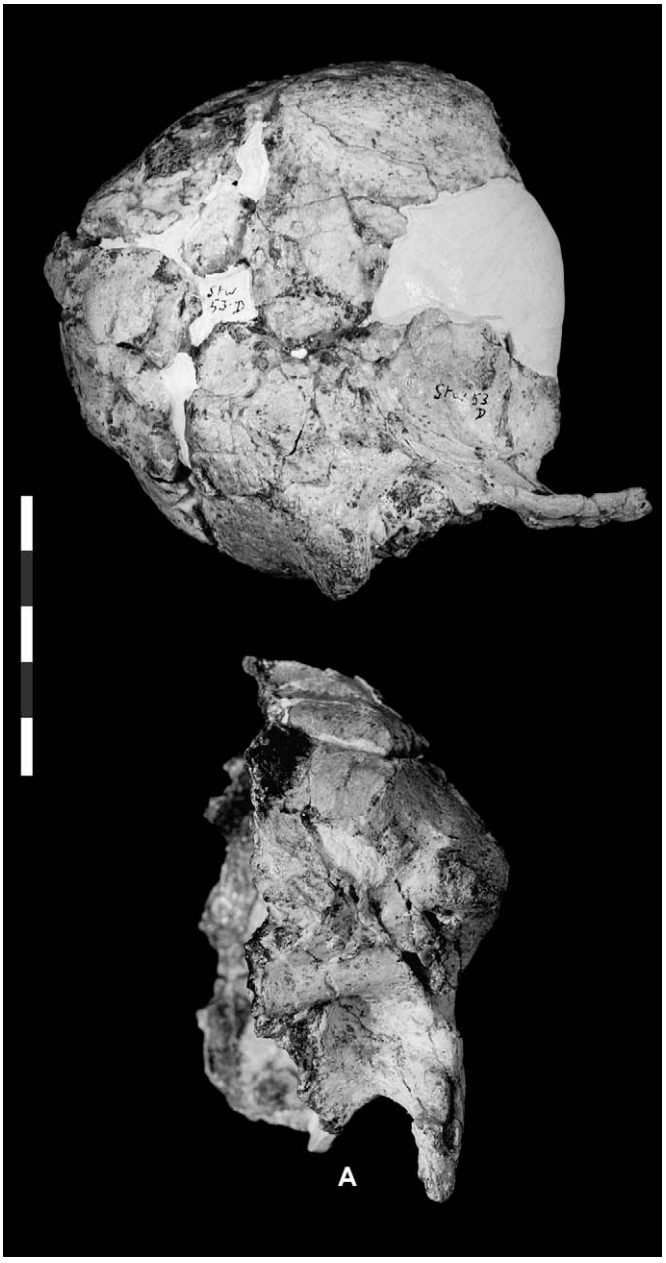

Fig. 4. Right parieto-occipito-temporal fragment of Stw 53: lateral aspect (top) and inferior aspect (bottom). Scale bar = 5 cm. A = anterior.

The right temporal of Stw 53 preserves the inferior two-thirds of the squamous part on its right side (Stw 53d; Fig. 4), with bony continuity from the posteromedial wall of the temporal fossa to the bone around asterion. It has a well-preserved mastoid part with intact process, external acoustic opening and meatus, and the mandibular fossa and the posterior part of the preglenoid plane (Fig. 4). The inferior two-thirds of the squamosal part are intact, but highly fragmented, with loss of outer table. The posterior margin of the temporal fossa and most of the zygomatic process of the temporal bone are intact.

The left petromastoid fragment preserves details of ectocranial and endocranial surfaces (see below). The tympanic part of this fragment has lost most of the superior border of the

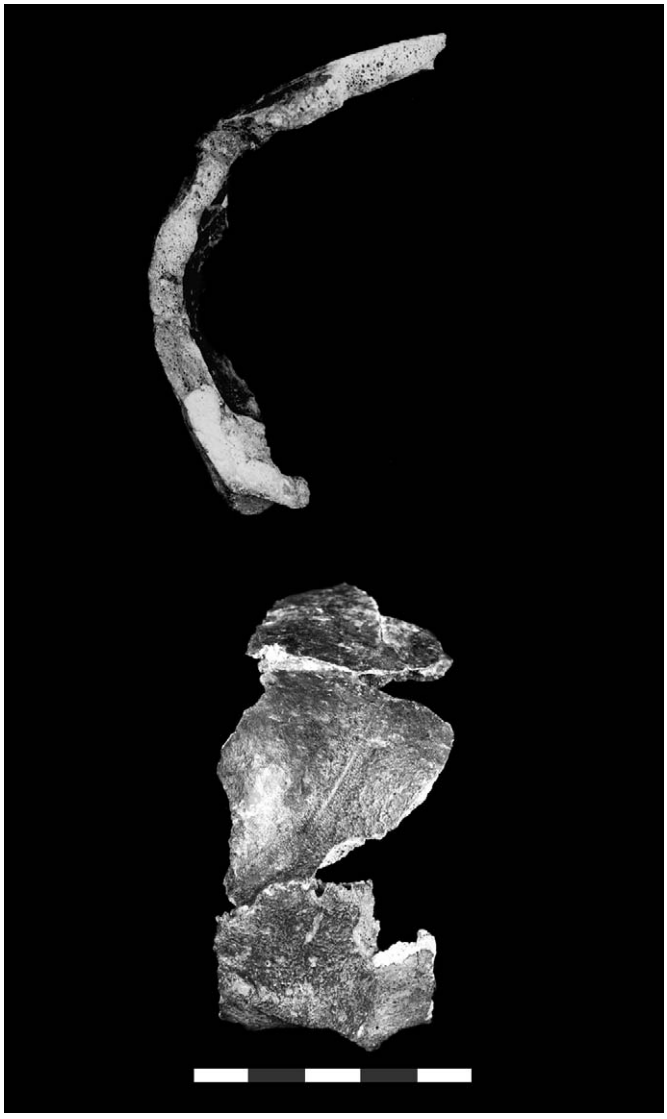

Fig. 5. Left parietal and occipital fragments of Stw 53: right lateral aspect (top) and posterior aspect (bottom). Photographs were taken prior to new restoration. Scale bar = 5 cm.

bony external ear, but retains the suprameatal triangle, tympanic plate, most of the acoustic meatus, and petrous temporal (quadrate area). A well-developed ossified styloid process and sheath are present (Fig. 6). The tympanomastoid suture may be followed for much of its course. A small stylomastoid foramen is preserved. The large opening to the carotid canal is present medial to the styloid process.

The mandibular ramus fragment (Fig. 7) preserves most of a delicate right ramus, the anterior border of which is broken away where it approaches the mandibular body. It lacks the condylar process, but retains the mandibular notch and coronoid process. An almost complete M^3 was recovered with Stw 53 (Fig. 7), with a cracked crown and most of the roots embedded in matrix (this specimen has not been fully cleaned due to its fragility). It has not previously been described, but was listed as belonging to Stw 53 by Kuman and Clarke (2000). The M^3 preserves sufficient enamel to provide reliable estimates of crown diameters. The fit of the occlusal surface of this specimen with that of the maxillary third molar of Stw 53 suggests they are from the same individual.

New reconstruction

Our new reconstruction of Stw 53 is illustrated in Fig. 8. The first stage of the reconstruction involved comparing the cranium, as initially assembled by Hughes and Clarke, with the later reconstruction by Clarke (1985). It became apparent that the anatomical placement of a number of critical bones differed between the two. Thus, two different interpretations of the morphology of Stw 53 have existed until now (i.e., studies of original remains, as assembled by Alun Hughes, and alterations to this restoration made on cast pieces by Clarke during his reconstruction). This situation is unsatisfactory because many researchers have either not acknowledged, or perhaps failed to realize, that these differences existed and assumed that both the restoration (glued together original fossil pieces) and the reconstruction (cranial model built from cast pieces) were identical.

It also became clear during our work that some fragments had been misaligned on the fossil. The problematic bone fragments and teeth were first disassembled using acetone to remove adhesive, and the opposing surfaces were thoroughly cleaned of adhesive using a fine paintbrush and acetone.

We disassembled the left lateral border of the piriform aperture and frontal process of the maxilla. Our restoration proved to be identical to that of Hughes and Clarke because of the existence of a join (fracture) that could not be seen until the pieces were separated. Left P^3 and P^4 were refitted in different positions from the earlier restoration. We made corrections to their heights so that the occlusal surfaces of the crowns aligned correctly with one another and with a plane projected from the occlusal surfaces of the posterior cheek teeth; their positions relative to each other in the maxillary dental arcade were also modified to provide increased space between them to allow for interalveolar septa.

The left M^1 alveolus, as restored by Hughes and Clarke (Fig. 1), allowed insufficient space for the tooth. We modeled the alveolus on the reconstructed crown dimensions of the antimere. On the original restoration, left M^{2-3} and the left maxillary tuberosity were positioned too far mesiad (the cause of the narrow M^1 alveolus). This was corrected concurrently with the above alteration; the buccolingual placement was judged from the position of the right homologues and the projected curvature along the left arcade.

The left parietal bone (two fragments) and left medial fragment of the occipital bone had been united as a single piece (Fig. 5). A small part of the mediolateral course of the lambdoid suture is retained on the occipital fragment and on the posterior margin of the left parietal (Fig. 5). They articulate well. In the original restoration, they were not joined along their natural articulation. Our restoration has resulted in altered placement of the left posterior parietal fragment on the coronal plane; it is now more elevated at its anterior end and placed further laterally from the median sagittal plane (Fig. 8a, c). The two parietal fragments were

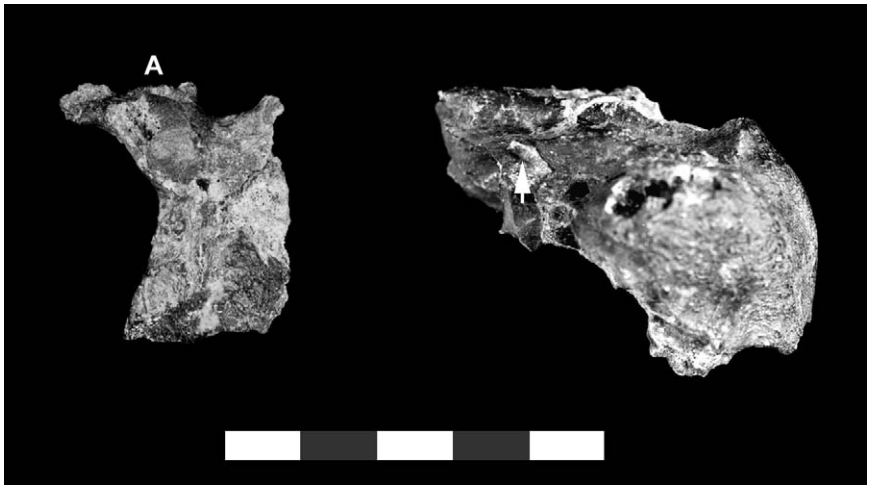

Fig. 6. Cranial base fragments: partial left margin of the foramen magnum (left) and left temporal fragment highlighting the well-preserved styloid process of Stw 53 (right). Scale bar = 5 cm. A = anterior.

separated, and after the removal of adhesive from their adjoining surfaces, we could find no natural join along corresponding surfaces. They were, therefore, left as separate fragments (Fig. 8a, c).

The right parieto-occipito-temporal fragment was subjected to severe plastic deformation, fragmentation, and erosion of the external table (Fig. 4). The original restoration assembled all of the fragments constituting this region as a single piece, with gaps filled with plaster (Fig. 4). It is evident upon close inspection that some pieces appear to align correctly, while owing to damage, others do not. The sheer complexity of the breakage patterns on this fragment, along with the loss of bone and the specimen's fragility, make it very difficult to take apart. We decided, therefore, to leave this fragment as originally restored and to attempt anatomical correction using a cast cut into pieces (see below).

Following the above changes to the original of Stw 53, the specimen was cast and a reconstruction was made. The restored maxillary bone and frontal bone were each cast as single pieces and their relative alignments proved relatively easy to judge. A section of the nasal bones missing below nasion was filled with plasticine (Fig. 8e). The amount lost was judged from the (1) tapering of the paired nasal bones, (2) the length of the remnant of the left nasal bone on the nasal part of the frontal bone, and (3) the vertical position of the maxilla, as judged from its angular placement relative to the Frankfurt Horizontal (in lateral aspect) and relative positions of the temporal process of the right zygomatic bone and the right zygomatic arch. Placement of the lateral surface of the right zygomatic bone was relatively straightforward (Fig. 8d, e). Its anteroposterior slope was judged from that of its left homologue.

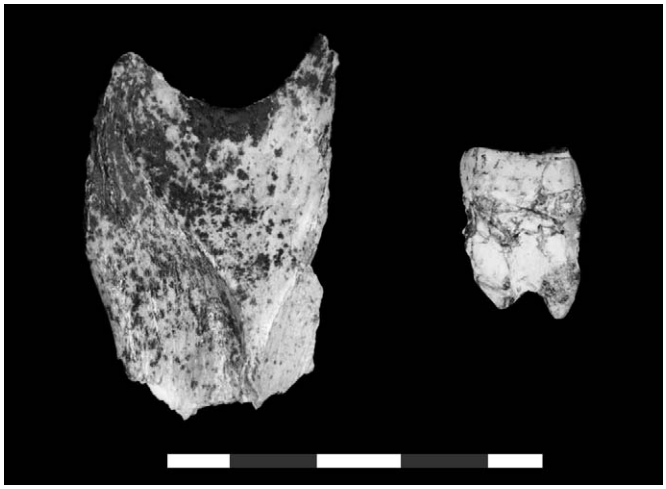

Fig. 7. Mandibular remains of Stw 53: partial ramus in medial aspect (left) and mandibular third molar (right). Scale bar = 5 cm.

The frontal bone was positioned with relative ease. The amount of bone missing from the interorbital part (maxillary process of the frontal and frontal process of the maxilla) was estimated. Sufficient bone is preserved on the squamous part of frontal to allow accurate reconstruction of its curvature (Fig. 8d, e). Judgement of the position of the left anterior parietal fragment, along the coronal plane, was relatively straightforward owing to the preservation on its posteromedial corner of two denticulations of the sagittal suture. By following the course of the left temporal line, we could estimate the position of the fragment along the sagittal plane. However, as this fragment is free-floating, its angle along the sagittal plane had to be estimated. Because this angle is a major factor determining the height and length of the calvaria, estimates of these dimensions in the new reconstruction may be unreliable.

Distortion of the facial skeleton and frontal bone

When viewed in inferior aspect, the median sagittal plane of the cranium can be seen to pass through the external occipital protuberance and the midline of the foramen magnum (Fig. 9). However, when this version of the midline reaches the posterior part of the palate, it lies to the left of the midline of the palate. Further anteriorly, it passes through the left canine alveolus (Fig. 9). Thus, the midline of the palate diverges more than 20° to the right of the median sagittal plane of the

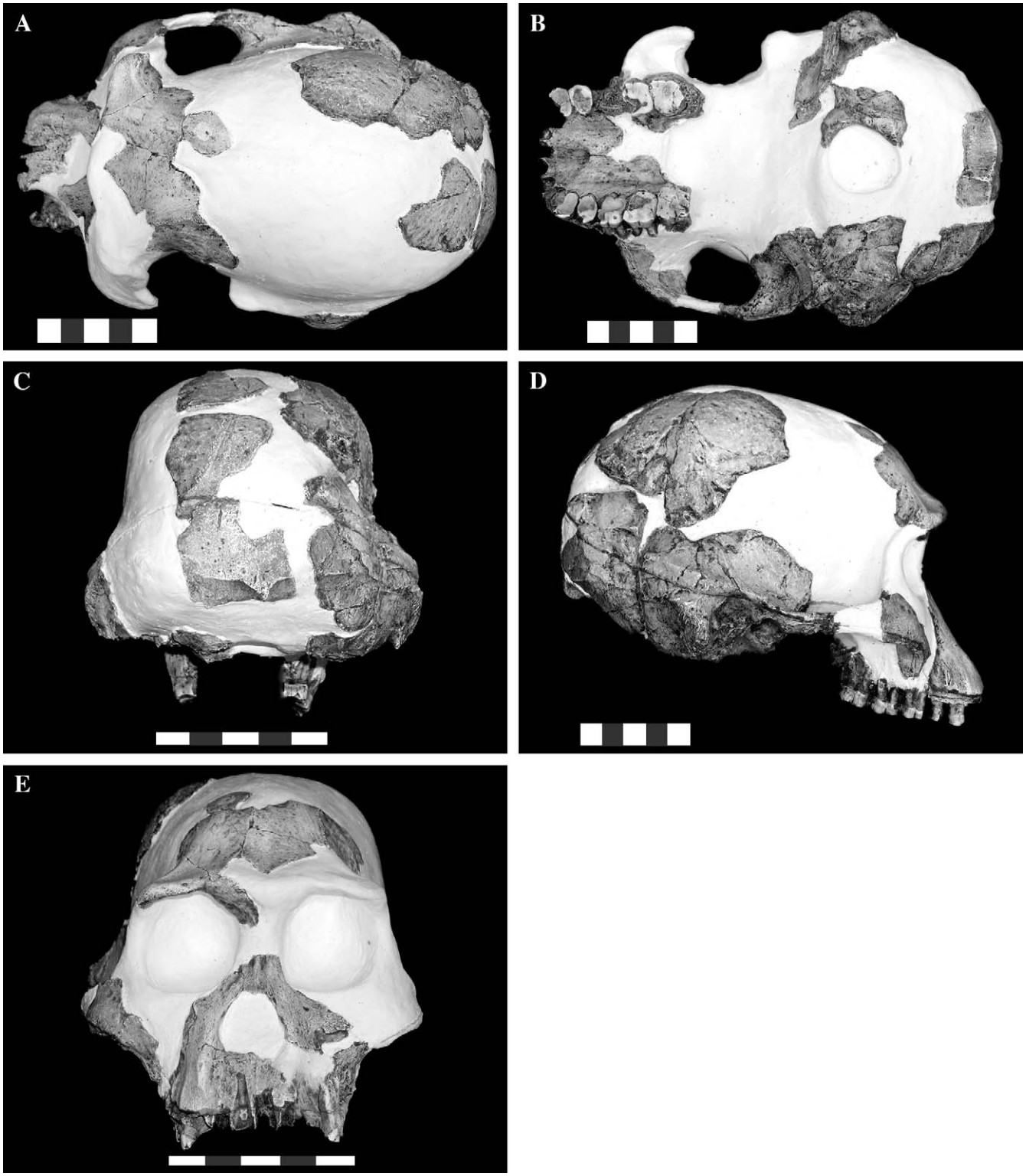

Fig. 8. New reconstruction of Stw 53 in (A) superior aspect, (B) inferior aspect, (C) occipital aspect, (D) right lateral aspect, and (E) anterior aspect. Cranium positioned in FH. Scale bar = 5 cm.

calvaria. This divergence is also evident in superior aspect, although it does not appear as pronounced. Thus, the whole facial skeleton of Stw 53 is twisted to the right of the median sagittal plane. We have not corrected for this in our reconstruction, as Clarke (1985) did in his, preferring instead to recognize more fully the extent of damage the specimen has suffered.

Judgement of parieto-occipital curvature is impaired by the loss of bone from the lateral and anterior parts of the left parietal and occipital bones, and by deformation of, and

Fig. 9. New reconstruction of Stw 53 in inferior aspect, highlighting distortion of the facial skeleton. The vertical line indicates the median sagittal plane (see text).

damage to, the right parieto-occipito-temporal fragment (Fig. 4). Transverse curvature of the vault was more difficult to reconstruct because of extensive distortion and damage, especially on the right parietal and temporal bones and on the right part of the occipital, and owing to a large area of missing bone on the left side (Fig. 5). A cast of the single restored right fragment was cut into three large pieces in order to correct for compression and distortion. We indicate in Fig. 10 where on a cast of the right parieto-occipito-temporal fragment we cut and distinguish between cuts involving articulated bone fragments and those through plaster. These pieces were placed on the coronal and sagittal planes by (1) following the curvature reconstructed along the left wall of the vault; (2) reconstructing the positions of the parietal eminences and maximum biparietal breadth; (3) projecting the frontal curvature posteriorly on left and right sides, aligning the right lateral and medial occipital fragments; and (4) estimating the lateral placement of the left and right mastoid processes, aligning the right zygomatic arch and temporal process of the right zygomatic bone, along with the relative placement of the foramen magnum and the left and right segments of the inferior nuchal line (Fig. 8b). The jugular processes of the occipital were also helpful as guides (Fig. 8b).

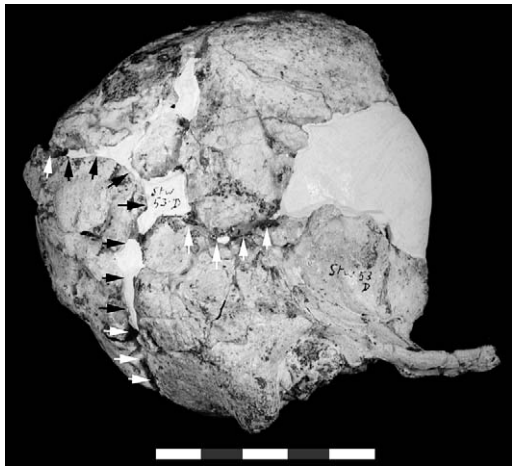

Fig. 10. Right parieto-occipito-temporal fragment of Stw 53 in lateral aspect showing where cuts were made in a cast during reconstruction (black arrows indicate cuts through plaster and white arrows, cuts through bone). Scale bar = 5 cm.

The placement of the preserved fragment of the foramen magnum, being slightly less than half of the original right margin, was relatively straightforward owing to good preservation of the left jugular process and jugular notch (Fig. 8b). The presence of the external occipital protuberance, preserved left and right halves of the nuchal plane, left and right external acoustic meatuses, and right jugular process aided reconstruction of the cranial base (Fig. 8b). Placement of the left temporal bone fragment was more difficult and much effort was devoted to placing this piece in the appropriate coronal and transverse horizontal planes, in its correct lie relative to the nuchal plane and petrous pyramid (as judged by symmetry with the right temporal fragment).

Comparison with earlier reconstruction

Above, we described changes made to the restoration of Stw 53. Here, we outline major differences between the new reconstruction of this specimen and the ''preliminary'' reconstruction of Clarke (1985). In lateral aspect (Fig. 11), the new reconstruction of the calvaria is longer and higher. This discrepancy results from a more posterior placement of the parietal, occipital, and temporal fragments, along with greater angulation of the squamous part of the frontal and parietal fragments. Table 1 compares some metrical features of the new reconstruction with those taken by us on Clarke's (1985) reconstruction. These data quantify differences, emphasizing in particular the greater length (+20 mm) and height (+7 mm) of the new reconstruction. Interestingly, an estimate of approximate auricular height in our new reconstruction (ca. 76 mm) is slightly less than in Clarke's reconstruction (ca. 79 mm). While our reconstruction has greater approximate basi-bregmatic height, it is slightly lower in its vertical height to vertex.

In superior aspect (Fig. 12), differences in breadth of the calvariae are clear. Constriction of the frontal behind the orbits

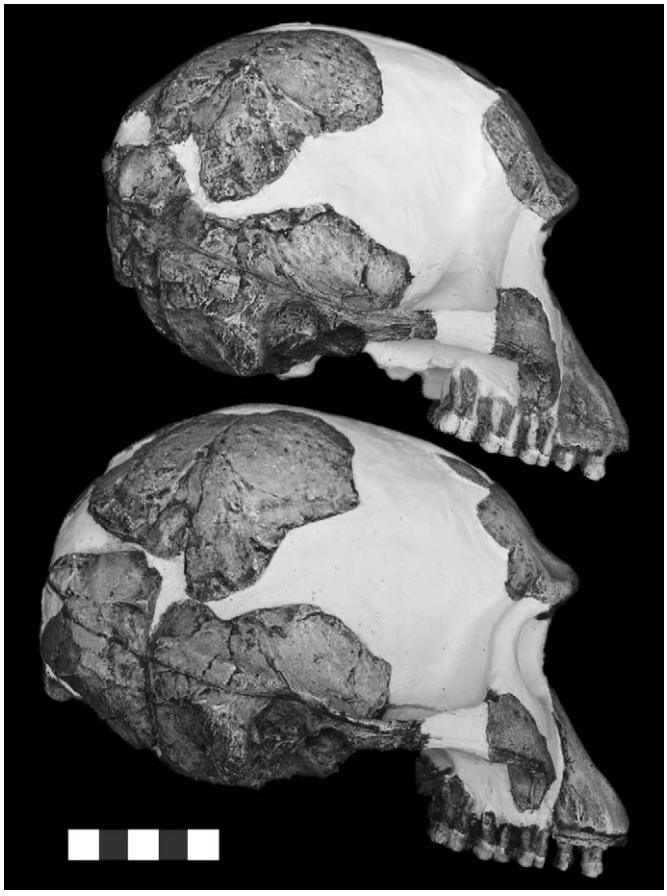

Fig. 11. New (bottom) and previous (top) reconstructions of Stw 53 in right lateral aspect. Crania positioned in FH. Scale bar = 5 cm.

(minimum frontal breadth) is less marked in the new reconstruction (−6 mm). Differences in maximum breadth across the temporals is large (−10 mm), while estimated biparietal breadth differs little (−1 mm). In inferior aspect (Fig. 13), corrections have been made to the placement of the left temporal. The foramen magnum has been

Table 1
Comparison of major dimensions (mm) of the new reconstruction with Clarke's (1985) "preliminary" reconstruction of Stw 53

Measurement	New reconstruction	Clarke's reconstruction	Difference
Maximum cranial length	ca. 167	ca. 147	+20
Cranial height	ca. 110	ca. 103	+7
Maximum breadth across mastoid processes	ca. 133	ca. 126	+7
Biporionic breadth	ca. 120	ca. 117	+3
Minimum frontal breadth	ca. 68	ca. 62	+6
Maximum temporal breadth	ca. 102	ca. 112	−10
Maximum parietal breadth	ca. 106	ca. 107	−1
Foramen magnum length	ca. 32	ca. 28	+4
Foramen magnum breadth	ca. 27	ca. 24	+3
Bidental breadth P^3	ca. 54	ca. 54	0
Bidental breadth P^4	ca. 57	ca. 59	−2
Bidental breadth M^2	ca. 60	ca. 64	−4
Bidental breadth M^3	ca. 60	ca. 62	−2
Superior facial height	ca. 70	ca. 72	−2
Bimaxillary breadth	ca. 96	ca. 93	+3

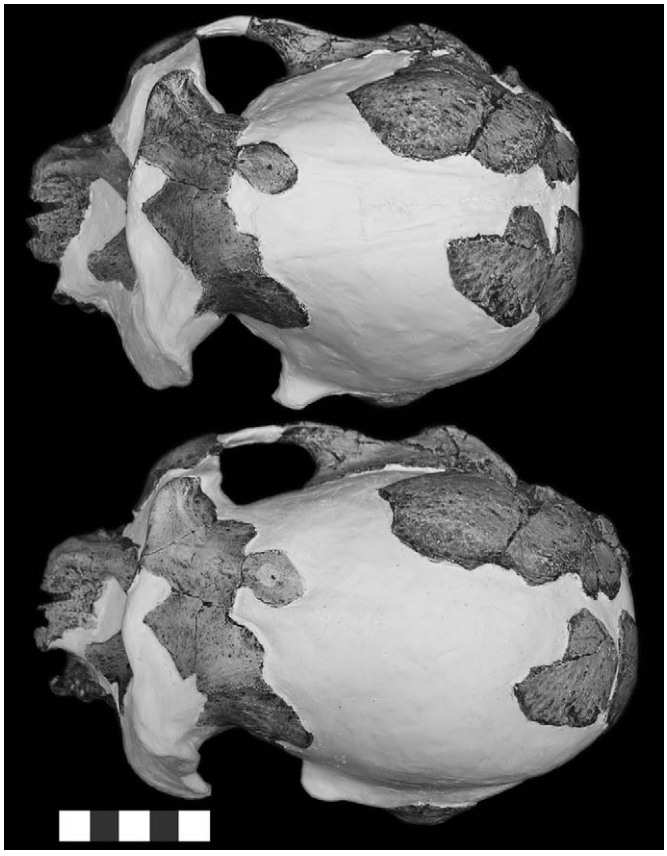

Fig. 12. New (bottom) and previous (top) reconstructions of Stw 53 in superior aspect. Crania positioned in FH. Scale bar = 5 cm.

reconstructed as larger (length +4 mm, breadth +3 mm). The new restoration of the maxilla has resulted in changes in the breadth of the upper dental arcade and palate. Most importantly, the arcade is narrower posteriorly (bidental at M^2, −4 mm; between the M^3s, −2 mm), reflecting an unusually narrow palate in Stw 53. The longer nuchal plane in the new reconstruction is also apparent. In posterior aspect (Fig. 14), the greater cranial height is obvious (+7 mm), as is the increased breadth across the mastoid processes (+11 mm).

The size of the face of Stw 53 differs between reconstructions (frontal aspect; Fig. 15). Superior facial height differs little (+2 mm), while the new reconstruction has a slightly narrower face (bimaxillary breadth, −3 mm).

Comparative morphology

The following section provides a comparison of the morphology of Stw 53 with that of other relevant Plio-Pleistocene fossils. Table 2 lists the species used for this purpose and their respective specimens. We regard KNM-ER 1470 as belonging to *Homo habilis* (Tobias, 1987, 1991, 2003; also see Miller, 2000), and we include this specimen in comparative samples for this taxon. However, in examining the morphology of Stw 53, we frequently refer to the conditions found in relevant individual Plio-Pleistocene crania, including comparisons with KNM-ER 1470. Specimen KNM-ER 1805 is listed separately because some researchers have assigned it to *Homo*

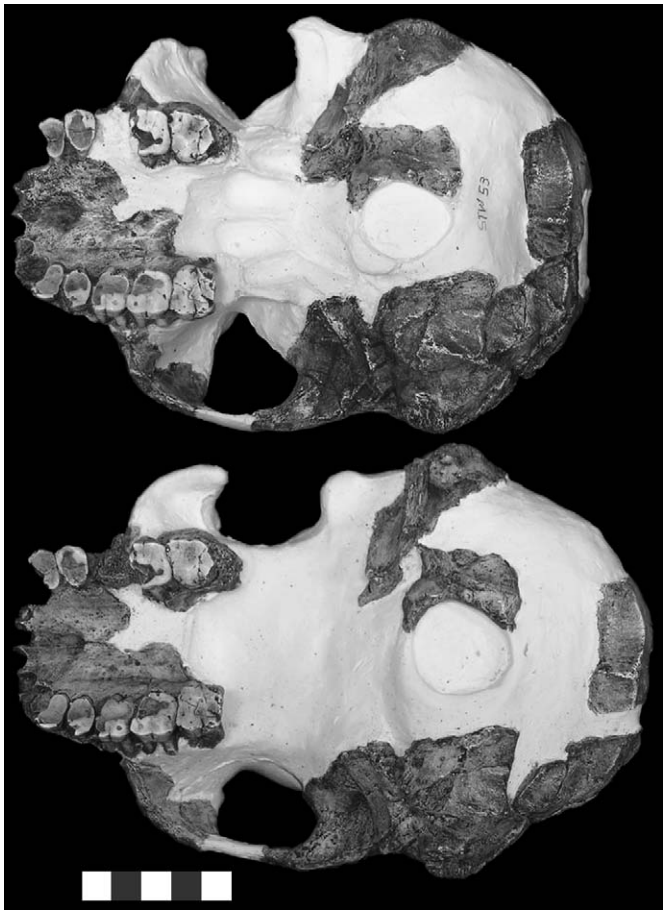

Fig. 13. New (bottom) and previous (top) reconstructions of Stw 53 in inferior aspect. Crania positioned in FH. Scale bar = 5 cm.

(e.g., Wood, 1992; Rightmire, 1993; Kimbel et al., 1997; Sherwood et al., 2002), while one of us (Tobias, 1991) regards this specimen as belonging to *Australopithecus boisei*. Specimen SK 847 is also given separate entry because the taxonomy of this specimen is considered in a separate section of the present contribution. We consider specimens frequently assigned to *Homo erectus* and *Homo ergaster* as belonging to *Homo sapiens* sensu lato (also see Jelinek, 1981; Aguirre, 1994; Wolpoff et al., 1994; Henneberg and Thackeray, 1995; Tobias, 1995; Curnoe and Thorne, 2003; Wu, 2004). We present data for Plio-Pleistocene representatives of this taxon for comparative purposes and list summary statistics for African (KNM-ER 3733 group), European (Dmanisi), and Southeast Asian (Sangiran and Trinil) samples separately. We use the term Plio-Pleistocene in its restricted sense, meaning fossils from the period spanning the final Pliocene and basal Pleistocene. We have restricted our craniometric samples to adult specimens and include KNM-WT 15000 only in dental comparisons.

In Tables 3–9 and Table 11, we provide data for a range of cranial and dental measurements and indices for Stw 53, comparing them with selected taxa and individual Plio-Pleistocene fossils. We use published craniometric data drawn from Jacob (1973), Bilsborough and Wood (1988), Tobias (1991), Wood (1991), Walker and Leakey (1993), Kimbel et al. (1997), Lockwood and Tobias (1999), Gabunia et al. (2000), and Vekua et al. (2002). Additional sources are listed in the text or in a footnote to the tables. Comparisons for all dental dimensions and indices are based on data in Tobias (1991), Wood (1991), Kimbel et al. (1997), and Blumenschine et al. (2003), with additional sources listed in the text or in a footnote to the tables.

Overall size and shape of the neurocranium

Maximum cranial length (see Fig. 8a,d) is estimated from the reconstruction to be ca. 167 mm long, greater than in the earlier reconstruction of Clarke (1985) (ca. 147 mm—see above). The difference results from the combined effect of two changes. First, in the new reconstruction the occipital plane is more elongate, as evidenced by an increased inion–opisthion length (ca. 40 mm vs. ca. 33 mm). Second, the curvature of the parietal bones in the sagittal plane is stronger as a result of altered placement of the left anterior parietal fragment (see above).

Fig. 14. New (right) and previous (left) reconstructions of Stw 53 in occipital aspect. Crania positioned in FH. Scale bar = 5 cm.

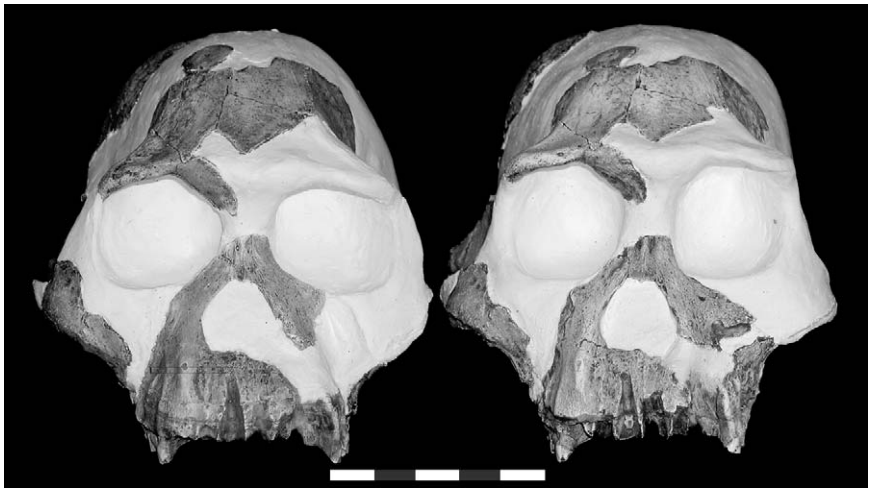

Fig. 15. New (right) and previous (left) reconstructions of Stw 53 in anterior aspect. Crania positioned in FH. Scale bar = 5 cm.

Maximum cranial length in Stw 53 is well above the sample medians for *A. africanus* and *H. habilis* (Table 3; see also Figs. 16, 17), but virtually identical to that estimated for KNM-ER 1470 (166 mm) (Fig. 18). While Stw 53 is below the median value for the European Plio-Pleistocene *H. sapiens* sensu lato sample, it is identical to the estimated length in D2282 (Table 3). The value for the southern African specimen is well below the sample medians for African and Southeast Asian Plio-Pleistocene *H. sapiens* sensu lato and outside of their ranges (Table 3).

As reconstructed, the Stw 53 calvaria is also high (estimated basi-bregmatic height is ca. 110 mm; Fig. 8d) compared with most Plio-Pleistocene taxa (Table 3; see also Figs. 16, 17), being similar to KNM-ER 3733 (108 mm) and identical to Sangiran 17. The precise position of bregma is not determinable, and the degree of angulation of the cranial base is difficult to estimate; these remain important uncertainties surrounding this dimension in Stw 53.

The greatest breadth of the reconstructed calvaria of Stw 53 is low (ca. 133 mm; see Fig. 8a,c), being widest across the mastoid processes. This value is below the median value for Plio-Pleistocene *H. sapiens* sensu lato but within the range for the Southeast Asian sample for this taxon (Table 3), and only just below (by 2 mm) the estimated maximum breadth across the mastoid processes in KNM-ER 3883. The value for this dimension in Stw 53 is above the ranges for *A. africanus* and *H. habilis* (Table 3). The mastoid processes of KNM-ER 1470 are not preserved. However, values for maximum breadth across the mastoid processes and supramastoid breadth are usually very close in *Homo* (see Table 3). Thus, the large supramastoid breadth in KNM-ER 1470 (ca. 138 mm) would probably have been accompanied by large maximum breadth across the mastoid processes (probably in excess of 130 mm). This would extend the *H. habilis* range and probably embrace the Stw 53 value. Supramastoid breadth in Stw 53 (ca. 130 mm) is well above the median values for *A. africanus* and *H. habilis* (Table 3), although it does lie within the sample range for the latter taxon, being less than the value in KNM-ER 1470. The Stw 53 value is greater than that of KNM-ER 1805. It is below the medians for African and European Plio-Pleistocene *H. sapiens* sensu lato samples and the average for the Southeast Asian sample of this group by only 3 mm in the case of the European sample median (Table 3). While all of these dimensions emphasize the broad cranial base of Stw 53 in relation to *A. africanus* and *H. habilis*, there is uncertainty surrounding these dimensions in this specimen owing to damage to the right parieto-occipito-temporal fragment and missing bone from the cranial vault and base (occipital and basioccipital).

Biporionic breadth (ca. 120 mm; Fig. 8c) is reconstructed to be large compared with smaller Plio-Pleistocene fossils (e.g., *A. africanus*, *H. habilis* specimens OH 24 and KNM-ER 1813, and KNM-ER 1805). It is well above sample medians for *A. africanus* and *H. habilis*, although below the value in KNM-ER 1470 (127 mm), and only just below (by 3 mm) sample medians for Plio-Pleistocene African and Southeast Asian *H. sapiens* sensu lato (Table 3). As reconstructed, the braincase is narrow across the parietal bones (corrected ca. 106 mm; Fig. 8a), and across the squamous part of the

Table 2
Species samples of teeth and crania used for taxonomic discussions

Australopithecus africanus[1]
MLD 1, MLD 11/30, MLD 6/23, MLD 9, MLD 18, MLD 28, MLD 37/38, MLD 45, TM 1511, TM 1512, TM 1514, TM 1527, TM 1561, Sts 1, Sts 2, Sts 3, Sts 7, Sts 8, Sts 12, Sts 17, Sts 22, Sts 24, Sts 28, Sts 32, Sts 36, Sts 37, Sts 47, Sts 48, Sts 50, Sts 51, Sts 52, Sts 53, Sts 54, Sts 55, Sts 56, Sts 61, Stw 187, Stw 505, Stw/H 2, Stw/H 6, Stw/H 13, Stw/H 18c, Stw 59, Stw/H 73, Taung 1

Homo habilis
A.L. 666-1, KNM-ER 1470, KNM-ER 1482, KNM-ER 1590, KNM-ER 1813, KNM-ER 3732, OH 7, OH 13, OH 15, OH 16, OH 22, OH 24, OH 37, OH 39, OH 40, OH 42, OH 62, OH 65

Homo sapiens sensu lato (Plio-Pleistocene)
KNM-ER 730, KNM-ER 806, KNM-ER 992, KNM-ER 3733, KNM-ER 3735, KNM-ER 3883, KNM-WT 15000, Trinil 1, Trinil 2, Trinil 4, Sangiran 2, Sangiran 3, Sangiran 4, Sangiran 9, Sangiran 10, Sangiran 11, Sangiran 12, Sangiran 15, Sangiran 16, Sangiran 17, Dmanisi D2280, D2282 and D2700

[1] DC prefers to classify this species in *Homo* (see Curnoe and Thorne, 2003).

Table 3
Dimensions and shape indices of the neurocranium

Measurements and indices[a]	Stw 53	*A. africanus*			*H. habilis*			ER 1805	SK 847	*H. sapiens* sensu lato Africa			*H. sapiens* sensu lato Europe			*H. sapiens* sensu lato East Asia		
		n	Med.	Range	n	Med.	Range			n	Med.	Range	n	Med.	Range	n	Avg./med.[d]	Range
Maximum cranial length (1)[b]	[ca. 167][c]	2	138	17	3	149	21	—	—	2	182	0	2	172	10	3	183	29
Cranial height (17)	[ca. 110]	2	97	9	2	90	1	—	—	2	104	8	2	99	13	4	105	8
Maximum breadth across mastoid processes	[ca. 133]	3	110	18	2	117	5	(128)	—	2	139	5	—	—	—	4	142	20
Supramastoid breadth	[ca. 130]	3	117	9	3	120	25	(122)	—	2	141	3	2	135	0	6	145 ± 9.2	27
Biporionic breadth	[ca. 120]	4	100	5	3	105	27	106	—	2	123	3	—	—	—	4	123	16
Maximum parietal breadth	[>99; ca. 106]	3	98	6	3	115	22	107	—	2	130	5	2	117	3	5	137 ± 5.3	14
Maximum temporal breadth	[ca. 102]	4	107	13	3	118	22	110	—	2	135	1	—	—	—	5	136 ± 6.6	15
Lambda–inion	[ca. 35]	4	36	10	2	56	5	—	—	2	55	12	—	—	—	5	50 ± 4.9	13
Minimum frontal breadth (9-1)	[ca. 68]	3	66	9	4	78	18	88	(64)	2	90	3	2	71	9	5	88 ± 8.2	20
Inion–opisthion	[ca. 40]	4	35	13	2	33	2	—	—	2	51	1	—	—	—	4	54	7
Occipital scale index	[ca. 114]	4	99	64	2	60	6	—	—	2	92	22	1	102	—	4	107	21
Mastoid length	26	4	23	7	1	20	—	24	20	—	—	—	—	—	—	2	26	2
Foramen magnum length (8)	[ca. 32]	3	28	3	2	29	0	—	—	2	33	5	—	—	—	2	39	1
Foramen magnum maximum width (16)	[ca. 27]	3	23	2	2	26	1	—	—	2	29	6	—	—	—	2	31	2
Occipital condyle maximum chord length	(ca. 15)	2	16	2	2	17	2	20	—	1	19	—	—	—	—	2	24	2
Occipital condyle maximum chord breadth	(ca. 7)	2	9	0	2	10	1	9	—	2	11	1	—	—	—	2	13	1
Occipital condyle computed area (mm^2)	(ca. 102)	2	144	18	2	162	36	180	—	1	209	—	—	—	—	2	301	49
Occipital condyle module	(ca. 10.8)	2	13	1	2	13	2	15	—	1	15	—	—	—	—	2	18	2
Occipital condyle breadth-length index (%)	(ca. 48)	2	57	7	2	56	0	45	—	1	58	—	—	—	—	2	52	0
Mandibular fossa length	13	4	16	5	3	15	7	19	15	3	19	1	—	—	—	2	22	1
Mandibular fossa breadth	21	4	29	5	3	26	3	(24)	26	3	30	6	—	—	—	1	24	—
Mandibular fossa depth	5	2	9	3	3	6	4	10	—	3	7	3	—	—	—	2	9	7
Mandibular fossa length-breadth index (%)	62	4	58	15	3	58	35	79	58	2	70	6	—	—	—	1	92	—
Mandibular fossa depth-length index (%)	38	2	56	23	3	40	51	53	—	2	31	9	—	—	—	2	40	31
Mandibular fossa depth-breadth index (%)	24	2	30	6	3	25	14	43	—	2	21	4	—	—	—	1	50	—

[a] All data in mm unless indicated.
[b] Numbers in parentheses after measurement names correspond to the measurements of Martin and Saller (1957).
[c] Values in brackets are estimates taken from the new reconstruction of Stw 53; numbers in parentheses are estimated/reconstructed values taken from original fossils (i.e., Stw 53, KNM-ER 1805, and SK 847).
[d] If $n < 5$, median is given; if $n \geq 5$, average is given; ± standard deviations of sample averages.

Table 4
Angles of the cranial base

Angles[a]	Stw 53	*A. africanus*			*H. habilis*			ER 1805	SK 847	*H. sapiens* sensu lato Africa			*H. sapiens* sensu lato Southeast Asia		
		n	Med.	Range	n	Med.	Range			n	Med.	Range	n	Med.	Range
Tympanomedian angle	[ca. 60][b]	4	75	10	2	95	0	(80)[c]	80	2	95	5	1	110	—
Mandibular fossa angle	[ca. 105]	4	100	10	3	105	5	90	80	2	113	5	1	95	—

[a] All data in degrees.
[b] Values in brackets are estimates taken from the new reconstruction of Stw 53.
[c] Values in parentheses are estimated/reconstructed values taken from original fossils.

temporal bones (ca. 102 mm; see Fig. 8a). These estimates are minima only, as the true breadth, which is likely greater, is difficult to reconstruct accurately due to missing bone in Stw 53.

In lateral aspect (Fig. 8d), the parieto-occipital region of Stw 53 is nearly subangular, the result of posterior expansion (''filling out'') of the parietal bones. In this regard, it resembles most closely KNM-ER 1813 (Fig. 17), differing from the more rounded profile present in *A. africanus* specimens such as Sts 5 (Fig. 16).

Frontal bone

The squamous part of the Stw 53 frontal is similar in height to that of Sts 5 (Fig. 16), OH 24, and KNM-ER 1813 (Fig. 17). Kimbel and Rak (1993) described differences in the morphology of the squamous frontal between *H. rudolfensis* (KNM-ER 1470 and KNM-ER 3732) and *H. habilis* sensu stricto (OH 24 and KNM-ER 1813). Specifically, the former taxon is described as possessing a flat squama, while the latter group is said to have a convex squama in the coronal plane of postorbital constriction. In Stw 53, this region is convex and rounded, exhibiting modest development of the bone in its median sagittal line. Thus, it has a rounded, domelike forehead, with the vault rising well above the orbits (as in KNM-ER 1813; Fig. 17). It is unclear whether development of the bone in the midline is a frontal midline ridge (or midline keel) of the form seen in Plio-Pleistocene *H. sapiens* sensu lato (also see Bräuer and Mbua, 1992). Although variable in presence and development, a frontal midline ridge is found in Dmanisi (Gabunia et al., 2000; Vekua et al., 2002) and Sangiran specimens, and is typically most developed as it approaches bregma. A frontal midline ridge is not found in *H. habilis*, including KNM-ER 1470, and is absent in KNM-ER 3733, although the latter specimen does possess a pre-bregmatic eminence. The frontal bone of Stw 53 preserves only the anterior third of the squama, making it impossible to judge whether this pre-bregmatic feature was present.

In superior aspect (Fig. 8a), Stw 53 is long and slightly ovoid, with moderate anterior tapering, having an outline similar to that of KNM-ER 1470 (Fig. 18). Minimum frontal breadth is low in Stw 53 (ca. 68 mm), being close to the sample median for *A. africanus* (Table 3), and outside of the sample range for *H. habilis* (although only 2 mm below the value in KNM-ER 1813). The Stw 53 value is also well below the medians for African and European Plio-Pleistocene *H. sapiens* sensu lato samples and the average for the Southeast Asian sample of this group (Table 3). It is, however, within the range for the European (Dmanisi) sample, being 2 mm broader than in D2282. In SK 847, the minimum frontal breadth (64 mm) is also low, being below the range for *A. africanus*, and within the range for robust australopiths.

The right superior and inferior temporal lines, or crests, are clearly marked from their origin behind the zygomatic process of the frontal bone and for much of their course on the right squamous part. The temporal lines of Stw 53 encroach on the lateral half of the supraorbital rim, as in SK 847 and *A. africanus* (see also Tobias, 1991; Grine, 2001). On the left side, the temporal lines are preserved for about the middle third of their course. The temporal crests reach towards the midline in Stw 53; this condition is similar to that in OH 16 (*H. habilis*) and the juvenile Dmanisi (D2700) cranium [as judged from photographs in Vekua et al. (2002)]. This morphology contrasts with that of OH 24 and KNM-ER 1813 (*H. habilis*), adult Dmanisi specimens (D2280 and D2282), and Plio-Pleistocene *H. sapiens* sensu lato, in which the temporal crests are well separated. The coronal lie of the temporal lines is a feature that has been used by Rightmire (1993) to distinguish KNM-ER 1470 from the small-brained OH 16,

Table 5
Estimates of cranial bone thickness

Measurements[a]	Stw 53	*A. africanus*			*H. habilis*			ER 1805	*H. sapiens* sensu lato Africa			*H. sapiens* sensu lato Southeast Asia		
		n	Med.	Range	n	Med.	Range		n	Med.	Range	n	Avg./med.[c]	Range
Parietal eminence	6	3	6	1	3	8	1.5	7	3	7.5	4	7	10 ± 1.5	4.5
Lambda	7[b]	1	7	—	3	7	5	6	3	9.5	3.5	4	9.5	3

[a] All data in mm.
[b] Taken slightly inferior to lambda and slightly lateral to median sagittal line.
[c] If $n < 5$, median is given; if $n \geq 5$, average is shown; $\pm$ standard deviation of sample average.

Table 6
Dimensions and indices of the viscerocranium and measures of facial projection

Measurements and indices[a]	Stw 53	*A. africanus*			*H. habilis*			ER 1805	SK 847	*H. sapiens* sensu lato Africa			*H. sapiens* sensu lato Europe			*H. sapiens* sensu lato Southeast Asia		
		n	Avg./med.[e]	Range	n	Med.	Range			n	Med.	Range	n	Med.	Range	n	Med.	Range
Superior facial height (48)[b]	[ca. 70][c]	4	75	20	3	67	24	71	84	1	83	—	1	(81)	—	1	(82)	—
Transverse extent of supraorbital torus[d]	[ca. 96]	4	87	11	3	103	2	—	93	2	110	6	—	—	—	—	—	—
Superior facial breadth	[ca. 84]	3	92	11	4	107	20	—	(101)	2	120	1	—	—	—	1	125	—
Bimaxillary breadth (46)	[ca. 92]	5	103 ± 7.8	18	2	105	16	—	(102)	2	123	34	—	—	—	1	(124)	—
Superior facial index (48/46)	[ca. 76]	4	73	19	2	74	11	—	(82)	1	78	—	—	—	—	1	66	—
Thickness of supraorbital margin	4	5	7 ± 3.9	4	4	9	6	—	7	2	11	5	2	11	1	3[f]	18	7
Orbital height	[ca. 31]	3	31	8	4	32	5	—	34	2	36	0.5	1	37	—	1	36	—
Orbital breadth	[ca. 27]	4	35	5	4	34	4	—	33	2	41	1	1	40	—	1	43	—
Nasal height (55)	[ca. 56]	6	50 ± 7.0	19	3	42	15	52	51	1	52	—	—	—	—	1	(61)	—
Nasal breadth (54)	25	8	23 ± 3.9	12	3	24	4	28	—	1	36	—	—	—	—	1	(30)	—
Nasal index (%) (54/55)	[ca. 45]	6	47 ± 6.3	16	3	55	10	54	—	1	69	—	—	—	—	1	(49)	—
Length of nasal bones (56)	[ca. 24]	5	26 ± 8.1	20	2	22	3	18	25	2	22	8	—	—	—	1	21	—
Inferior breadth of nasal bones (57-3)	8	5	11 ± 1.1	3	3	10	3	11	(12)	2	17	4	—	—	—	1	11	—
Piriform aperture height (55-1)	21	5	26 ± 2.5	5	3	28	18	34	27	1	30	—	—	—	—	1	41	—
Height/breadth index of piriform aperture (%) (54/55-1)	119	5	89 ± 17.9	40	3	82	45	82	—	1	120	—	—	—	—	1	73	—
Orbito-foraminal height	[ca. 13]	5	13 ± 3.1	8	1	15	—	—	—	—	—	—	—	—	—	—	—	—
Malar thickness	(ca. 9)	3	10	8	2	8	2	—	12	1	19	—	—	—	—	1	(15)	—
Alveolar height (48-1)	(ca. 25)	4	28	9	2	26	2	21	32	1	31	—	—	—	—	1	(25)	—
Prosthion–nasospinale projected distance	[ca. 13]	4	20	9	4	18	17	—	16	1	13	—	—	—	—	1	18	—
Proj./direct index (%)	[ca. 52]	4	75	17	4	64	22	—	53	1	47	—	—	—	—	1	62	—
Facial angle (°)	[ca. 66]	2	60	10	3	70	7	—	65	1	78	—	—	—	—	1	75	—
Alveolar profile angle (°)	[ca. 50]	3	40	15	3	50	2	—	55	1	63	—	—	—	—	1	75	—
Nasal profile angle (°)	[ca. 75]	2	73	5	3	75	12	—	—	1	88	—	—	—	—	1	80	—

[a] All data in mm unless indicated.
[b] Numbers in parentheses after measurement names correspond to the measurements of Martin and Saller (1957).
[c] Values in brackets are estimates taken from the new reconstruction of Stw 53; numbers in parentheses are estimated/reconstructed values taken from original fossils (i.e., Stw 53, KNM-ER 1805, and SK 847).
[d] Measured in Stw 53 as the reconstructed distance between points on the lateral borders of the torus at the approximate level of glabella, after Bilsborough and Wood (1988). Data for comparative taxa for this dimension taken from Bilsborough and Wood (1988), but note that in *A. africanus*, the average is given.
[e] If $n < 5$, median is given; if $n \geq 5$, average is shown; ± standard deviations of sample averages.
[f] Includes data from Rightmire (1990).

Table 7
Dimensions of the maxillary dental arcade and palate

Measurements and indices[a]	Stw 53	*A. africanus*			*H. habilis*			SK 847	*H. sapiens* sensu lato Africa[f]	*H. sapiens* sensu lato Southeast Asia[g]
		n	Avg./med.[e]	Range	n	Avg./med.[e]	Range			
Maxillo-alveolar length (60)[b]	(ca. 67)[c]	3	77	10	2	61	0	65	(63)	67
Canine interalveolar distance	24	8	29 ± 1.6	5	5	30 ± 2.3	6	26	34	(40)
P^3 interalveolar distance	26	8	29 ± 3.2	9	6	34 ± 3.4	9	27	35	(48)
P^4 interalveolar distance	27	6	31 ± 2.4	6	3	35	6	26	36	—
M^2 interalveolar distance	(ca. 25)	7	35 ± 4.9	14	5	40 ± 4.8	12	31	38	(35)
M^3 interalveolar distance	(ca. 24)	3	39	8	5	39 ± 2.3	6	30	—	(27)
Palatal height (64)[d]	(ca. 9)	6	14 ± 2.9	8	5	16 ± 2.7	5	12	(20)	14

[a] All data in mm unless indicated.
[b] Numbers in parentheses after measurement names correspond to the measurements of Martin and Saller (1957).
[c] Numbers in parentheses are estimated/reconstructed values taken from original fossils.
[d] On Stw 53, this measurement was taken with an imaginary line between distal faces of M^1s (not midpoint) and the reconstructed height of the alveolar processes.
[e] If n < 5, median is given; if n ≥ 5, average is shown; ±standard deviations of sample averages.
[f] Data from KNM-ER 3733.
[g] Data from Sangiran 17.

OH 24, and KNM-ER 1813 specimens. As outlined here, there is considerable variation in the latter group, suggesting that this feature has limited phyletic value.

Occipital bone

In lateral aspect (Fig. 8d), the occipital bone is moderately sloped (as in KNM-ER 1813, but contrasting with Sts 5; Figs. 16, 17). Inion is positioned below the Frankfurt Horizontal (FH) and opisthocranion. The latter two features distinguish Stw 53 from Plio-Pleistocene *H. sapiens* sensu lato (see Day and Stringer, 1982; Tobias, 1991) and align it with *H. habilis*. The occipital squama of Stw 53 is short (lambda–inion ca. 35 mm; see Fig. 8d) and nearly identical to the sample median for *A. africanus* (Table 3). It lies well outside of the ranges for *H. habilis* and Plio-Pleistocene *H. sapiens* sensu lato (Table 3). Note that the position of lambda has been reconstructed for measurement in Stw 53, adding an estimated uncertainty of approximately 2–3 mm to this dimension.

A striking feature of our new reconstruction when viewed in inferior and lateral aspects (Fig. 8b,d) is its elongate occipital (nuchal) plane. Estimated length (inion–opisthion ca. 40 mm) is long compared to most Plio-Pleistocene groups. While it is above the median values for *A. africanus* and *H. habilis* (see Figs. 16, 17), it does lie within the ranges of these taxa (Table 3). The Stw 53 value is outside of the ranges for Plio-Pleistocene *H. sapiens* sensu lato samples. We have also estimated the occipital scale index (lambda–inion/inion–opisthion) in Stw 53 (ca. 114%). This is well above the median values for *A. africanus*, *H. habilis*, and samples of Plio-Pleistocene *H. sapiens* sensu lato (Table 3). However, the estimated value for this specimen does lie within the range for *A. africanus*. A considerable amount of bone is missing from the occipital plane (Fig. 8b), and the posterior border of the foramen magnum is also missing (Figs. 6, 8b), adding uncertainty to our estimate of inion–opisthion length. We believe the

Table 8
Difference (%) between anterior, middle, and posterior maxillary interalveolar distances

Taxon/specimen	$P^3/\underline{C}$	$P^4/\underline{C}$	M^3/P^3	M^3/P^4
Stw 53	+8	+13	−8	−11
SK 847	+4	0	+11	+15
A. africanus				
MLD 9	0	−3	—	—
Sts 5	−7	+14	+48	+21
Sts 17	+7	+22	(+34)	(+18)
Sts 52	−7	−4	—	—
Sts 53	0	+10	+10	0
Sts 60	−11	(+15)	—	—
Sts 71	+14	—	—	—
Stw 13	+3	—	—	—
Avg./med.[a]	−0.13 ± 8.2	+9 ± 10.4	+34	+18
H. habilis				
OH 13	+7	—	(+19)	—
OH 24	+11	+11	+33	+33
OH 65	—	—	+7	—
KNM-ER 1813	+14	+25	+28	+17
KNM-ER 1470	+18	—	—	—
A.L. 666-1	+9	+19	(+6)	(−3)
Avg./med.[a]	+11.8 ± 4.3	+19	+18.6 ± 12.1	+25
H. sapiens sensu lato				
KNM-ER 3733	+3	+6	—	—
Sangiran 17	+20	—	−44	—
Med.	+12	—	—	—

[a] If n < 5, median is given; if n ≥ 5, average is shown; ± standard deviations of sample averages.

Table 9
Anterior maxillary tooth alveolus dimensions of Stw 53[a]

Tooth	Side	Mesiodistal diameter (mm)	Labiolingual diameter (mm)	Alveolus area (mm^2)
I^1	R	10.7	—	—
I^2	L	ca. 9.4[b]	ca. 5.2	ca. 48.9
	R	ca. 8.7[c]	ca. 4.0[d]	ca. 34.8
$\underline{C}$	R	8.8	ca. 10.3[d]	ca. 90.6

[a] Inner maximum dimensions taken for all alveoli.
[b] Reconstructed to allow for damage on mesial margin.
[c] Reconstructed to allow for damage on labial margin.
[d] Reconstructed to allow for damage on labial and distal margins.

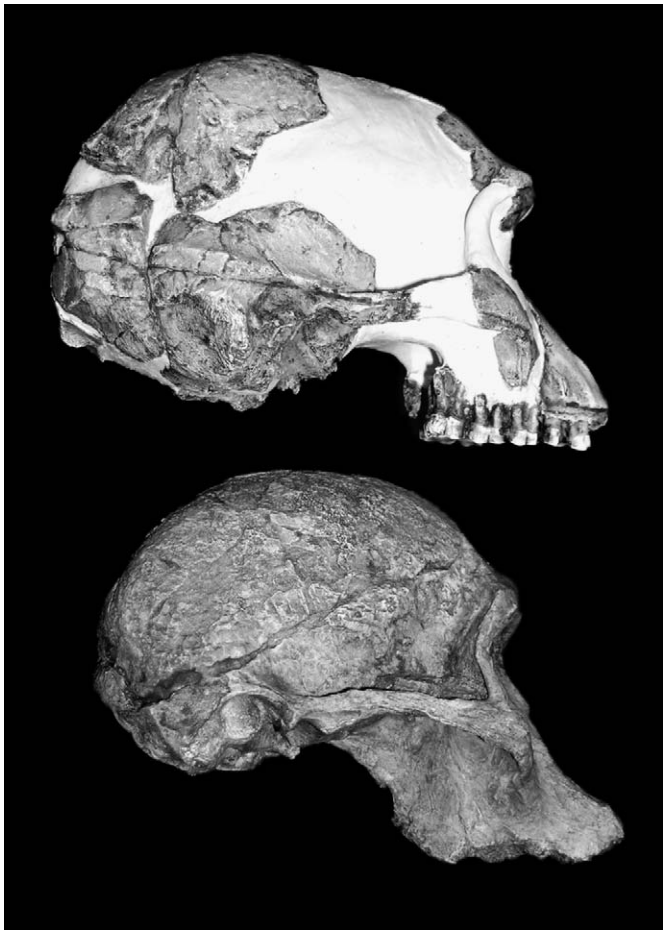

Fig. 16. Casts of Stw 53 (top) and Sts 5 (bottom) in right lateral aspect.

Fig. 17. Casts of Stw 53 (top) and KNM-ER 1813 (bottom) in right lateral aspect.

occipital plane of Stw 53 is unlikely to have been longer than we have reconstructed it to be, suggesting that it has its strongest affinity with *A. africanus* and *H. habilis* in terms of absolute size. However, the loss of some bone makes the assessment of affinities based on shape, especially using the occipital scale index value, less certain.

There is a slightly asymmetrical occipital torus in Stw 53, better developed laterally on its left side (Fig. 5). Rightmire (1993) used this feature to support a distinction between KNM-ER 1470 (torus lacking) and small-brained crania from Olduvai and Koobi Fora (torus present). A slight supratoral sulcus is present in Stw 53. Such a sulcus is found in *H. habilis* (e.g., OH 16) and *A. africanus* (e.g., Sts 5 and Sts 25). The presence of an occipital torus serves to align Stw 53 with OH 16 (*H. habilis*), and to a lesser extent, OH 13 and OH 24 (*H. habilis*), in which it is laterally constricted, and MLD 1 (*A. africanus*).

Temporal bone

In occipital aspect (Fig. 8c), Stw 53 is distinguishable from specimens such as OH 24 and KNM-ER 1813 by its strong lateral protrusion of the mastoid-supramastoid complex relative to the temporal squama. In this respect, it is similar to some *A. africanus* specimens and robust australopiths. Rightmire (1993) used this feature to distinguish KNM-ER 1470 (protrusion present) from OH 13, OH 24 (and probably OH 16), KNM-ER 1805, and KNM-ER 1813 (protrusion absent). It also aligns KNM-BC 1 with the latter group (Sherwood et al., 2002). Specimen Stw 53 has much stronger protrusion than any of these fossils. The mastoid process and mastoid crest are also laterally swollen in Stw 53, which aligns it with KNM-ER 1470 and KNM-ER 1805 (Rightmire, 1993), but distinguishes it from OH 24 and KNM-ER 1813. The length of the right mastoid process (measured by the method of Wood, 1991) in Stw 53 (26 mm) is long (Fig. 4), being identical to the median for the African Plio-Pleistocene *H. sapiens* sensu lato sample (Table 3). Although it lies above the median values for all other samples, the length of the mastoid process in Stw 53 is within the range for *A. africanus* (Table 3). They also project downwards and somewhat forwards. The mastoid processes of Stw 53 are reminiscent of those of Sangiran 17 in their size (see Table 3) and those of Sts 5, Sts 71, and OH 24 in their projection and level of pneumatization.

Mandibular fossa dimensions for Stw 53 follow the definitions of Wood (1991). Other measurements may be used that provide more comprehensive coverage of the articular surface of the mandibular fossa (e.g., measurements of Weidenreich, 1943; Tobias, 1991). However, we used Wood's dimensions in order to maximize available comparative data. The mandibular fossa is short in anteroposterior length (13 mm). It is

Fig. 18. Casts of Stw 53 (left) and KNM-ER 1470 (right) in superior aspect.

below the medians for *A. africanus* and *H. habilis*, below the value for SK 847, and well below the value for KNM-ER 1805, as well as the medians for the samples of Plio-Pleistocene *H. sapiens* sensu lato (Table 3). The mandibular fossa of Stw 53 is mediolaterally narrow (21 mm), being the narrowest of the Plio-Pleistocene fossils included here. Its value is outside of the range for all taxa (Table 3). The mandibular fossa of Stw 53 is shallow (5 mm), being identical to values for KNM-ER 3733 and Sangiran 4. Its value is below the median for *A. africanus*, but only just below (by 1 mm) the median for *H. habilis* (Table 3).

The mandibular fossa length-breadth index value for Stw 53 (62%) is identical to the value for Sts 71, slightly above (by 4%) the value in SK 847 (Table 3), but well below that of KNM-ER 1805. It is slightly above the median values for *A. africanus* and *H. habilis*, which are identical (Table 3). Thus, as in these taxa, the mandibular fossa in Stw 53 is relatively short anteroposteriorly. The value for this index in Stw 53 is well below the median values for samples of Plio-Pleistocene *H. sapiens* sensu lato. In Stw 53, the mandibular fossa depth-length index value (38%) is moderate, being well below the median for *A. africanus*, and virtually indistinguishable from the median values for *H. habilis* and eastern African Plio-Pleistocene *H. sapiens* sensu lato, which are identical (Table 3). The mandibular fossa depth-breadth index value is low (24%), being below the median for *A. africanus*, virtually identical to the median for *H. habilis*, above the median for African Plio-Pleistocene *H. sapiens* sensu lato (by 3%), but well below the value in Sangiran 17 (Table 3).

The mandibular fossa of Stw 53 exhibits a prominent articular eminence (Fig. 19), as seen in OH 24 and KNM-ER 1813. The postglenoid process in Stw 53 (Fig. 19) is asymmetrical and much reduced compared with *A. africanus*. Laterally, the posterior articular surface is formed by the continuous postglenoid process and the tympanic (Fig. 19). In *A. africanus*, the

Fig. 19. Right parieto-occipito-temporal fragment of Stw 53 (inferior aspect), highlighting salient features of the mandibular fossa: 1 = prominent articular eminence, 2 = reduced postglenoid process that is continuous with the tympanic, 3 = absence of both medial recess and anteromedial recess, and 4 = large petrous crest. Divisions of scale bar are each 10 mm. A = anterior.

lateral posterior wall of the mandibular fossa is formed exclusively by the postglenoid process (Kimbel and Rak, 1993). The medial recess of the mandibular fossa (described by Weidenreich, 1943) is clear in *H. habilis* and Plio-Pleistocene *H. sapiens* sensu lato and is absent in Stw 53 (Fig. 19). The anteromedial recess (a feature described by Tobias, 1991), seen clearly in specimens such as Sts 5, Sts 19, and MLD 37/38 (*A. africanus*), but lacking in early *Homo* (Tobias, 1985) and KNM-BC 1 (Sherwood et al., 2002), is absent in Stw 53 (also see Bräuer and Mbua, 1992). The petrous crest in Stw 53 (Fig. 19) is well developed and merges with the anterior face of the mastoid (observable on the left side), being identical to the condition in OH 24, and a diagnostic feature of *H. habilis* (Kimbel and Rak, 1993). Specimen Stw 53 possesses a well developed styloid process (Fig. 6). This feature is variable in both *A. africanus* and *H. habilis*.

Most of the preglenoid plane of Stw 53 is missing; however, its angle with the anterior wall of the mandibular fossa is steep (about 50°), as seen in KNM-ER 1813. The angle is acute in OH 24 (Tobias, 1991; Kimbel and Rak, 1993; Ahern, 1998). In KNM-ER 1470, the angle of the preglenoid plane is more horizontal (Kimbel and Rak, 1993), as in *A. africanus*.

Cranial base

As judged by the anteroposterior distance between the mandibular fossa and M^2/M^3, the new reconstruction of Stw 53 has a cranial base that is relatively short, as observed in OH 24 and KNM-ER 1813, and shorter than in KNM-ER 3733 and Sts 5. The foramen magnum sits well beneath the cranium (Fig. 8b) and is in approximately the same anteroposterior position as in KNM-ER 1813, but posterior to its position in comparison to that of Sts 5 and OH 24.

As noted, less than half of the left margin of the foramen magnum is present, the preserved part comprising the anterior rim (Fig. 6). The reconstructed length (basion–opisthion, ca. 32 mm) is above the medians for *A. africanus* and *H. habilis*, almost identical to the value for KNM-ER 3733, but below that for Sangiran 17. Its estimated breadth (ca. 27 mm) is almost identical to the *H. habilis* median, above the *A. africanus* median, but below median values for Plio-Pleistocene African and Southeast Asian *H. sapiens* sensu lato (Table 3).

The preserved occipital condyle of Stw 53 (Fig. 6) is broken off anteriorly, but it is possible to estimate its original size. The reconstructed computed area (ca. 102 mm^2) and module (ca. 11 mm) are well below the range for Plio-Pleistocene taxa (Table 3). The occipital condyle breadth-length index value in Stw 53 (ca. 48%) is closest to that of KNM-ER 1805 (Table 3). However, comparative samples are small for all taxa and the significance of small occipital condyles in Stw 53 is difficult to assess.

The petrous pyramids are incomplete in Stw 53. However, it is possible to approximate the orientation of the left pyramid relative to the sagittal plane. Using a cast of Clarke's (1985) Stw 53 reconstruction, Ahern (1998) determined petrous pyramid orientation (petromedian angle) to be 36°. In our new reconstruction of Stw 53, this angle is estimated at ca. 35°. According to Kimbel and Rak (1993) and Ahern (1998), this feature serves to distinguish *A. africanus* and *H. habilis*, the former exhibiting more sagittally oriented petrous pyramids (Dean and Wood, 1982), and the latter more coronally oriented pyramids. Specimen Stw 53 possesses the same condition as seen in *H. habilis*.

Table 4 lists a further two angles of the cranial base that we have been able to estimate in the new reconstruction of Stw 53. The tympanomedian angle (between the long axis of the tympanic bone and the long axis of the petrous pyramid; Weidenreich, 1943) of Stw 53 (ca. 60°) is low and well outside of the range for Plio-Pleistocene groups. The mandibular fossa angle (between the long axis of the fossa and the sagittal axis of the cranium; see Wood, 1991) in Stw 53 is moderate (ca. 105°), being identical to the median value for *H. habilis* (Table 4). Although we have corrected for distortion in the cranium, these estimates for Stw 53 are likely to contain some error.

Vault thickness

Thickness of the cranial vault can be determined at two locations on Stw 53: at the position of the parietal eminence (right side) and close to lambda (measured slightly below and lateral to the median sagittal plane). Values for Stw 53 are as follows: parietal right eminence, 6 mm; near lambda, 7 mm. The parietal value is identical to the median value for *A. africanus* (Table 5) and below the median values for *H. habilis* (by 2 mm) and Plio-Pleistocene African *H. sapiens* sensu lato (by 1.5 mm) (Table 5), below the value in KNM-ER 1805 (by 1 mm), and well below the sample average for the Southeast Asian *H. sapiens* sensu lato sample (by 5 mm) (Table 5). The occipital value is identical to the median values for *A. africanus* and *H. habilis* (Table 5), slightly larger than the value in KNM-ER 1805 (by 1 mm), but below the median values in African and Southeast Asian *H. sapiens* sensu lato samples (by 2.5 mm) (Table 5).

Interior of the calvaria

The endocranial surface of the temporal bone of Stw 53 preserves some of the middle cranial fossa, including much of the tegmen tympani (left and right), and with the occipital, much of the right posterior cranial fossa. The tegmen tympani is reduced in size compared with those in modern humans, but is about the same size as in Sts 19. In Sts 19, SK 847, and modern humans, the anterior and posterior surfaces of the petrous meet at an acute angle, with widening of the angle from anteromedial (AM) to posterolateral (PL). However, in Stw 53, the configuration of the petrous pyramid is very different. It has a moderately acute angle, but this angle becomes more acute from AM to PL, as in chimpanzees.

We have not examined the morphology of this region in other specimens. To evaluate whether the morphology of the petrous pyramid is likely to be relevant for the assessment of the affinities of Stw 53, we examined a sample of 30 Zulu and Sotho South African modern human crania (15

male and 15 female) housed in the Raymond Dart Collection (University of the Witwatersrand) to assess within-group variation. The petrous pyramids of the male crania had, for the most part, the human modal form, with an acute angle widening from AM to PL (as in Sts 19 and SK 847). However, the opposite AP trend was found in two of the female crania, which showed a narrowing of the angle from AM to PL (as in Stw 53). A small number of males and females had equally sized angles from AM to PL. We conclude that the endocranial petrous pyramid morphology of Stw 53 is likely to have little relevance in assessing its affinities.

Venous sinus impressions of Stw 53 show no enlargement of the occipital and marginal sinuses, a feature shared with *A. africanus* (cf. Taung, Stw 187), *H. habilis*, and Plio-Pleistocene *H. sapiens* sensu lato.

The internal acoustic meatus of Stw 53 is narrow, and its long axis is about 45° to the horizontal plane. This morphology is identical to that seen in Sts 19, but distinct from the internal acoustic meatus seen in SK 847 and most modern humans, which have a large, sub-circular opening. The posterior cranial fossa of Stw 53 is relatively large (long, wide, and deep), indicating that it had housed relatively large cerebellar hemispheres (see below).

Endocranial surfaces of the left parietal fragments preserve grooves for the parietal and frontal branches of the middle meningeal vessels (Fig. 20). It is evident that the vascular pattern of this vessel is complex, with a radiating array of branches, especially the frontal branches; Stw 53 resembles OH 24, KNM-ER 1813, KNM-ER 3733, and Sangiran in this respect (see Tobias, 1991). Good convolutional detail is preserved on the internal surface of the frontal bone, with impressions of the superior frontal, middle frontal, and inferior frontal (left only) gyri clearly indicated. They are separated by the superior and inferior frontal sulci, which are especially clear on the left side; they are humanlike in form, a morphology shared with OH 24, KNM-ER 1813, and KNM-ER 3733 (Falk, 1983). In *A. africanus*, they are more apelike (Falk, 1983; Tobias, 1991). The endocast is rounded towards the anterior pole of the frontal lobe. It is interesting to note that the endocast of Arago XXI, although larger, has a frontal lobe that is similar in morphology to Stw 53. The regions overlying Broca's and Wernicke's areas are not preserved in Stw 53.

A right frontal petalia pattern is evident, suggesting the presence of cerebral asymmetry, seen in most human fossils. However, poor preservation of the endocranial surfaces of the occipital fragments makes it impossible to detect the presence of occipital petalia. The impression of the cerebellum of Stw 53 is large and rounded, and appears to sit forward of the cerebral occipital pole, as in OH 24, but differing from its more posterior location in *A. africanus* (Tobias, 1987).The cerebellar lobes are tucked under the occipital poles of the cerebrum in *A. boisei* and some *Australopithecus afarensis* specimens.

At this stage, we have not endeavored to arrive at an estimate of the endocranial capacity, but we hope to address this problem in the future, by way of the virtual imaging approach.

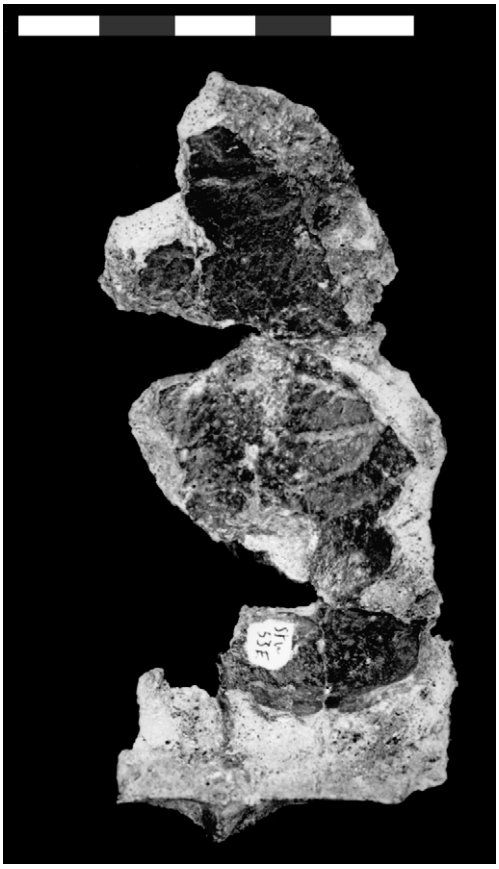

Fig. 20. Left parietal fragments (inferior aspect), highlighting impressions of cerebral vasculature.

Overall size and shape of the viscerocranium

In its overall size, the face of Stw 53 is most like that of specimens such as Sts 5 (Fig. 21) and KNM-ER 1813 (Fig. 22): it is short, with a reconstructed superior facial height (ca. 70 mm) just above the *H. habilis* median (Table 6). Howell (1978) and Bilsborough and Wood (1988) have used the typically short facial height of *H. habilis* to distinguish this taxon from other Pliocene and Plio-Pleistocene taxa, and we confirm its importance in distinguishing between these groups.

Facial breadth is estimated here for Stw 53 using three dimensions: (1) the transverse extent of the supraorbital torus (after Bilsborough and Wood, 1988), by measuring from the lateral margin of the supraorbital torus on the right side to the approximate position of glabella (midline) and doubling the value; (2) superior facial breadth, by measuring the distance from right frontotemporale to the midline and doubling the value; and (3) midfacial breadth, by reconstructing bimaxillary breadth, i.e., measuring from the right zygomaxillare to the median sagittal line, and doubling the value.

Transverse breadth of the supraorbital torus in Stw 53 (ca. 96 mm) is below the median values for *H. habilis* (by 7 mm; Table 6; also see Fig. 22) and Plio-Pleistocene African *H. sapiens* sensu lato (by 14 mm; Table 6), and similar to the value for SK 847 (below by 3 mm). It is, however, above the median for *A. africanus* (by 9 mm; Fig. 21). Superior facial breadth in

Fig. 21. Casts of Stw 53 (left) and Sts 5 (right) in anterior aspect.

Stw 53 (ca. 84 mm) is well below median values for all taxa (Table 6), but it lies within the range for *A. africanus* (Fig. 21). Estimated bimaxillary (midfacial) breadth is low in Stw 53 (ca. 92 mm), and again lies below average and median values for all taxa (Table 6). Kimbel and Rak (1993) noted that the superior facial breadth exceeds midfacial breadth in *H. habilis* sensu stricto, whereas in KNM-ER 1470 (*H. rudolfensis*) the opposite condition is found. Specimen Stw 53 has the same condition as that in KNM-ER 1470 (Fig. 23), and this condition is typical of *A. africanus* (Fig. 21) and Plio-Pleistocene African *H. sapiens* sensu lato (Table 6). In SK 847, superior facial breadth is also less than midfacial breadth (by 1 mm) (Table 6).

Rightmire (1993) described KNM-ER 1470 as possessing a "massive visceroskeleton," in contrast to smaller Olduvai and Koobi Fora early *Homo* crania. Specimen KNM-ER 1470 has a long (superior facial height, 90 mm) and broad (bimaxillary breadth, 113 mm) face; to examine its shape, we calculated Virchow's superior facial index. This index expresses superior facial height as a percentage of bimaxillary breadth (Table 6). The superior facial index value for KNM-ER 1470 (ca. 80%) shows that this fossil has a relatively long face (Fig. 23), being second only to SK 847 (ca. 82%) in its relative height. Specimen Stw 53 (ca. 76%) has a face of moderate length relative to its breadth, identical to the median values for *A. africanus* (Fig. 21) and *H. habilis* (Table 6; Fig. 22), and similar to KNM-ER 3733 (78%). Sangiran 17 has a relatively short face (66%).

Supraorbital torus

The supraorbital torus of Stw 53 is well defined but small in vertical height (4 mm), being the thinnest of Plio-Pleistocene toral specimens we examined (Table 6; Fig. 3). The supraorbital part in Stw 53 is divided into a superciliary arch and supraorbital trigone (Fig. 3), as is the case in OH 16 and OH 24. The location of its thickest part in Stw 53 is medial (nasal portion) and not over its center, the latter location being a distinguishing feature of crania such as OH 24 and KNM-ER 1813 (Kimbel and Rak, 1993).

A supratoral sulcus is present in Stw 53, but it is shallow and confined to the lateral part of the frontal bone (Fig. 3). Kimbel and Rak (1993) described the presence of a supratoral sulcus as a feature distinguishing crania such as OH 24 and KNM-ER 1813 (sulcus present) from KNM-ER 1470 (sulcus shallow and laterally constricted). There is, however, variation in

Fig. 22. Casts of Stw 53 (left) and KNM-ER 1813 (right) in anterior aspect.

Fig. 23. Casts of Stw 53 (left) and KNM-ER 1470 (casts) in anterior aspect.

opinion about the configuration of the supraorbital region in KNM-ER 1470 (e.g., Leakey, 1973; Wood, 1991; Rightmire, 1993; Kimbel and Rak, 1993). Although incomplete, the glabella of Stw 53 would have formed a broad, rounded, anterior projection extending between one supraorbital notch and the other (Fig. 8a). However, it is similar in its development to OH 24, and contrasts with KNM-ER 1470, which has a massive glabella.

Orbits

When Stw 53 is oriented in the Frankfurt Horizontal, the superior and inferior orbital margins lie in approximately the same coronal plane (Fig. 8d), as in KNM-ER 1813 (Fig. 17) and KNM-ER 1470. This contrasts with KNM-ER 3733 and *A. africanus* (Fig. 16), in which the superior orbital margin projects anteriorly, beyond the inferior orbital margin.

The inferomedial margin of the left orbit of Stw 53 is sharp. The orbits themselves, as reconstructed, are tall (Fig. 8e): estimated height taken on the right side is ca. 31 mm. The orbits of the specimen are narrow: breadth on the right side, between bone on the superomedial orbital wall and the inferiormost preserved part of the zygomatic process of the frontal, is ca. 27 mm. It is not possible to determine how close these estimates are to actual maximum values in this specimen. We believe out estimate of orbital height is likely to be a reasonable approximation (within 2 mm), while breadth is likely to be an underestimate (by at least 5 mm). This is in keeping with the summary statistics for various taxa (Table 6). Our height estimate is indistinguishable from median values for shorter faced taxa, such as *A. africanus* and *H. habilis*, while our orbital breadth estimate is well below the values for all groups, typically by about 6–8 mm.

Interorbital region

The interorbital part is narrow, resembling Sts 5 and KNM-ER 1813 in this regard (Figs. 16, 17). Nasion is set posterior to the plane of the orbits (anterior margin of the superior orbital rim to the anterior margin of the inferior orbital rim; Fig. 8d). In *A. africanus* and specimens belonging to *H. habilis*, nasion is within or posterior to this plane (see Figs. 16, 17), in contrast to the robust australopiths, where it is located anteriorly. This condition reflects greater transverse ‘‘bending’’ across this region in the former taxa (Tobias, 1991). Breadth of the interorbital part inferiorly has nearly equal contributions from the frontal processes of the maxilla and from the nasal bones. The frontal process of the maxilla remains narrow as it approaches the body of the maxilla (Figs. 1, 8e), as in OH 24, KNM-ER 1813 (Fig. 22), and KNM-ER 3733, but unlike in Sts 5 (Fig. 21), in which it widens rapidly. In Sts 5, this is related to the possession of lower orbital height and a much flatter inferomedial orbital rim.

Nasal part

The nasal height (nasion–nasospinale) of Stw 53 (ca. 56 mm) is high (Fig. 8e), being well above the average value for *A. africanus* and the median value for *H. habilis*, and within the range for Plio-Pleistocene *H. sapiens* sensu lato (Table 6). Its value is 1 mm below the estimate for KNM-ER 1470 (ca. 57 mm; Fig. 23). Piriform aperture breadth (nasal breadth; Table 6; Fig. 1) in Stw 53 (25 mm) is only 2 mm above the average value for *A. africanus* and 1 mm above the median for *H. habilis.* Piriform aperture breadth is one component of total midfacial breadth, and the narrowness of this feature reinforces the finding of a narrow face in Stw 53 (Fig. 8e). This specimen is well below the values for specimens with broader faces, such as KNM-ER 3733 (11 mm difference). The nasal index value (ca. 45%) is closest to the median value for *A. africanus* (Table 6), but well below the *H. habilis* median (Table 6). It is, however, similar to the value in KNM-ER 1470 (47%). The value in KNM-ER 1805 (54%) is indistinguishable from the *H. habilis* median, being well above the value in Stw 53. The index value in KNM-ER 3733 is well above that of Stw 53 (69%), but the estimated value in Sangiran 17 is only 4% greater than the southern African

specimen. There is considerable uncertainty surrounding some of these estimates, owing to missing bone in the interorbital region of Stw 53 (Fig. 8e).

The nasal bones are individually narrow and waisted (Fig. 1); this condition distinguishes *H. habilis* specimens, such as OH 24 and KNM-ER 1813 (Fig. 22), along with the Plio-Pleistocene *H. sapiens* sensu lato juvenile cranium D2700 (Vekua et al., 2002), from *A. africanus* (Fig. 21). The breadth of the paired nasal bones at their inferior extremity is provided in Table 6. In Stw 53, the nasal bones are narrow (8 mm) inferiorly (Fig. 1), being within the range of robust australopiths.

The reconstructed chord length of the nasal bones of Stw 53 (ca. 24 mm) is below the average for *A. africanus* (by 2 mm), and larger than the median values for *H. habilis* and Plio-Pleistocene *H. sapiens* sensu lato (Table 6). This feature serves to distinguish *A. africanus*, typically with long nasal bones, from early *Homo*, with its reduced nasal bone length. Missing bone in Stw 53 (Fig. 8e) makes our estimate of nasal bone length uncertain, and combined with our reconstruction of its length as being midway between the median values for *A. africanus* and median values for *H. habilis*/African Plio-Pleistocene *H. sapiens* sensu lato, the relevance of this feature to an assessment of the affinities of Stw 53 is uncertain. There is a midnasal elevation or bony ridge along the internasal suture in Stw 53 (Fig. 1), a feature seen also in MLD 6, Stw 13, Sts 52a (*A. africanus*), and OH 24 (*H. habilis*).

The height of the piriform aperture in Stw 53 (21 mm) is short (Fig. 1), being identical to that of OH 24, but well below the sample average for *A. africanus* and median for *H. habilis* (Table 6). The piriform apertures of KNM-ER 1805, SK 847, KNM-ER 3733, and Sangiran 17 are taller than Stw 53 (Table 6). The value for the breadth-height index of the piriform aperture in this specimen (119%) is virtually identical to that in KNM-ER 3733 (120%) and only 5% above the value in OH 24 (114%). While piriform aperture shape in D2700 is described as similar to that in KNM-ER 3733, Vekua et al. (2002) provided no data for comparison with Stw 53. The value in Stw 53 is well above the sample average for *A. africanus* and the median for *H. habilis* (Table 6) and the values in KNM-ER 1805 and Sangiran 17.

The margins of the piriform aperture of Stw 53 are thickened and possess an anterior pillar (Fig. 1) of the form found in OH 24 and D2700 (Vekua et al., 2002). Tobias (1991) has described this feature as found only along the lateral margin of the lower half of the piriform aperture, forming a canine buttress leading to the canine jugum in the Olduvai crania. Parenthetically, we correct here the previous observation of Curnoe (2001a), who stated that Stw 53 possessed "robust" anterior pillars; they are, in fact, slender. It is worth noting that this feature is variable in its development in *A. africanus* (e.g., comparing Sts 5 with Sts 52 and Sts 71).

An anterior nasal spine (*crista spinalis anterior*) sits within the nasal cavity of Stw 53 (Fig. 1). However, its true development is difficult to determine due to the loss of surface bone from much of the anterior parts of the maxilla, from the point of entry to the floor of the nasal cavity down to the alveoli of the medial incisors. Judging from the thickness of the bone in the surrounding region, it would have sat just anterior to the coronal plane through rhinion, the condition seen in *H. habilis*. It was also probably not as large as in OH 24, being apparently similar to that in OH 62 (Johanson et al., 1987), and certainly stronger than the spine of KNM-ER 3733.

Maxillary sinuses

The exposed maxillary sinuses of Stw 53 are large but not loculated. There is a large posterior chamber, with septal division from the smaller anterior chamber located at the level of P^4/M^1. This is similar to the morphology described in early *Homo* (Kimbel et al., 1997).

Infraorbital region

The malars of Stw 53 are short (Fig. 8e), as seen in *A. africanus* (see Fig. 21) and *H. habilis* [KNM-ER 1813 (Fig. 22), with the exception of KNM-ER 1470, in which they are long (Fig. 23)]. On its left side (Fig. 8e), the infraorbital plate in Stw 53 is flat medially (zygomatic process), while laterally, it slopes gradually posteriorly (zygomatic). In OH 24, the malars slope anteroinferiorly (Bilsborough and Wood, 1988); in KNM-ER 1470, the cheeks are flat. In *A. africanus*, the infraorbital plate is transversely flat or even concave (Kimbel and Rak, 1993). In Stw 53, the superior margin of the temporal process sits just above the level of the inferior orbital rim (Fig. 8d). This is the same configuration as seen in Sts 5 (Fig. 16) (Rak, 1983). In OH 24, SK 847, and KNM-ER 3733, the temporal process of the zygomatic bone is located about or below the level of the inferior orbital rim.

The vertical position of the infraorbital foramen has been used to distinguish *A. africanus* from *H. habilis* (Tobias, 1991). In Stw 53, Tobias (1991) estimated the orbito-foraminal height to be 8.3 mm, whereas, in our new reconstruction it is likely to be closer to 13 mm. This is identical to the median value for *A. africanus* and short of the value in OH 24 by ca. 2 mm. There are no other published estimates for early *Homo*, limiting comparison, and thus making the importance of this feature to systematics difficult to assess.

Zygomatic process

The root of the zygomatic process of the maxilla is comparatively thin anteroposteriorly: malar thickness is ca. 9 mm in Stw 53. This value is midway between the median values for *A. africanus* and *H. habilis*, below SK 847 (by 3 mm), and well below values in KNM-ER 3733 and Sangiran 17 (Table 6). Specimen Stw 53 possesses a small malar notch, as in OH 24 and KNM-ER 1813 (*H. habilis*), SK 847, Dmanisi, and Plio-Pleistocene Southeast Asian *H. sapiens* sensu lato. It also exhibits a small malar tubercle, a feature not seen in OH 24, KNM-ER 1813, or the juvenile D2700 (Vekua et al., 2002), but present in D2282 (Gabunia et al., 2000) and Plio-Pleistocene Southeast Asian *H. sapiens* sensu lato.

The anterior part of the root of the zygomatic process of the maxilla of Stw 53 leads down to P^4/M^1 (Fig. 8d). Kimbel and

Rak (1993) identified the position of the anterior limit of the zygomatic process as a feature distinguishing KNM-ER 1470 (*H. rudolfensis*) from OH 24 and KNM-ER 1813 (*H. habilis*). They described placement over P^4/M^1 or M^1 as the *H. habilis* condition, in contrast to placement above the premolars in *H. rudolfensis*. In a recent examination of this feature by Lockwood and Tobias (1999), the anterior limit of the zygomatic process was shown to vary considerably within Plio-Pleistocene groups. It lies above P^4 in KNM-ER 1470, KNM-ER 1813, and A.L. 666-1, and above P^4/M^1 in OH 24 and KNM-ER 1805. These workers also described the position in Stw 53 as above P^4/M^1. Thus, recent analyses of this feature contradict the findings of Kimbel and Rak (1993) and undermine the utility of this feature for taxonomic discrimination in early *Homo.*

Nasoalveolar clivus

The nasoalveolar clivus of Stw 53 is short, slightly convex in both the sagittal and transverse planes, and positioned in a different plane from that of the canine-P^3 eminences and the lateral margins of the piriform aperture (note: as stated above, the external table is missing here and this may lead to error in our observations). A convex nasoalveolar clivus is a feature that distinguishes the smaller Olduvai Gorge crania (including OH 62) and Koobi Fora remains from KNM-ER 1470 (Rightmire, 1993); Stw 53 resembles the former group in this respect. In *A. africanus*, the nasoalveolar clivus is of moderate length (on average), concave, and located on the same plane as the anterior pillars. Entry into the nasal cavity is smooth in Stw 53 (McCollum et al., 1993), a feature shared with robust australopiths.

The alveolar height (nasospinale–prosthion) of Stw 53 (ca. 25 mm) is similar to that in OH 24, and identical to the values in Sts 53, KNM-ER 1813, and Sangiran 17. It is just below the median values for *A. africanus* and *H. habilis* (Table 6).

On the right lateral face of the alveolar process, there is a mediolaterally shallow but anteroposteriorly long fossa above P^{3-4}, similar to that found in *A. africanus* crania. The anteroposterior continuity of this sulcus is interrupted by an eminence formed by the mesiobuccal root of P^4. A similar feature was described for D2700 (Vekua et al., 2002).

Facial projection

Specimen Stw 53 exhibits low midfacial projection, as evidenced by its flat nasal bones (viewed in lateral aspect) and consequent posteriorly positioned rhinion relative to the infraorbital plane (Fig. 8d). This is the condition in *H. habilis* (Fig. 17), and it contrasts with *A. africanus*, in which rhinion typically sits more anteriorly relative to the infraorbital plane and the nasal bones are generally more concave (Fig. 16; but note that this feature is variable—contrast Sts 5 with Sts 52a and Sts 71). In Plio-Pleistocene *H. sapiens* sensu lato (e.g., KNM-ER 3733), the midface projects to a considerable extent anteriorly, with the nasal bones showing marked curvature (concave) and rhinion being located well anterior to the infraorbital plate.

Specimen Stw 53 shows weak projection of the nasoalveolar clivus beyond the canine alveoli when viewed in lateral aspect (Fig. 8d), in contrast with many other Plio-Pleistocene crania, which display such projection, but similar to other early *Homo* specimens (especially Plio-Pleistocene *H. sapiens* sensu lato). This hints at its low level of prognathism.

The ratio of projected prosthion–nasospinale to the chord of prosthion–nasospinale was employed by Kimbel et al. (1997) to compare levels of prognathism in Plio-Pleistocene crania. These workers found that more prognathic crania, such as those belonging to *A. africanus*, have values ranging from 65–82% (Table 6: Proj./direct ratio). According to their data, OH 62, KNM-ER 1813, and A.L. 666-1 have values that overlap this range (63–69%), in contrast to the orthognathic KNM-ER 1470, SK 847, KNM-ER 3733, and Sangiran 4, whose values lie below this range (47–62%). The value for Stw 53 (ca. 52%) is well below the median values for *A. africanus* and *H. habilis*, virtually indistinguishable from SK 847, above KNM-ER 3733, but below Sangiran 4 (Table 6), indicating that Stw 53 has low prognathism.

The facial angle is the angle the nasion–prosthion line makes with the Frankfurt Horizontal. The closer this angle is to 90° the more orthognathic is the face. Estimated facial angle for Stw 53 (ca. 66°), using a goniometer, compares well with values using the same method (see Wood, 1991) for KNM-ER 1470 (est. 65°) and SK 847 (65°), but is well below values in KNM-ER 3733 and Sangiran 17 (Table 6). The value in Stw 53 is above the median value for *A. africanus* by 6°, but below the *H. habilis* median by 4° (Table 6). The second angular estimate of prognathism we employ is the alveolar profile angle (measured with a goniometer, after Wood, 1991). The value for Stw 53 (ca. 50°) is above the median value for *A. africanus* (Table 6) and identical to the median value for *H. habilis* (Table 6) and individual values for Sts 52a, OH 24, and KNM-ER 1470. It is below (by 5°) the value for SK 847 (Table 6) and well below values for KNM-ER 3733 and Sangiran 17 (Table 6). The third angle we employ to estimate projection is the nasal profile angle (estimated using a goniometer, after Wood, 1991). This angle in Stw 53 (ca. 75°) is slightly above (by 2°) the median value in *A. africanus* (Table 6), and identical to the median value for *H. habilis* (Table 6) and values for Sts 71 and OH 24. It is, however, well below values for KNM-ER 3733 and Sangiran 17 (Table 6).

To summarize, Stw 53 shows low midfacial (nasal) projection and low prognathism, which aligns it most closely with *H. habilis*: flat to moderately projecting midface and moderate to slight prognathism [as indicated by measurements used here; see also descriptions of facial projection for this taxon in Howell (1978) and Bilsborough and Wood (1988)]. We correct here an earlier description by one of us (Curnoe, 2001a), which stated that Stw 53 exhibits high prognathism. It is clear that Stw 53 differs from the pattern of facial projection observed in *A. africanus* (low to moderate midfacial projection and moderate to strong prognathism) and *H. sapiens* sensu

lato (moderate to strong midfacial projection and low prognathism).

Alveolar process and palate

Maxillo-alveolar length provides an estimate of the length of the alveolar process of the maxilla (prosthion–maxillary tuberosity). We have estimated this dimension from prosthion to a line projected to the median sagittal line from the posterior wall of the left maxillary tuberosity. Maxillo-alveolar length in Stw 53 (ca. 67 mm) is moderate, being identical to the value in Sangiran 17, and similar to SK 847 (65 mm). It is well below the *A. africanus* median (Table 7), above the *H. habilis* median, and above the value in KNM-ER 3733 (Table 7).

Due to a loss of bone in Stw 53, palatal length and breadth cannot be estimated using standard measurements. Interalveolar breadths show the palate of Stw 53 to be unusually narrow (Table 7). Canine interalveolar breadth in this specimen (24 mm) is below the averages for *A. africanus* (by 5 mm) and *H. habilis* (by 6 mm) (Table 7), and well below values for other Plio-Pleistocene specimens (Table 7). Interalveoar breadth at P^3 (26 mm) is narrow, being below the average values for *A. africanus* (by 3 mm) and *H. habilis* (by 8 mm) (Table 7), and within the range for the robust australopiths. Interalveoar breadth at P^4 (27 mm) is also narrow, being below the average value for *A. africanus* (by 3 mm), below the median for *H. habilis* (by 8 mm) (Table 7), and within the range of the robust australopiths. These values in Stw 53 are also well below values in KNM-ER 3733 and Sangiran 17 (P^3–P^3 only) (Table 7). They are, however, very similar to values in SK 847 (Table 7). In Stw 53, M^2 and M^3 interalveolar breadths have the lowest values among all Plio-Pleistocene crania examined. Interalveolar breadth at M^2 (ca. 25 mm) is very low, well below the average values for *A. africanus* (by 10 mm) and *H. habilis* (by 15 mm) (Table 7), and well below values in other Plio-Pleistocene specimens examined. Interalveolar breadth at M^3 (ca. 24 mm) is very low, well below the median value for *A. africanus* (by 15 mm) and the average for *H. habilis* (by 15 mm) (Table 7), and again outside of the range for other Plio-Pleistocene specimens. The congenital absence of M^3s in KNM-ER 3733 means that M^3 interalveolar breadth in this specimen is unreliable.

Palatal height shows Stw 53 to have a shallow palate (ca. 9 mm), being below the average value for *A. africanus* (by 5 mm), below the average for *H. habilis* (by 7 mm) (Table 7) and within the range for robust australopiths. The palate of KNM-ER 3733 is deep (Table 7), but in Sangiran 17 it is identical to the average value for *A. africanus* (Table 7). Specimen SK 847 also has a shallow palate, being below average values for *A. africanus* and *H. habilis* (Table 7).

The maxillary dental arcade of Stw 53 is characterized by progressive incurvation posteriorly, from P^4 to M^3, as judged from successive interalveolar distances (Table 7). In Figs. 24–26, palate shape expressed as successive interalveolar distances is depicted in Stw 53 and other Plio-Pleistocene specimens. Specimens Stw 53, OH 24, and KNM-ER 1813 (Fig. 24) have similar intercanine distances, but A.L. 666-1 contrasts with them in having greater intercanine distance. The greatest interalveolar breadth is located at the P^4s in Stw 53, M^2 in A.L. 666-1, and M^3 in OH 24 and KNM-ER 1813. However, Stw 53 and A.L. 666-1 share a medial placement of the M^3s (relative to their M^2s). Specimen SK 847 (Fig. 25) differs from Stw 53 in having greatest interalveolar breadth across M^2 (as seen in A.L. 666-1). However, it shares posterior incurvation with Stw 53 and A.L. 666-1. As Fig. 26 indicates, there is also considerable variation of palate shape in *A. africanus*. One specimen (Sts 53) has maximum interalveolar breadth at M^2 (like A.L. 666-1) and two specimens (Sts 5 and Sts 17) have maximum interalveolar breadth at M^3 (as in OH 24 and KNM-ER 1813). Thus, Stw 53, like A.L. 666-1 and SK 847, exhibits medial placement of the M^3s (relative to its M^2s), but is unusual in having maximum interalveolar breadth across its anterior cheek teeth.

Another way to compare palate shape is to calculate the percentage change from anterior to mid-palatal interalveolar distances (P^3/$\underline{C}$ and P^4/$\underline{C}$; Table 8), and mid- to posterior palatal interalveolar distances (M^3/P^3 and M^3/P^4; Table 8). In Stw 53, the P^3/$\underline{C}$ and P^4/$\underline{C}$ index values show moderate increase in breadth from anterior to mid-palate (+8% and +13%, respectively), but moderate decrease in breadth from the mid- to posterior palate (−8% and −11%, respectively). In contrast, *A. africanus* typically shows a small decrease in interalveolar breadth from canine to P^3 and a moderate average increase from canine to P^4 (Table 8). In *H. habilis*, interalveolar breadth shows a moderate average increase from canine to P^3 and typically a large increase from canine to P^4 interalveolar breadth (Table 8). The small sample for Plio-Pleistocene *H. sapiens* sensu lato shows that this group is characterized by a moderate increase in interalveolar breadth from canine to P^3 and a moderate average increase from canine to P^4 (Table 8). Thus, Stw 53 is most like specimens belonging to Plio-Pleistocene *H. sapiens* sensu lato. Specimen SK 847 shows small (increase) or no change from anterior to mid-palatal breadths (Table 8).

The contrast in mid- versus posterior palatal (interalveolar) breadths between *A. africanus*, *H. habilis*, and SK 847, on the one hand, and Stw 53 and Plio-Pleistocene *H. sapiens* sensu lato (particularly Sangiran 17), on the other, is striking: the former typically exhibit moderate to large increase in interalveolar breadth from P^3 to M^3 and P^4 to M^3, while the latter are characterized by moderate to large decreases in interalveolar breadth from P^3 to M^3 and P^4 to M^3 (Table 8). Thus, Stw 53 most closely resembles Plio-Pleistocene *H. sapiens* sensu lato in possessing a palate that shows moderate increase in breadth from anterior to mid-palate and decrease in breadth from mid- to posterior palate. Interestingly, the A.L. 666-1 early *Homo* specimen shares with *A. africanus*, *H. habilis*, and SK 847 a moderate M^3/P^3 breadth increase, but with Stw 53 and Sangiran 17, M^3/P^3 breadth decrease.

Mandibular ramus

The mandibular ramus of Stw 53 is shown in Fig. 7. On its lateral surface, the insertion area for the masseter muscle is visible. On the medial surface, an endocoronoid crest forms

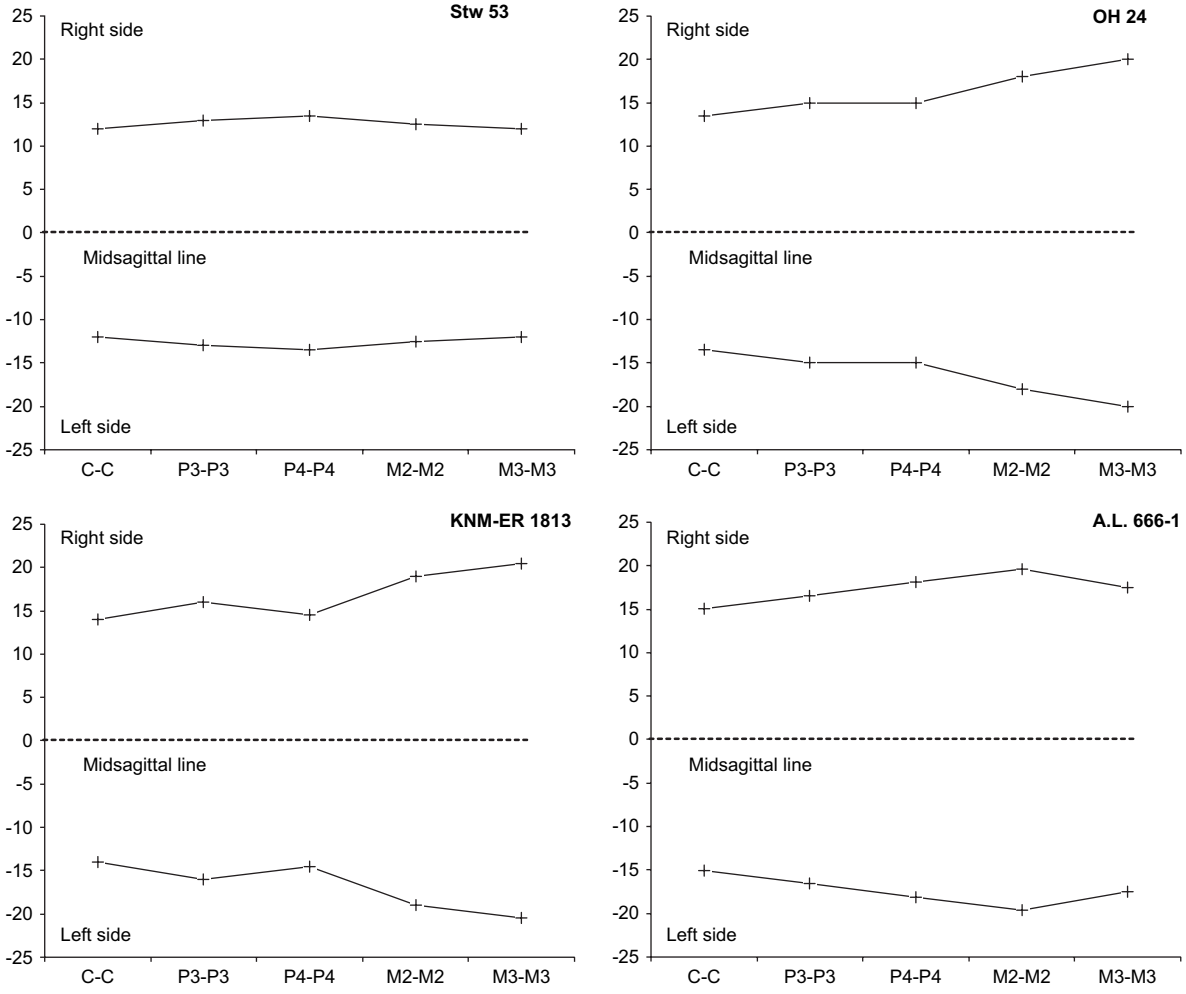

Fig. 24. Palate shape illustrated with interalveolar distances, comparing Stw 53 with *H. habilis* specimens.

a ridge running anteriorly at an angle of about 45° to the anterior margin of the ramus. The endocoronoid crest meets with the smaller, less prominent, endocondyloid ridge running to the anterior part of the condylar process. After merging, a strong and sharp ridge—the *torus triangularis rami* of Weidenreich (1936)—travels inferiorly along the ramus as far as the line of breakage. The posterior part of the ramus is broken away immediately anterior to the mandibular foramen. The anterior wall of the mandibular foramen is preserved above.

What remains of the ramus suggests that it was broad, being similar in size to that of Sts 52b. An interesting feature of the mandibular ramus of Stw 53 is the small angle between the endocoronoid and endocondyloid crests, a feature shared with OH 13 (*H. habilis*) and some *A. africanus* specimens (Tobias, 1991).

Dentition

The presence of erupted maxillary and mandibular M3s with moderate occlusal wear demonstrates the adult status of Stw 53. From the standards developed by Hurme (1948, 1949, 1957), Tobias (1991) determined that the M^3s erupt between the ages of 16.5 and 27 years in 95% of modern human populations. A recent study of eruption patterns in wild chimpanzees (Zihlman et al., 2004) provided an estimate of 12.4 years, with a minimum 10.8 years and a maximum 14.2 years. The amount of tooth wear on the M^3s of Stw 53 suggests that this individual was of relatively advanced age, regardless of which taxon is used as a standard against which to assess its adult status.

A helicoidal occlusal plane (Ackermann, 1941) is strongly expressed in Stw 53 (Tobias, 1978). The position of the "helicoid pitch," or zone of transition between mesial (ad palatum) and distal (ad vestibulum) occlusal relationship, in Stw 53 lies in the distal quarter of the M^2 or even between M^2 and M^3. The pattern of tooth wear is asymmetrical in Stw 53, with the left P^3, P^4, M^2, and M^3 showing more occlusal wear than their antimeres. This pattern was also found on OH 16, which resulted from pathology on the right M^2 (Tobias, 1991). In Stw 53, no pathology is discernible, suggesting that a crossbite of developmental origin may have been responsible for the asymmetry.

Anterior dentition

The mesiodistal (MD) and labiolingual (LL) diameters for the anterior alveoli of Stw 53 are provided in Table 9. It is not

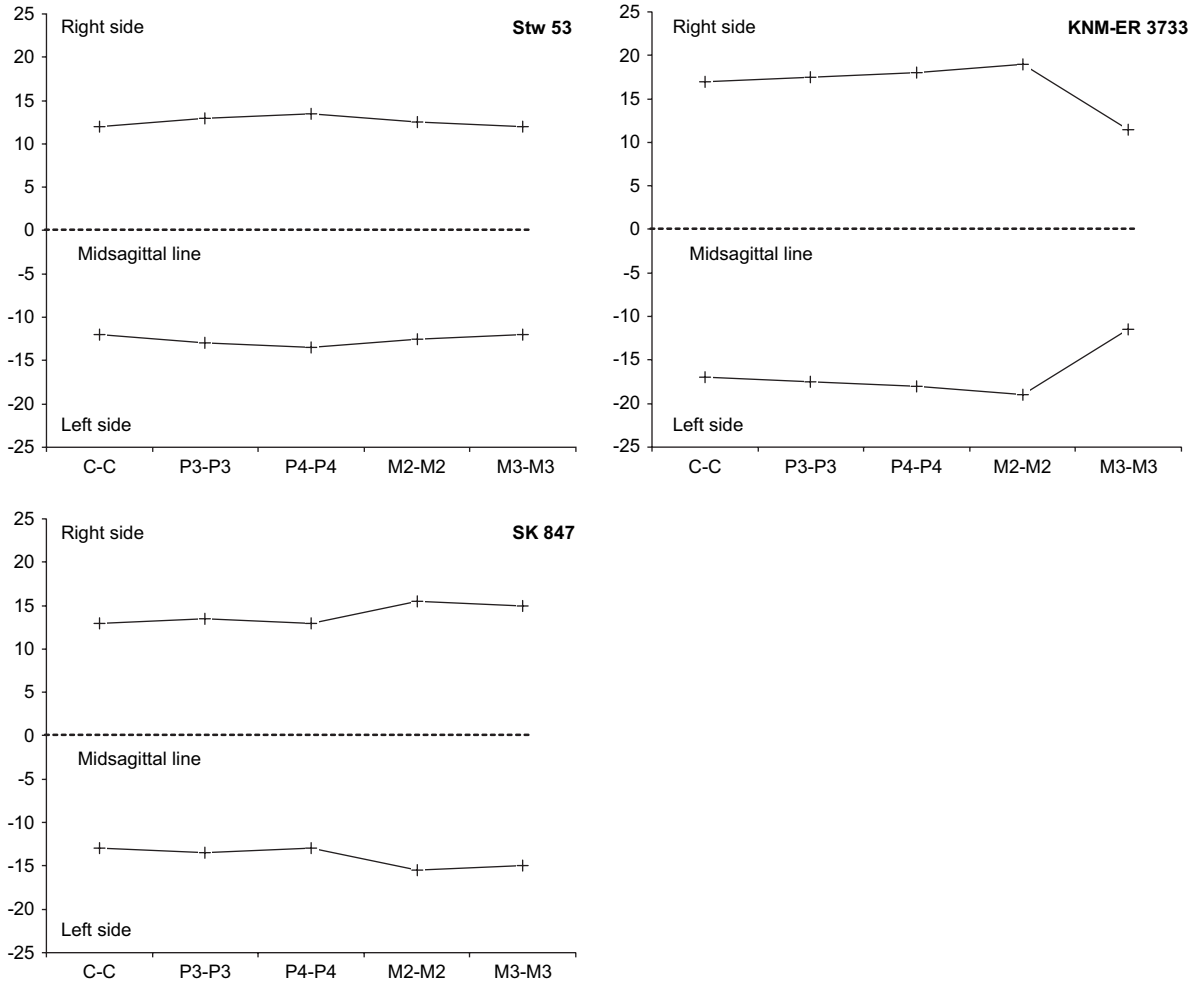

Fig. 25. Palate shape illustrated with interalveolar distances, comparing Stw 53 with KNM-ER 3733 (*H. sapiens* sensu lato) and SK 847.

possible to use I^1 or I^2 alveolus dimensions to reliably estimate the dimensions of their tooth crowns. In contrast, canine alveoli have been shown to provide good approximations of crown size in some Plio-Pleistocene groups (Tobias, 1991). In Table 10, we provide summary statistics for canine crown size (MD, LL, crown area, and crown module) and crown shape (MD/LL) for *A. africanus*, *H. habilis*, and Plio-Pleistocene *H. sapiens* sensu lato for comparison with our estimates in Stw 53. We restrict our comparison to these taxa, because Stw 53 has not been suggested to sample another group.

Canine alveolus MD diameter in Stw 53 (8.8 mm) is small compared to average and median values for all comparative samples, while the LL alveolus diameter (ca. 10.3 mm) is large compared to the sample averages for *A. africanus* and *H. habilis*, but smaller than the sample median for Plio-Pleistocene *H. sapiens* sensu lato (Table 10). Estimated canine alveolus area (ca. 90.6 mm^2) and crown module (ca. 9.6 mm) in Stw 53 are almost indistinguishable from the sample average for *A. africanus*, but well below the average for *H. habilis* and the median value for Plio-Pleistocene *H. sapiens* sensu lato (Table 10). The reconstructed canine crown shape index value (85%) is well below the average for *A. africanus*, outside of the range for *H. habilis*, but slightly (3.8%) above the median for Plio-Pleistocene *H. sapiens* sensu lato (Table 10).

Premolars

In Table 11, we provide MD, buccolingual (BL), crown area, crown module, and shape (MD/BL) index values for the P^3s and P^4s of Stw 53. In Table 12, we provide summary statistics of these crown dimensions and crown shape index values for *A. africanus*, *H. habilis*, and Plio-Pleistocene *H. sapiens* sensu lato. For the purposes of comparison, we use only corrected values for Stw 53 [premolars and molars (below)]; where both teeth are present in this specimen and individuals in comparative samples, we use the average values for left and right [again, premolars and molars (below)].

In Stw 53, P^3 MD (ca. 9.6 mm) and BL (ca. 12.2 mm) diameters are virtually indistinguishable from sample averages for *A. africanus* and *H. habilis*, but well above the average for Plio-Pleistocene *H. sapiens* sensu lato (Table 12). The P^3 crown area (ca. 116.7 mm^2) is close to the average for *A. africanus*, below the average but well within the range for *H. habilis*, and outside of the range for Plio-Pleistocene *H. sapiens* sensu lato (Table 12). For crown module (10.88 mm), Stw 53

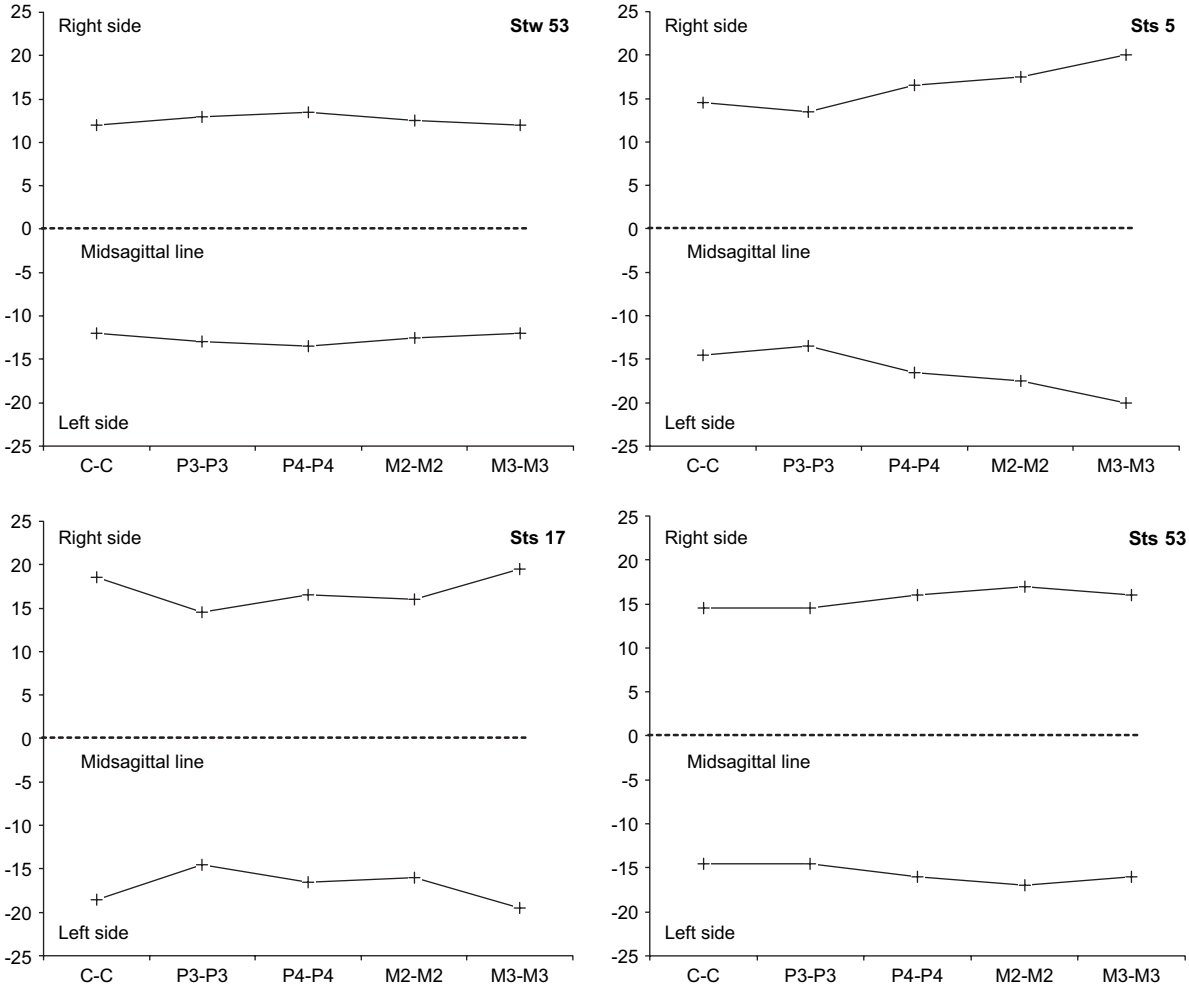

Fig. 26. Palate shape illustrated with interalveolar distances, comparing Stw 53 with *A. africanus* specimens.

is very close to the average values for *A. africanus* and *H. habilis* but outside the range for Plio-Pleistocene *H. sapiens* sensu lato (Table 12). Its P^3 crown shape index value (ca. 77.9%) is high, showing marked MD elongation in this tooth. This value is above sample averages but within the ranges for *A. africanus*, *H. habilis*, and Plio-Pleistocene *H. sapiens* sensu lato (Table 12)—each of these taxa have very similar average crown shape index values (differing by only 1–2%).

Table 10
Summary statistics of maxillary canine crown dimensions and shape index values for comparative taxa

Measurements and indices[a]	*A. africanus*			*H. habilis*			*H. sapiens* sensu lato		
	n	Avg.[b]	Range	n	Avg.[b]	Range	n	Med.	Range
MD	7	9.5 ± 0.4	1.1	8	9.9 ± 0.8	3.0	3	9.5	0.5
LL	6	9.6 ± 0.5	1.3	7	10.2 ± 1.4	4.0	3	11.7	2.7
Crown area (mm^2)	6	91.2 ± 8.1	17.2	7	102.9 ± 23.2	70.9	3	111.2	30.3
Module	6	9.5 ± 0.4	0.9	7	10.1 ± 1.1	3.5	3	10.6	1.6
Shape index (%)	6	96.6 ± 9.0	27.1	7	97.7 ± 6.2	15.7	3	81.2	18.0

[a] All data in mm unless indicated.
[b] ± standard deviations of sample averages.

The P^4 MD diameter in Stw 53 (ca. 10.6 mm) is large, outside of the ranges for *A. africanus* and Plio-Pleistocene *H. sapiens* sensu lato, and well above the average but within the range for *H. habilis* (Table 12). Its BL diameter (ca. 12.5 mm) is close to the average for *H. habilis*, below the average and within the range for *A. africanus*, but outside of the range for Plio-Pleistocene *H. sapiens* sensu lato (Table 12). The P^4 crown area (ca. 127.5 mm^2) and crown module (11.48 mm) are closest to the average value for *A. africanus*, within the ranges for *H. habilis*, but outside of the ranges for Plio-Pleistocene *H. sapiens* sensu lato (Table 12). Its P^4 crown shape index value (ca. 83.6%) is high, showing marked MD elongation in this tooth. This value is outside of the range for all comparative taxa, being just above the maximum value for *H. habilis* (Table 12).

In Table 13, we present values for indices that relate tooth crown sizes progressively within the maxillary arcade for Stw 53 and summary statistics for these index values in comparative taxa. The P^3 module of Stw 53 is 113.9% of the size of its $\underline{C}$ module, virtually identical to the median for a small sample of *A. africanus* specimens (Table 13), but also within the range for *H. habilis* (Table 13). The P^4 module of Stw 53 is 120.2% of the size of its $\underline{C}$ module, which is well above the value for a single

Table 11
Crown dimensions and shape index values for the dentition of Stw 53[a]

Tooth	Side	Mesiodistal diameter (mm)	Buccolingual diameter (mm)	Crown area (mm^2)	Crown module (mm)	Crown shape index[d] (%)
P^3	L	7.8 [ca. 9.3][b]	[ca. 11.6]	ca. 107.88	ca. 10.45	ca. 80.2
	R	8.3 [ca. 9.8]	[ca. 12.8]	ca. 125.44	ca. 11.30	ca. 75.6
P^4	L	9.5 (ca. 10.7)[c]	[ca. 12.5]	ca. 133.75	ca. 11.60	ca. 85.6
	R	8.8 (ca. 10.2)	[ca. 12.5]	ca. 127.50	11.35	ca. 81.6
M^1	R	—	—	—	—	—
M^2	L	—	ca. 15.2[f]	—	—	—
	R	13.5 (ca. 14.3)	ca. 15.3[f]	ca. 218.79	ca. 14.80	ca. 94.6
M^3	L	14.1 (ca. 15.6)[e]	16.9[f]	ca. 263.64	ca. 16.25	ca. 92.3
	R	14.3 (ca. 16.1)	16.4[f]	ca. 264.04	ca. 16.25	ca. 98.2
M_3	L	14.5	14.8	214.60	14.65	98.0

[a] To avoid systematic error from rounding second decimal place, even digit down, odd digit up.
[b] Values in brackets reconstructed from incomplete crowns; estimates of crown area, crown module, and crown shape index use mesiodistal dimensions corrected for interproximal wear.
[c] Values in parentheses corrected for interproximal wear.
[d] Index is mesiodistal diameter/buccolingual diameter * 100.
[e] Amount of enamel lost on distal margin of crown estimated from RM^3.
[f] Maximum diameter measured on mesial half of crown.

A. africanus specimen (Sts 52), and outside of the ranges for *H. habilis* and Plio-Pleistocene *H. sapiens* sensu lato (Table 13).

The P^4 MD of Stw 53 is about 110.4% of the size of its P^3 MD, a value that is outside of the range for *H. habilis* (Table 13), but within the ranges for *A. africanus* and Plio-Pleistocene *H. sapiens* sensu lato (Table 13). The P^4 BL of Stw 53 is about 102.5% of its P^3 BL, a value that is outside of the ranges for all three taxa (Table 13). The P^4 module of Stw 53 is about

Table 12
Summary statistics for crown dimensions and shape index values for the cheek teeth of comparative taxa

Measurements and indices[a]	*A. africanus*			*H. habilis*			*H. sapiens* sensu lato		
	n	Avg.[b]	Range	n	Avg./med.[b]	Range	n	Avg./med.[b]	Range
P^3									
MD	11	9.3 ± 0.2	0.7	10	9.5 ± 0.8	2.8	5	8.1 ± 0.7	2.0
BL	11	12.4 ± 0.8	3.2	10	12.7 ± 1.7	5.9	5	11.3 ± 1.1	2.7
Crown area (mm^2)	11	114.8 ± 9.4	35.0	10	121.8 ± 26.3	90.1	5	92.4 ± 16.3	38.9
Module	11	10.8 ± 0.5	1.8	10	11.1 ± 1.2	4.0	5	9.7 ± 0.9	2.1
Shape index (%)	11	75.9 ± 4.9	16.9	10	74.8 ± 5.6	17.5	5	73.9 ± 5.1	14.0
P^4									
MD	8	9.8 ± 0.6	1.7	8	9.4 ± 0.8	2.2	6	8.0 ± 0.3	0.9
BL	8	13.2 ± 0.7	1.6	8	12.2 ± 0.9	2.9	6	11.0 ± 0.9	2.3
Crown area (mm^2)	8	130.3 ± 12.0	35.7	8	115.0 ± 17.6	53.5	6	87.6 ± 9.4	22.5
Module	8	11.5 ± 0.5	1.5	8	10.8 ± 0.8	2.5	6	9.5 ± 0.5	1.3
Shape index (%)	8	74.3 ± 4.4	13.3	8	76.6 ± 4.4	12.4	6	73.2 ± 5.4	12.2
M^2									
MD	12	14.0 ± 0.9	2.9	8	13.1 ± 1.0	3.1	7	12.6 ± 0.8	2.4
BL	12	15.5 ± 1.0	3.0	9	14.9 ± 1.4	4.1	7	13.2 ± 1.3	3.4
Crown area (mm^2)	12	217.5 ± 27.8	86.9	8	194.1 ± 33.2	100.5	7	165.9 ± 21.6	66.1
Module	12	14.7 ± 0.9	2.9	8	13.2 ± 1.2	3.6	7	12.9 ± 0.8	2.5
Shape index (%)	12	88.6 ± 4.5	15.0	8	87.4 ± 4.7	12.9	7	95.2 ± 11.2	26.2
M^3									
MD	12	13.8 ± 1.3	4.2	6	12.5 ± 1.1	3.1	4	10.4	1.9
BL	12	15.6 ± 1.3	4.3	7	14.9 ± 1.3	3.3	4	13.6	2.8
Crown area (mm^2)	12	216.8 ± 37.8	113.4	6	185.4 ± 34.2	81.2	4	136.1	46.9
Module	12	14.7 ± 1.2	3.7	7	13.6 ± 1.2	2.9	4	11.8	1.9
Shape index (%)	12	89.0 ± 6.1	20.2	7	84.9 ± 4.3	11.2	4	74.6	12.3
M_3									
MD	11	15.7 ± 1.2	4.0	4	15.4	1.3	7	13.9 ± 0.9	2.8
BL	11	14.1 ± 0.6	2.1	5	13.5 ± 1.0	2.4	7	12.1 ± 0.7	1.9
Crown area (mm^2)	9	222.1 ± 26.9	82.8	4	201.7	49.5	7	169.6 ± 19.6	59.4
Module	9	14.7 ± 0.9	2.9	4	14.3	1.7	7	13.0 ± 0.8	2.4
Shape index (%)	9	112.3 ± 5.8	18.2	4	117.6	8.5	7	114.8 ± 4.5	10.5

[a] All data in mm unless indicated.
[b] ±standard deviations of sample averages; if $n < 5$, median is given; if $n \geq 5$, average is shown.

Table 13
Relative size of maxillary tooth crowns in Stw 53 and summary statistics for relative size of maxillary tooth crowns for comparative taxa (%)

Indices	Stw 53	*A. africanus*			*H. habilis*			*H. sapiens* sensu lato		
		n	Avg./Med.[a]	Range	n	Avg.[a]	Range	n	Med.	Range
$P^3/\underline{C}$ module index	113.9	2	113.7	6.8	5	109.4 ± 6.9	16.3	1	98.4	—
$P^4/\underline{C}$ module index	120.2	1	110.3	—	6	108.8 ± 6.2	15.1	2	97.8	3.4
P^4/P^3 MD	110.4	5	104.2 ± 5.9	13.0	8	100.0 ± 2.7	7.8	3	129.0	47.0
P^4/P^3 BL	102.5	5	106.0 ± 2.5	6.3	8	100.6 ± 1.7	4.4	3	100.0	52.5
P^4/P^3 module	105.5	5	105.2 ± 3.0	6.8	8	100.7 ± 2.1	6.6	3	99.5	25.0
M^2/P^4 MD	134.9	3	144.3	8.6	8	142.3 ± 5.4	15.7	4	154.3	50.2
M^2/P^4 BL	122.4	3	115.0	16.6	8	119.7 ± 14.0	44.9	4	120.3	79.9
M^2/P^4 module	128.9	3	127.7	13.6	8	129.1 ± 5.1	16.8	4	135.7	14.0
M^3/M^2 MD	111.2	5	95.0 ± 8.7	23.1	5	94.1 ± 5.0	12.6	2	80.2	7.5
M^3/M^2 BL	109.1	5	99.8 ± 4.3	10.9	5	99.0 ± 3.0	7.0	2	110.6	18.2
M^3/M^2 module	109.8	5	97.4 ± 5.7	14.0	5	96.0 ± 2.6	7.2	2	89.2	11.6

[a] If $n < 5$, median is given; if $n \geq 5$, average is shown; ± standard deviations of sample averages.

105.5% of the size of its P^3 module; this value lies outside of the range for *H. habilis*, but is within the ranges for *A. africanus* and Plio-Pleistocene *H. sapiens* sensu lato (Table 13).

An interesting feature of the premolars of Stw 53 is the number and complexity of their roots. Both P^3s and P^4s possess three roots each, two buccal and one lingual. The P^3 root number falls within the range of variation of root form seen in most Plio-Pleistocene groups. However, P^4 root number distinguishes Stw 53 from *A. africanus*, which seems to possess only two-rooted P^4s, and aligns it with SK 847 (Robinson, 1953) and *H. habilis*.

Molars

In Table 11, we provide MD, BL, crown area, crown module, and crown shape (MB/BL) index values for the M^2s and M^3s of Stw 53. In Table 12, we provide summary statistics of size dimensions, crown module, and crown shape index values for these teeth in *A. africanus*, *H. habilis*, and Plio-Pleistocene *H. sapiens* sensu lato.

The M^2 MD (ca. 14.3 mm) and BL (ca. 15.3 mm) diameters, crown area (ca. 218.8 mm^2), and crown module (ca. 14.8 mm) values are closest to the sample averages for *A. africanus* and are also within the range for *H. habilis* (the BL value is also within the range for Plio-Pleistocene *H. sapiens* sensu lato) (Table 12). The M^2 crown shape index value (ca. 94.6%) is high, being almost indistinguishable from the average for Plio-Pleistocene *H. sapiens* sensu lato (Table 12).

As shown in Table 13, the M^2 MD of Stw 53 is about 134.9% of the size of its P^4 MD. This value is well below sample averages/medians for all taxa and only within the range for *H. habilis*. The M^2 BL of Stw 53 is about 122.4% of the size of its P^4 BL, being closest to the sample median for Plio-Pleistocene *H. sapiens* sensu lato, but within the ranges for all three taxa (Table 13). The M^2 module of Stw 53 is about 128.9% of the size of its P^4 module, virtually indistinguishable from the average value for *H. habilis*, and within the ranges for *A. africanus* and Plio-Pleistocene *H. sapiens* sensu lato (Table 13).

In Stw 53, M^3 MD diameter (ca. 15.9 mm) is large and only within the range for *A. africanus* (Table 12). The Stw 53 crown dimension is identical to the median for Swartkrans robust australopiths (Grine, 1993: 110). In BL diameter (ca. 16.7 mm), Stw 53 is large and lies within the ranges for *A. africanus* and *H. habilis* (Table 12). This crown dimension in Stw 53 is virtually indistinguishable from the average for Swartkrans robust australopiths (less by 0.1 mm) (Grine, 1993: 110). The M^3 crown area (ca. 263.8 mm^2), crown module (16.25 mm), and crown shape index value (ca. 95.3%) for Stw 53 lie only within the ranges for *A. africanus* (Table 12).

Examining indices that relate tooth crown sizes progressively within the maxillary arcade (Table 13) shows that the M^3 MD of Stw 53 is 111.2% of the size of its M^2 MD. This is outside of the ranges for comparative taxa. The M^3 BL of Stw 53 is 109.1% of the size of its M^2 BL, a value that is virtually indistiguishable from the median for Plio-Pleistocene *H. sapiens* sensu lato and outside of the ranges for other taxa (Table 13). The M^3 module of Stw 53 is about 109.8% of the size of its M^2 module, outside of the ranges for comparative taxa (Table 13). Thus, the M^3 of Stw 53 is larger than M^2 for all size estimates, and in this respect, it most closely resembles the typical condition seen in *A. robustus* (Table 17; see also Curnoe, 2002). The M^3 of *A. africanus* is on average slightly smaller than M^2 (Tables 12, 13).

Maxillary tooth material

In Fig. 27, we compare maxillary "tooth material" for Stw 53 with Plio-Pleistocene taxa as summed premolar crown areas (Fig. 27a), summed molar (M^{2-3}) crown areas (Fig. 27b), and summed premolar and M^2 crown areas (Fig. 27c). The summed premolar crown area for Stw 53 is virtually indistinguishable from the median values for *A. africanus* and *H. habilis* (Fig. 27a), but outside of the range for Plio-Pleistocene *H. sapiens* sensu lato and *A. robustus*. The summed molar crown area for Stw 53 (Fig. 27b) is large and outside of the range for *H. habilis* and Plio-Pleistocene *H. sapiens* sensu lato, much larger than the single *A. africanus* specimen for which data are available, but within the range for *A. robustus*. Finally, summed premolar and M^2 crown area in Stw 53 (Fig. 27c) is virtually indistinguishable from the median value for *A. africanus*, within the broad range for *H. habilis*, but outside of the ranges for Plio-Pleistocene *H. sapiens* sensu lato and *A.*

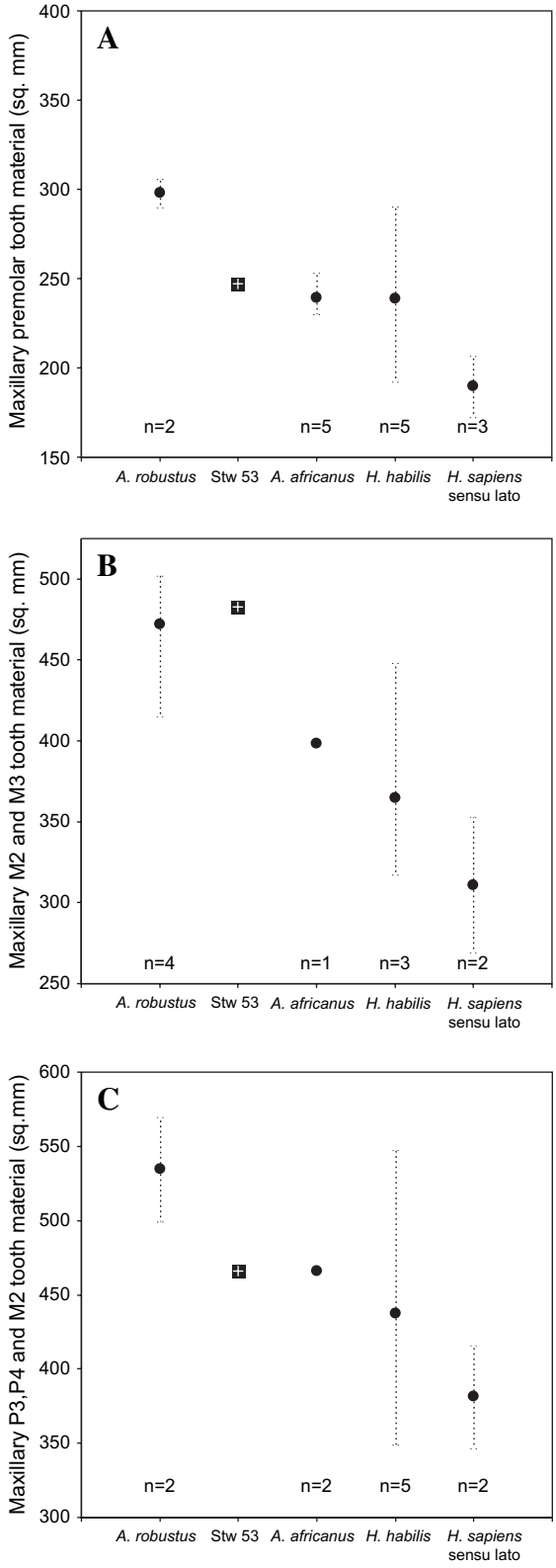

Fig. 27. Average/median and range of maxillary tooth material for: (a) summed P^3 and P^4 cross-sectional crown areas; (b) summed M^2 and M^3 cross-sectional crown areas; and (c) summed P^3, P^4, and M^2 cross-sectional crown areas. Average shown for samples in which $n \geq 5$; median given for sample sizes of $n < 5$.

robustus. Thus, in terms of its total (summed) premolar crown size, Stw 53 is indistinguishable from *A. africanus* and *H. habilis*. However, in terms of the tooth material for its cheek teeth (P^3, P^4, and M^2), Stw 53 is most like *A. africanus*.

Maxillary tooth roots

The M^1, M^2s, and M^3s of Stw 53 possess a distinctive root system in which each is furnished with two buccal roots and a robust lingual root. However, the roots are manifestly double for all molars and are partially bifid at their apices. The duality of each of the three roots is more pronounced in M^2 than in M^1, as is the degree of separation of each pair of the two root components. The gradation of development of root doubling of the mesiobuccal root is continued to the M^3, where it is most pronounced in the marked distal recurvation of its lingual moiety.

Mandibular molar

In Table 11, we provide MD, BL, crown area, crown module, and crown shape (MB/BL) index values for the M_3 of Stw 53. In Table 12, we provide summary statistics of size dimensions, crown module, and crown shape index values for these teeth in *A. africanus*, *H. habilis*, and Plio-Pleistocene *H. sapiens* sensu lato. The M_3 MD diameter in Stw 53 (ca. 14.5 mm) is within the ranges for *A. africanus* and Plio-Pleistocene *H. sapiens* sensu lato (Table 12). However, the BL diameter in this specimen (ca. 14.8 mm) is large and outside of the ranges for all of the comparative taxa (Table 12). The M_3 crown area (ca. 214.6 mm^2) is most similar to the average value for *A. africanus*, and lies also within the range for Plio-Pleistocene *H. sapiens* sensu lato (Table 12). Crown module (14.7 mm) is identical to the average for *A. africanus* and within the range for *H. habilis* (Table 12). The M_3 crown shape index value in Stw 53 is unusually low (98%), emphasizing its very short MD dimension, and outside of the ranges for all comparative taxa (Table 12).

Classification of Stw 53

Generic classification

The first question to consider about the classification of Stw 53 is its generic status. Following reconstruction, the description and comparison of Stw 53 to other Pliocene and Plio-Pleistocene specimens suggests that this fossil shares several features with *Homo* [as conventionally defined (Leakey et al., 1964; Tobias, 1991); but see Curnoe and Thorne (2003)]. However, the accurate identification of some of these features is not possible because of missing bone or postburial distortion in this specimen. Therefore, in considering the classification of Stw 53, we confine our remarks to morphological features that are well preserved, or reliably reconstructed, in this cranium. The following features support its assignment to *Homo*:

- **Neurocranium**: parieto-occipital region nearly subangular; moderately sloped occipital plane; mandibular fossa

shallow compared to its length, lacking an anteromedial recess, and with a steep preglenoid plane relative to the anterior wall of the mandibular fossa (variable in *H. habilis*); well developed styloid process; coronal orientation of petrous pyramids; vascular pattern and impressions of gyri and sulci humanlike; low petromedian angle; cerebellum inferred to be positioned anterior to the occipital pole.

- **Viscerocranium**: the frontal process of the maxilla remains narrow as it approaches the body; nasal bones individually narrow and waisted (variable in Plio-Pleistocene *H. sapiens* sensu lato); a malar notch; nasoalveolar clivus short and convex in both sagittal and transverse planes, positioned on a different plane to canine and P^3 eminences and the lateral margin of the piriform aperture (features variable in *H. habilis*); reduced prognathism; reduced maxillo-alveolar length; relatively broad anterior palate, but relatively narrow posterior palate, with M^3s postioned medially (variable in *H. habilis*); large posterior chamber of the maxillary sinus floor.

Some features described in Stw 53 are shared apparently exclusively with species of *Australopithecus*. Of the better preserved:

- **Neurocranium**: occipital squama (upper scale) is short; absence of medial recess.
- **Viscerocranium**: superior margin of temporal process sits above the level of inferior orbital rim; temporal lines encroach on the lateral half of the supraorbital rim; entry of nasoalveolar clivus into nasal cavity smooth; nasal bones inferiorly very narrow.
- **Dentition**: Small canine crown; P^4 crown enlarged relative to P^3 crown; molar crowns enlarged; M^3 crown larger than M^2 crown.

The first feature of the viscerocranium, which desribes the vertical position of the temporal process of the zygomatic relative to orbitale, is shared with *A. afarensis*, *A. africanus*, *A. robustus*, and *A. boisei* (in which we include KNM-WT 17000; see Curnoe, 2001b). The second feature, absence of medial recess, is characteristic of *A. africanus*, however, it is replaced in this species with the anteromedial recess, a feature lacking in Stw 53. The third feature, temporal lines that encroach on the lateral half of the supraorbital rim, is usually associated with *A. africanus* and is variable in expression within this taxon. However, it is found also in SK 847, a specimen usually assigned to *Homo* (see discussion below and Clarke et al., 1970; Howell, 1978; Tobias, 1991). The fourth feature, smooth entry into the nasal cavity, is a derived feature of robust australopiths and is absent in *A. afarensis* and *A. africanus*. Like *A. africanus*, but unlike *H. habilis* and Plio-Pleistocene *H. sapiens* sensu lato, the canine crown is small (but note that other purported early *Homo* from Sterkfontein Member 5 also show canine crown reduction; see below). As in *A. africanus*, the P^4 crowns (modules) of Stw 53 are enlarged relative to P^3 crowns (they are typically of equivalent size in *H. habilis* and Plio-Pleistocene *H. sapiens* sensu lato). Diagnostic of *Australopithecus* is the possession of larger molar tooth crowns compared with *Homo*. In Stw 53, the maxillary molar crown areas and M_3 area are large. The M^3 crowns are larger than the M^2 crowns in Stw 53, as is typically found in *A. robustus* (Curnoe, 2002).

In our judgement, the generic classification of Stw 53 is clearcut, and we reaffirm its assignment to *Homo* (Hughes and Tobias, 1977; Tobias, 1978, 1991; Clarke, 1985; Chamberlain, 1987; Grine et al., 1993, 1996; Kimbel et al., 1997; Curnoe, 1999, 2001a, 2002; Grine, 2001). While we recognize that there are similarities in molar crown size between Stw 53 and *A. africanus*, important differences exist between them, including tooth root numbers.

Species classification

Stw 53 shares a number of features with *H. habilis* that are diagnostic of this taxon:

- **Neurocranium**: rounded, domelike frontal squama; inion located below FH and opisthocranion; occipital squama short; slightly developed occipital torus; mandibular fossa shallow compared with its breadth; a prominent articular eminence, small postglenoid process; tympanic element that merges with the postglenoid process; well-developed petrous crest that merges with the anterior face of mastoid process; moderate mandibular fossa angle.
- **Viscerocranium**: relatively flat midface; absolutely narrow midface (piriform aperture breadth); superior and inferior orbital margins that lie in approximately the same plane; supraorbital torus in two parts; distinct anterior nasal spine located anterior to the coronal plane of rhinion.
- **Dentition**: P^4s triple-rooted.

There are four morphological features of Stw 53 that we have identified as shared with Plio-Pleistocene *H. sapiens* sensu lato to the exclusion of *H. habilis*, namely, long mastoid processes, presence of a malar tubercle, LL expansion of the maxillary canine crown (high crown shape index value), and M^2 crown enlongated mesiodistally. Sample sizes for Plio-Pleistocene *H. sapiens* sensu lato are small for some of these features, and thus we cannot reliably assess how typical they are of this group as a whole. Regardless, Stw 53 exhibits features not found in this taxon: absence of medial recess, possession of thin cranial vault bones, thin root of the zygomatic process and thin malars, short malars, a short face (absolute height) but moderate height relative to its breadth (superior facial index), a narrow midface, slender supraorbital torus, anterior pillars, absolutely short and narrow piriform aperture, low midfacial (nasal) projection, a shallow palate, small occipital condyle area, short occipital squama (upper scale), cheek tooth crown enlargement, and triple-rooted P^4s. We believe that the presence of these features in Stw 53 argues strongly against its assignment to *H. sapiens* sensu lato. Thus, Stw 53 exhibits a close

phenetic relationship with fossils in the *H. habilis* hypodigm, as well as possessing unique features of this taxon. On this basis, we believe Stw 53 is best accommodated within *H. habilis* (see also Tobias, 1991; Kimbel et al., 1997).

Sterkfontein Member 5 dental specimens

In Table 14, we provide an updated list of specimens from Member 5 of the Sterkfontein Formation that have been classified as *Homo* or have been suggested to show closest affinity with this genus. Our odontometric data for these specimens are provided in Table 15 (for Stw 53 ondontometric data, see Tables 9, 11) and comparative data are provided in Tables 10, 12, 16, and 18. The comparisons that follow include data for Stw 151, a juvenile specimen described as sharing derived morphology with early *Homo* (Moggi-Cecchi et al., 1998) and believed to have been recovered from Member 4 of the Sterkfontein Formation (Kuman and Clarke, 2000). Odontometric data for this specimen have been taken from Moggi-Cecchi et al. (1998). We also include early *Homo* specimens from Swartkrans (data from Wood, 1991) and Drimolen (data from Keyser et al., 2000). Many of the Member 5 specimens are isolated teeth, and therefore dental comparions provide the only information on which to make taxonomic judgements about them. We also include sample data for *A. robustus* in our comparisons (Tables 16 and 17), as this taxon has also been recovered from Sterkfontein Member 5 (Kuman and Clarke, 2000) and alongside early *Homo* from deposits of similar age at the nearby sites Swartkrans, Kromdraai, and Drimolen.

Maxillary deciduous second molar

In Fig. 28, we provide a bivariate plot of crown module versus crown shape index values for dm^2. For crown size, SE 255 is indistinguishable from the median for *A. africanus* and lies within the ranges for *H. habilis* and *A. robustus* (Table 16). The crown shape index value in SE 255 is only within the range for *H. habilis* (Table 16). Thus, like *H. habilis*, the dm^2 crown of SE 255 is characterized by MD elongation. The crown module values in SK 27 and SKX 267 are very similar to typical *A. africanus* specimens (Table 16). The crown

Table 14
Sterkfontein Member 5 fossils referred to *Homo*

Specimen	Description	Date of Discovery	Locality	References
SE 255	Juvenile maxilla with RM^1, dm^1, and dm^2	1957	Member 5 Extension Site	Robinson (1958, 1962), Tobias (1965), Tobias and Wells (1967)
SE 1508	RM^2	1957	Member 5 Extension Site	Robinson (1958, 1962), Tobias (1965, 1978), Tobias and Wells (1967)
SE 1579	L maxillary molar fragment	1957	Member 5 Extension Site	Robinson (1958, 1962), Tobias (1965, 1978), Tobias and Wells (1967)
SE 1937	L lower C	1958	Member 5 Extension Site	Robinson (1958, 1962), Tobias (1965, 1978), Tobias and Wells (1967)
SE 2396	Lingual half probably of LP^3	1958	Member 5 Extension Site	Robinson (1958, 1962), Tobias (1965, 1978), Tobias and Wells (1967)
SE 2398	Post-canine dens, vertebra	1958	Member 5 Extension Site	Robinson (1958, 1962), Tobias (1965, 1978), Tobias and Wells (1967)
Stw 19a[a]	Premolar (?R maxillary) buccal 3/4 of crown	1973	Member 5 Extension Site	Tobias et al. (1977)
Stw 19b[a]	Maxilla with RM^2 and RM^3	1973	Member 5 Extension Site	Tobias et al. (1977)
Stw 27[a]	Distal third of R metacarpal	1973	Member 5 Extension Site	Tobias et al. (1977)
Stw 33	RP^4	1973	Member 5 Extension Site	Unpublished
Stw 34[a]	Left antimere Stw 19b M^2, lingual ½ of crown	1977	Member 5 Extension Site	Kuman and Clarke (2000)
Stw 42[b]	RI^2	1975	Member 5 Extension Site	Tobias et al. (1977)
Stw 53	Cranium	1976	Member 5 Stw 53 breccia	Hughes and Tobias (1977)
Stw 75-79	Left I^1–P^3	1979	Member 5 Stw 53 breccia	Kuman and Clarke (2000)
Stw 80	Mandible, tooth crowns	1979	Member 5 West	Kuman and Clarke (2000)
Stw 84	Mandibular corpus, tooth crowns	1980	Post-Member 6, but probably eroded from Member 5	Kuman and Clarke (2000)
Stw 85	Mandibular corpus, no teeth	1979	Member 5 East	Kuman and Clarke (2000)
Stw 311	Right femoral head	1980	Member 5 East	Kuman and Clarke (2000)
Stw 559	M2 or M3	1992	Member 5 East	Kuman and Clarke (2000)
Stw 567	Right distal tibia	1993	Member 5 East	Kuman and Clarke (2000)
Stw 571	Right proximal ulna	1981	Member 5 Stw 53 breccia	Kuman and Clarke (2000)
Stw 572	Lumbar vertebra	1980	Member 5 East	Kuman and Clarke (2000)

[a] Labeled Dump 18, but most likely Dump 3.
[b] Recovered from Dumps 1 and 3 of Robinson's 1957–1958 excavation.

Table 15
Dimensions and shape index values of teeth (excluding Stw 53) from Sterkfontein Member 5 assigned to *Homo*[a]

Tooth	Specimen	Mesiodistal diameter (mm)		Labiolingual/buccolingual diameter (mm)		Crown area (mm^2)		Crown module (mm)		Crown shape index[b] (%)	
		L	R	L	R	L	R	L	R	L	R
dm^2	SE 255	—	10.6 (ca. 10.8)	—	11.0	—	ca. 118.80	—	ca. 10.9	—	ca. 98.3
I^1	Stw 75-79	11.8	—	8.4	—	99.12	—	10.1	—	140.5	—
I^2	Stw 42	—	6.2	—	6.4	—	39.68	—	6.3	—	96.9
	Stw 75-79	7.4	—	6.2	—	—	45.88	—	6.8	—	119.4
UC	Stw 75-79	10.1	—	8.4	—	84.84	—	9.25	—	120.2	—
P^3	SE 2396	ca. 8.4	—	—	—	—	—	—	—	—	—
	Stw 75-79	8.9	—	11.0	—	97.90	—	9.95	—	80.9	—
P^4	Stw 33[c]	—	ca. 8.6 (ca. 9.3)	—	ca. 12.5	—	ca. 116.25	—	ca. 10.9	—	ca. 74.4
M^1	SE 255	—	13.5	—	13.4	—	180.90	—	13.5	—	100.7
M^2	SE 1508	—	13.1 (ca. 13.5)	—	14.3	—	ca. 193.05	—	ca. 13.9	—	ca. 94.4
	Stw 19b	—	13.1 (ca. 14.2)	—	13.8	—	ca. 195.96	—	ca. 14.0	—	ca. 102.9
	"Stw 34"[d]	13.3	—	—	—	—	—	—	—	—	—
M^3	Stw 19b	—	13.3 (ca. 13.5)	—	13.9	—	ca. 187.65	—	ca. 13.7	—	ca. 97.1
LC	SE 1937	8.4	—	9.0	—	75.60	—	8.7	—	93.3	—

[a] To avoid systematic error from rounding second decimal place, even digit down, odd digit up; values in parentheses are corrected for interproximal wear; estimates of crown area and crown shape index use mesiodistal dimensions corrected for interproximal wear.
[b] Index is mesiodistal diameter/buccolingual diameter, multiplied by 100.
[c] Most likely RP^4 and probably belongs to the same individual as Stw 19.
[d] Left antimere of Stw 19b M^2.

shape index value in SK 27 lies only within the range for *H. habilis*, while the value for this index in SKX 267 lies just within the ranges for *A. africanus* and *A. robustus* (Table 16). The crown of Stw 151 is unusually small in size, while its shape index value is close to typical values for *A. africanus* (Table 16). The absence of Plio-Pleistocene *H. sapiens* sensu lato specimens preserving the dm^2 crown limits our comparisons.

Table 16
Summary statistics for dm^2, I^1, I^2, and mandibular canine crown dimensions and shape index values for comparative taxa

Measurements and indices[a]	*A. africanus*			*A. robustus*[b]			*H. habilis*			*Homo sapiens* sensu lato		
	n	Avg./med.[c]	Range	n	Avg./med.[c]	Range	n	Avg./med.[c]	Range	n	Med.	Range
dm^2												
MD	4	10.7	1.0	5	10.9 ± 0.5	1.2	5	12.9 ± 2.2	5.1	—	—	—
BL	4	11.5	1.8	6	12.2 ± 0.6	1.6	5	12.7 ± 1.7	4.0	—	—	—
Crown area (mm^2)	4	124.3	26.4	5	130.3 ± 8.6	18.1	5	168.9 ± 45.3	103.1	—	—	—
Module	4	11.2	1.2	5	11.4 ± 0.4	0.8	5	12.9 ± 1.8	4.2	—	—	—
Shape index (%)	4	92.7	12.0	5	91.0 ± 5.2	12.3	5	102.5 ± 4.0	11.0	—	—	—
I^1												
MD	2	11.1	2.8	15	9.2 ± 0.7	2.6	5	11.1 ± 0.8	2.3	—	—	—
LL	2	8.2	0.4	13	7.7 ± 0.5	1.8	5	7.9 ± 0.4	1.0	—	—	—
Crown area (mm^2)	2	90.5	19.0	13	68.8 ± 8.8	30.4	5	99.5 ± 10.5	26.4	—	—	—
Module	2	9.6	1.2	13	8.3 ± 0.5	2.0	5	9.6 ± 0.6	1.5	—	—	—
Shape index (%)	2	136.2	40.1	13	116.1 ± 8.8	35.7	5	144.5 ± 9.1	22.2	—	—	—
I^2												
MD	4	7.0	1.3	12	7.4 ± 1.0	4.0	3	7.0	1.0	1	7.9	—
LL	4	6.8	1.6	11	7.2 ± 0.9	2.9	3	7.0	1.9	1	8.4	—
Crown area (mm^2)	4	47.6	17.9	11	53.3 ± 10.4	38.7	3	50.5	12.6	1	66.4	—
Module	4	6.9	1.4	11	7.3 ± 0.8	3.0	3	7.2	0.9	1	8.2	—
Shape index (%)	4	101.8	12.0	11	104.5 ± 15.4	53.4	3	100.0	30.7	1	94.0	—
Mandibular canine												
MD	7	9.6 ± 0.6	1.5	13	7.9 ± 0.5	1.8	3	8.1	1.0	2	8.0	2.0
BL	7	10.6 ± 1.1	2.9	15	8.0 ± 0.6	2.0	3	7.7	2.5	2	9.2	0.7
Crown area (mm^2)	7	102.7 ± 16.1	42.4	13	63.6 ± 8.2	26.9	3	61.6	28.8	2	73.6	23.9
Module	7	10.1 ± 0.8	2.1	13	8.0 ± 0.5	1.7	3	7.9	1.7	2	8.6	1.4
Shape index (%)	7	91.1 ± 6.2	15.9	13	99.5 ± 6.4	19.6	3	101.3	19.5	2	87.1	15.2

[a] All data in mm unless indicated.
[b] Includes data from Keyser (2000) and Keyser et al. (2000).
[c] If $n < 5$, median is given; if $n \geq 5$, average is shown; ± standard deviations of sample averages.

Table 17
Summary statistics of maxillary canine, premolar, and molar crown dimensions and shape index values for *Australopithecus robustus*

Measurements and indices[a]	n	Avg.[b]	Sample range
Maxillary canine			
MD	18	8.6 ± 0.6	2.3
BL	18	9.9 ± 0.7	2.8
Crown area (mm^2)	18	85.6 ± 10.2	37.7
Module	18	9.3 ± 0.6	2.1
Shape index (%)	18	87.6 ± 6.9	27.9
P^3			
MD	17	9.9 ± 0.5	2.1
BL	15	14.3 ± 0.7	2.4
Crown area (mm^2)	15	142.1 ± 13.2	45.8
Module	15	12.9 ± 0.6	1.9
Shape index (%)	15	69.7 ± 3.0	8.5
P^4			
MD	19	11.1 ± 0.7	2.7
BL	19	15.9 ± 0.9	2.8
Crown area (mm^2)	19	176.2 ± 18.1	66.0
Module	19	13.5 ± 0.7	2.6
Shape index (%)	19	69.4 ± 2.7	9.1
M^1			
MD	17	13.3 ± 0.4	1.5
BL	17	14.8 ± 0.7	3.5
Crown area (mm^2)	17	197.0 ± 13.6	58.0
Module	17	14.1 ± 0.5	2.1
Shape index (%)	17	90.1 ± 4.2	16.5
M^2			
MD	17	14.4 ± 1.1	4.0
BL	17	15.7 ± 0.9	2.9
Crown area (mm^2)	17	226.8 ± 25.1	90.5
Module	17	15.1 ± 0.8	3.1
Shape index (%)	17	91.6 ± 6.8	26.6
M^3			
MD	21	15.1 ± 1.1	5.1
BL	21	17.0 ± 1.1	4.0
Crown area (mm^2)	21	257.3 ± 31.3	131.2
Module	21	16.0 ± 1.0	4.2
Shape index (%)	21	88.5 ± 4.6	16.0

[a] Includes data from Keyser (2000) and Keyser et al. (2000); all data in mm unless indicated.
[b] ± standard deviations of sample averages.

Maxillary incisors

Figure 29 is a plot of I^1 size-shape. The I^1 crown size (module) in Stw 75-79 is large and well within the *A. africanus* range (Table 16). In terms of its crown shape index value, Stw 75-79 is midway between the median for *A. africanus* and the average for *H. habilis.* Thus, it lies well within the ranges for both taxa. In terms of their size, the I^1 crowns in Stw 151 and SKX 339 are most like those of *A. robustus* (Table 16). However, the crown shape index value for Stw 151 places it within the ranges for *A. africanus* and *A. robustus*, while the index value for SKX 339 lies within the range for *H. habilis* (Table 16). Thus, Stw 151 has strong affinities with the australopiths in its I^1 crown size and shape, while SKX 339 is most like *H. habilis* in its crown shape. The absence of Plio-Pleistocene *H. sapiens* sensu lato specimens that preserve the I^1 crown limits our comparisons.

In Fig. 30, we compare I^2 crown size and crown shape index values. The crown module in Stw 42 lies only within the ranges for australopith taxa (Table 16). Its shape index value lies within the ranges for *A. robustus* and *H. habilis* (Table 16) and is similar to the value in KNM-WT 15000. In terms of its crown size (module), Stw 75-79 is virtually indistinguishable from the median for *A. africanus* (Table 16). Its crown shape index value is high and lies within the ranges for *H. habilis* and *A. robustus* (Table 16). Crown size values in Stw 151, DNH 45, and SK 847 are similar and lie only within the ranges for australopith taxa (Table 16). The crown shape index value for Stw 151 is midway between the median value for *A. africanus* and the average for *A. robustus* (Table 16). The value in DNH 45 is closest to the median for *H. habilis* but is also close to the median for *A. africanus* (Table 16). The shape index value for SK 847 lies only within the range for *A. robustus* (Table 16). The crown module in SK 27 is within the upper part of the ranges for *H. habilis* and *A. robustus* (Table 16). The module in SKX 610 is virtually indistinguishable from the average for *A. robustus* and is also within the range for *H. habilis* (Table 16). Crown shape index values in SK 27 and SKX 610 are virtually identical and lie midway between the median value for *H. habilis* and the average value for *A. robustus* (Table 16). The existence of only a single Plio-Pleistocene *H. sapiens* sensu lato specimen with preserved I^2 crown limits our comparisons.

Maxillary canine

In Fig. 31, we provide a plot of maxillary canine size-shape. The crown size (module) value in Stw 75-79 is large and virtually indistinguishable from the average for *A. robustus*, while its crown shape index value is high and lies outside of the range for all taxa (Tables 10, 17). The reconstructed canine crown module in Stw 53 is virtually indistinguishable from the average for *A. africanus*, while its reconstructed crown shape index value is closest to the average for *A. robustus*, but also well within the range for Plio-Pleistocene *H. sapiens* sensu lato (Tables 10, 17). The crown module in Stw 151 is similar to the average value for *A. robustus*, while its crown shape index value is high and lies only within the range for this taxon (Tables 10 and 17). For SK 27, the crown module is closest to the median for Plio-Pleistocene *H. sapiens* sensu lato, while its crown shape index value is within the ranges for *H. habilis* and *A. robustus* (Tables 10, 17).

Maxillary premolars

Figure 32 is a plot of P^3 size-shape. The crown module in Stw 75-79 is closest to the average value for Plio-Pleistocene *H. sapiens* sensu lato (Tables 12 and 17), while its crown shape index value is high and lies within the ranges for *A. africanus* and *H. habilis* (Tables 12, 17). Specimen Stw 53 has a much larger crown module value, but its shape index value is similar

Table 18
Summary statistics of dimensions and shape index values of M^1 for comparative taxa

Measurements and indices[a]	*A. africanus*			*H. habilis*			*H. sapiens* sensu lato		
	n	Avg.[b]	Range	n	Avg.[b]	Range	n	Med.	Range
MD	11	12.7 ± 0.5	1.7	13	13.0 ± 1.0	3.5	4	11.8	0.9
BL	11	13.6 ± 0.7	2.3	13	13.0 ± 0.8	2.9	3	12.9	1.5
Crown area (mm^2)	11	173.8 ± 14.0	53.4	13	170.2 ± 21.9	74.3	3	152.2	19.5
Module	11	13.2 ± 0.5	2.0	13	13.0 ± 0.8	2.9	3	12.4	0.8
Shape index (%)	11	94.9 ± 4.8	15.6	13	98.0 ± 6.8	26.4	3	91.5	10.0

[a] All data in mm unless indicated.
[b] ± standard deviation of sample averages.

to that in Stw 75-79. The crown module in SK 27 is about midway between sample averages for *H. habilis* and *A. robustus* (Tables 12, 17), while its crown shape index value is about midway between average values for Plio-Pleistocene *H. sapiens* sensu lato and *A. robustus* (Tables 12, 17).

Figure 33 is a plot of P^4 size-shape. The crown module in Stw 33 is virtually indistinguishable from the average value for *H. habilis*, while its crown shape index value is indistinguishable from the sample average for *A. africanus* (Tables 12, 17). The crown module in Stw 53 is larger and its crown shape index value much higher, the specimen having markedly different values to those of Stw 33.

Maxillary molars

In Fig. 34, M^1 crown size (module) and shape index values are compared. The crown module value in SE 255 is about midway between average values for *A. africanus* and *A. robustus* (Tables 17 and 18). Its crown shape index value is well within the range for *H. habilis* and closest to the average value for this taxon (Tables 17, 18). The crown modules for Stw 151, SKX 268, and DNH 70 are almost identical to the average value for *H. habilis* (Tables 17, 18). The crown module value for SK 27 is about midway between the average values for *A. africanus* and *A. robustus*, although it is within the range for *H. habilis* (Tables 17, 18). The shape index values for Stw 151, DNH 70, and SK 27 are close to the average value for *H. habilis*, while the shape index value for SKX 268 lies within the range only of this taxon (Tables 17, 18).

Figure 35 is a plot of M^2 size-shape. Crown module values in Stw 19b and SE 1508 are virtually indistinguishable from the *H. habilis* average (Tables 12, 17), and contrast with the large value for Stw 53. The crown shape index value in SE 1508, like Stw 53, is virtually indistinguishable from the average for Plio-Pleistocene *H. sapiens* sensu lato (Tables 12, 17). The crown shape index value for Stw 19b is very high and lies within the range only of Plio-Pleistocene *H. sapiens* sensu lato (Tables 12, 17). The crown module value for Stw 151 is virtually identical to the average value for *H. habilis*, while the value in SK 27 lies about midway between the average values for *H. habilis* and *A. africanus* (Tables 12, 17). The crown shape index value in Stw 151 lies very close to the average value for *A. africanus*, while in SK 27

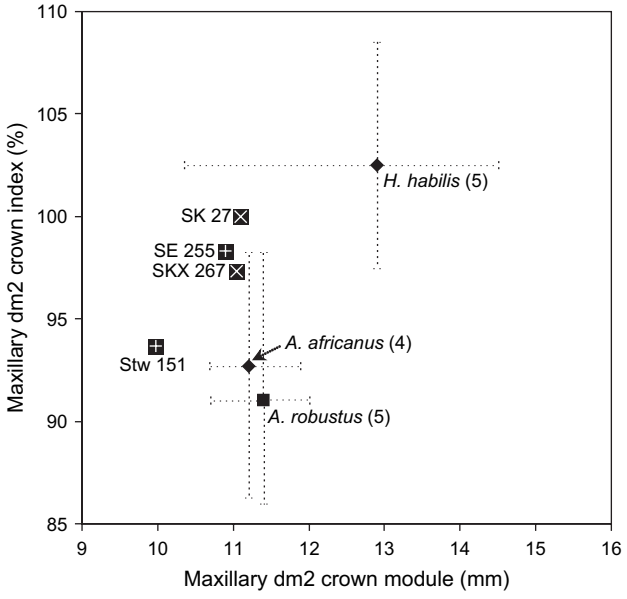

Fig. 28. Size-shape plot: dm^2 crown module vs. crown shape index value. Error bars represent ranges for samples. Average shown for samples in which $n \geq 5$; median given for sample sizes of $n < 5$; numbers in parentheses after taxon names are sample sizes.

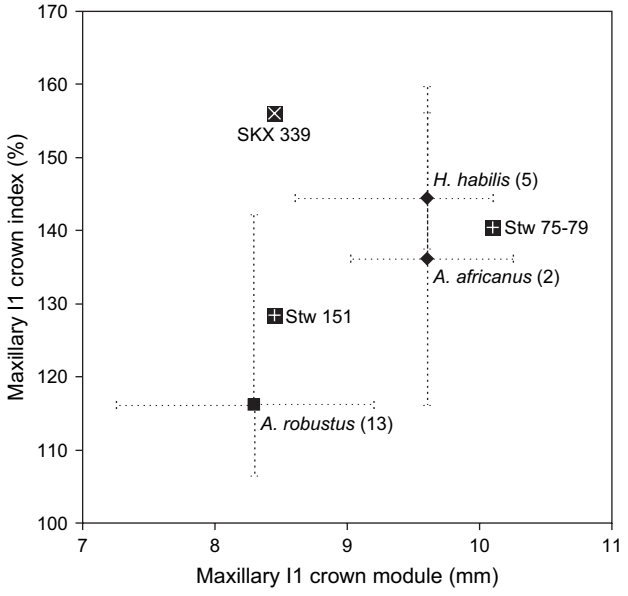

Fig. 29. Size-shape plot: I^1 module vs. crown shape index value. Error bars represent ranges for samples. Average shown for samples in which $n \geq 5$; median given for sample sizes of $n < 5$; numbers in parentheses after taxon names are sample sizes.

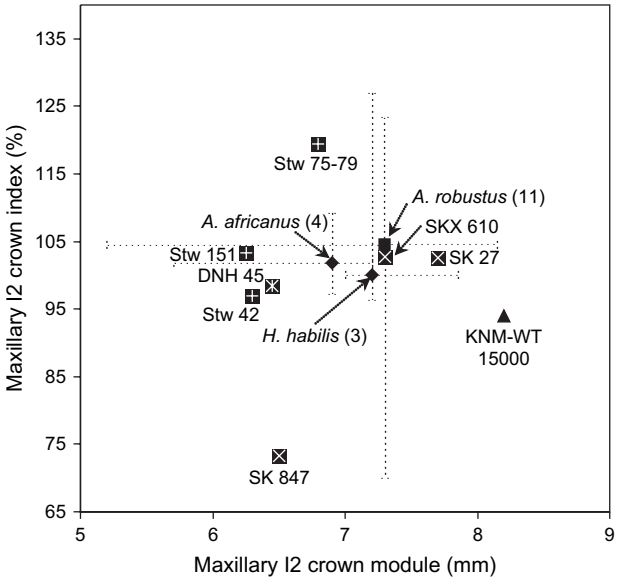

Fig. 30. Size-shape plot: I^2 module vs. crown shape index value. Error bars represent ranges for samples. Average shown for samples in which n ≥ 5; median given for sample sizes of n < 5; numbers in parentheses after taxon names are sample sizes.

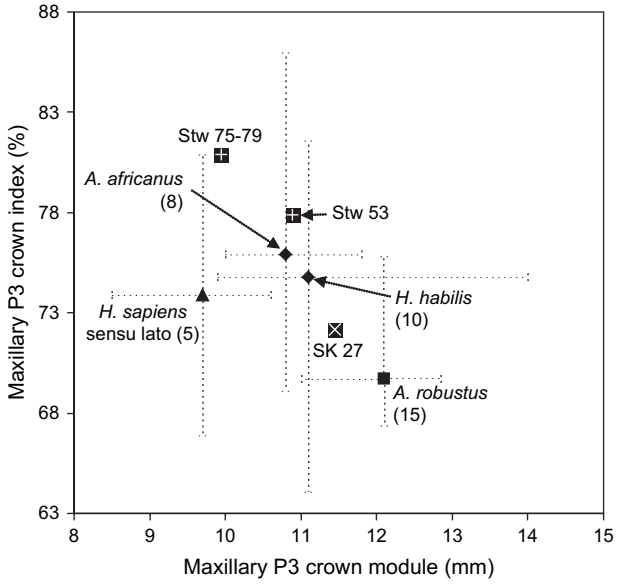

Fig. 32. Size-shape plot: P^3 module vs. crown shape index value. Error bars represent ranges for samples. Average shown for samples in which n ≥ 5; median given for sample sizes of n < 5; numbers in parentheses after taxon names are sample sizes.

the value is about midway between the average values for Plio-Pleistocene *H. sapiens* sensu lato and *A. africanus* (Tables 12 and 17).

In Fig. 36, we compare M^3 crown size and shape values. The crown module values for Stw 19b and SK 847 are almost identical to the median value for *H. habilis*, and contrast with the large crown module value in Stw 53 (Tables 12, 17). Crown shape index values for Stw 19b and Stw 53 are high and lie within the ranges only of australopiths (Tables 12, 17). The crown shape index value for SK 847 is low and lies within the ranges for *H. habilis* and Plio-Pleistocene *H. sapiens* sensu lato (Tables 12, 17).

Mandibular canines

Figure 37 compares mandibular canine crown module and shape index values. The crown module value for SE 1937 is almost identical to the median value for Plio-Pleistocene *H. sapiens* sensu lato, while its crown shape index

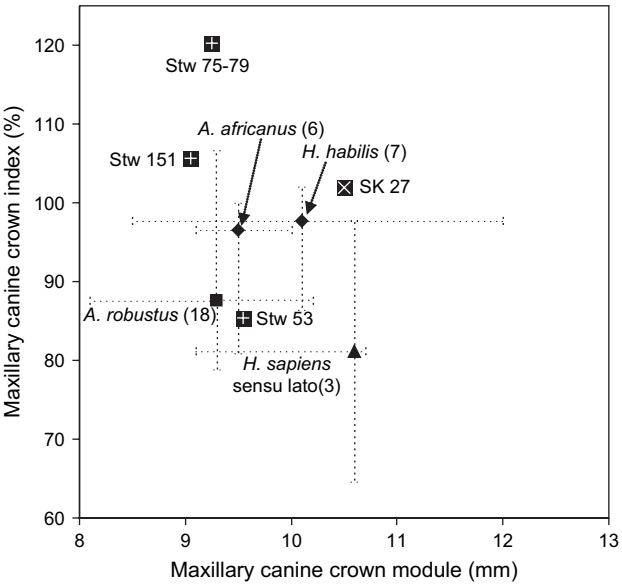

Fig. 31. Size-shape plot: Maxillary canine module vs. crown shape index value. Error bars represent ranges for samples. Average shown for samples in which n ≥ 5; median given for sample sizes of n < 5; numbers in parentheses after taxon names are sample sizes.

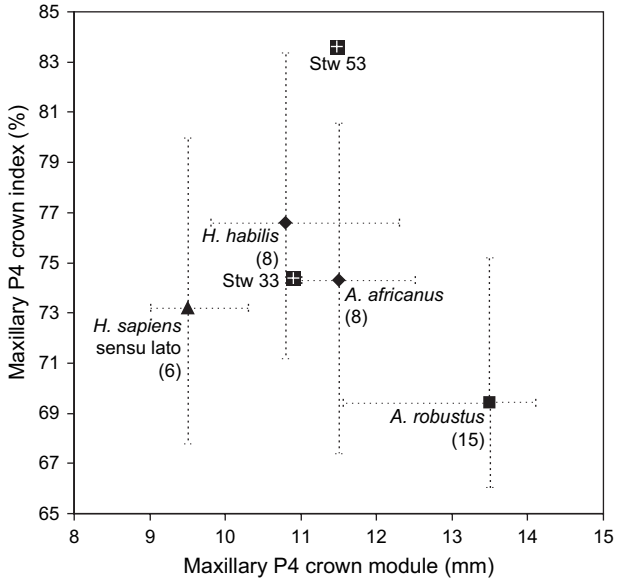

Fig. 33. Size-shape plot: P^4 module vs. crown shape index value. Error bars represent ranges for samples. Average shown for samples in which n ≥ 5; median given for sample sizes of n < 5; numbers in parentheses after taxon names are sample sizes.

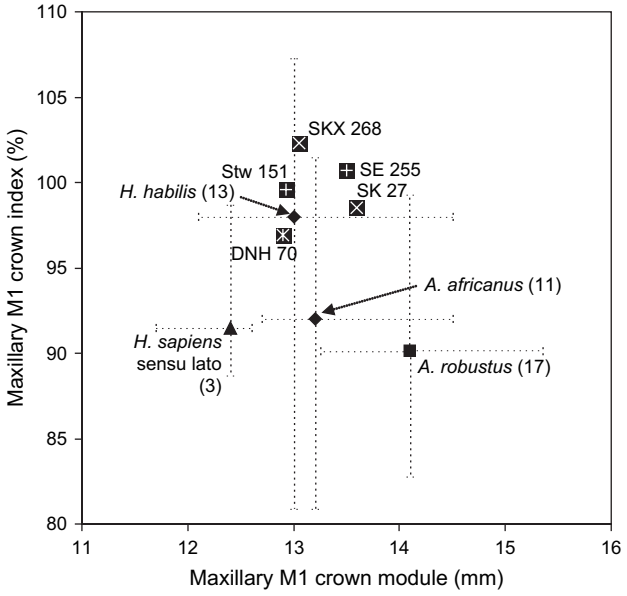

Fig. 34. Size-shape plot: M^1 module vs. crown shape index value. Error bars represent ranges for samples. Average shown for samples in which n ≥ 5; median given for sample sizes of n < 5; numbers in parentheses after taxon names are sample sizes.

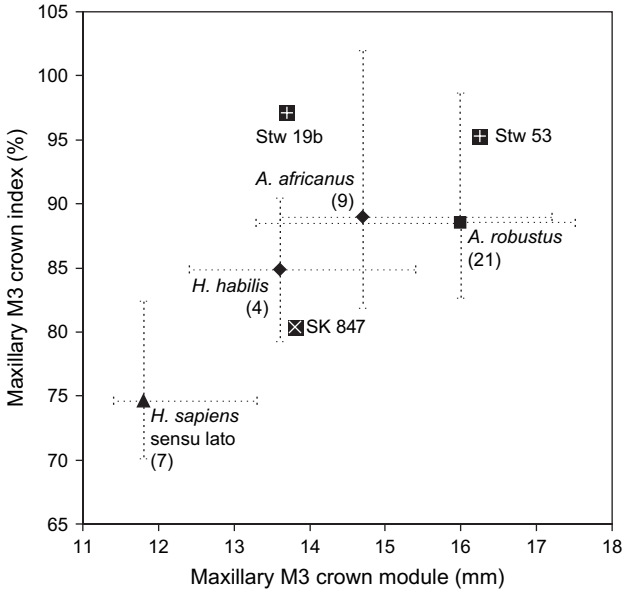

Fig. 36. Size-shape plot: M^3 module vs. crown shape index value. Error bars represent ranges for samples. Average shown for samples in which n ≥ 5; median given for sample sizes of n < 5; numbers in parentheses after taxon names are sample sizes.

value lies closest to the average value for *A. africanus* (Table 16).

Taxonomic assignments

In Table 19, we provide our proposed classification for the Sterkfontein Member 5 dental specimens and, in Table 20, proposed classifications for dental remains from Swartkrans and Drimolen. Taxonomic assignments are based on the comparisons we have made above. We believe that only two specimens from Sterkfontein Member 5 (Stw 33 and Stw 42) can be assigned at the species level with confidence. For remains from other southern African Plio-Pleistocene sites, we are confident about the assignment of three of them (SK 27, SKX 268, and DNH 70).

Comparison of Stw 53 and SK 847

Discussion of the classification of Stw 53 naturally leads to consideration of its affinities with the Swartkrans cranium

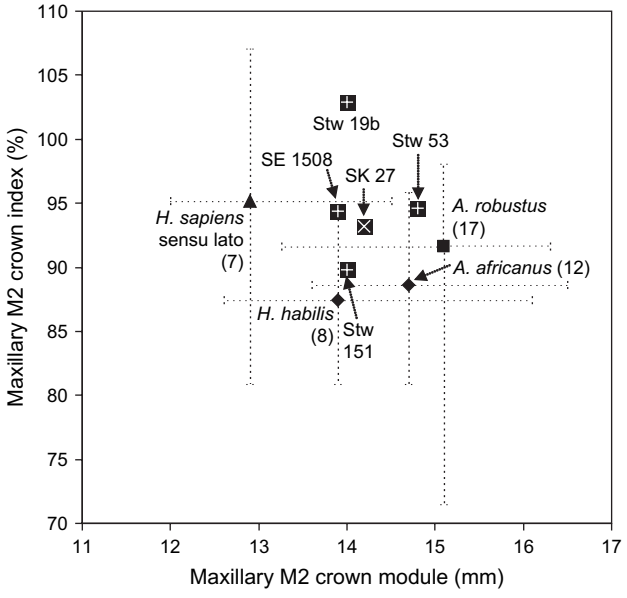

Fig. 35. Size-shape plot: M^2 module vs. crown shape index value. Error bars represent ranges for samples. Average shown for samples in which n ≥ 5; median given for sample sizes of n < 5; numbers in parentheses after taxon names are sample sizes.

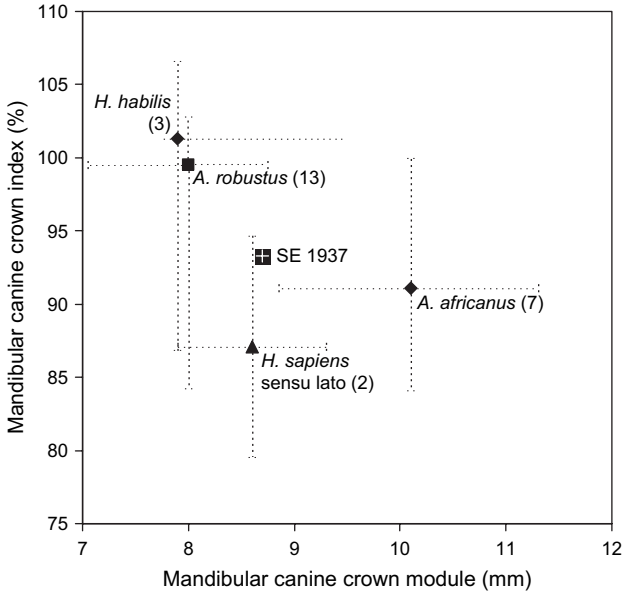

Fig. 37. Size-shape plot: mandibular canine module vs. crown shape index value. Error bars represent ranges for samples. Average shown for samples in which n ≥ 5; median given for sample sizes of n < 5; numbers in parentheses after taxon names are sample sizes.

Table 19
Proposed classification for dental specimens from Sterkfontein Member 5

Specimen	Classification
SE 255	*Homo* aff. *H. habilis*
SE 1508	*Homo* aff. *H. sapiens*
SE 1937	*Homo* aff. *H. sapiens*
Stw 19b	*Homo* aff. *H. habilis*
Stw 33	*Homo habilis*
Stw 42	*Homo habilis*
Stw 75-79	*Homo* aff. *H. habilis*

SK 847. Similarities between Stw 53 and SK 847 have been described (Grine et al., 1993, 1996; Curnoe, 1999, 2001a, 2002; Grine, 2001). Specimen SK 847 has been likened mainly to *H. erectus* (Clarke et al., 1970; Clarke, 1977a,b, 1985; Walker, 1981; Tobias, 1991; Kimbel et al., 1997). However, Clarke and Howell (1972) described similarities between SK 847 and OH 13, and Howell (1978) referred the Swartkrans cranium to *H. habilis*. Analyses by Bilsborough and Wood (1988) showed that "facial dimensions align SK 847 firmly with the smaller 'early *Homo*' specimens" (p. 82), such as OH 24 and KNM-ER 1813.

In Table 21, we compare 37 features of Stw 53 and SK 847 with their morphological conditions in *H. habilis* and Plio-Pleistocene *H. sapiens* sensu lato. Both specimens are characterized by postorbital constriction of the frontal bone, particularly SK 847, in which the value for minimum frontal breadth is especially low (Table 3) and within the range for robust australopiths. Absolutely low minimum frontal breadth is a feature both specimens share that distinguishes them from *H. habilis* and Plio-Pleistocene *H. sapiens* sensu lato (Table 3). The mastoid processes of Stw 53 are long, distinguishing the specimen from SK 847 and *H. habilis*, but aligning it with Plio-Pleistocene *H. sapiens* sensu lato (Table 3). Specimens Stw 53 and SK 847 also share the feature of encroachment of the temporal lines on the lateral half of the supraorbital rim, present and variable in *A. africanus*, but absent from early *Homo*.

The supraorbital torus distinguishes the two specimens (Fig. 38; Table 6), being vertically thin in Stw 53, with a shallow and laterally constricted supratoral sulcus, but of moderate development in SK 847, which possesses a true sulcus. Specimen SK 847 is more like specimens of Plio-Pleistocene *H. sapiens* sensu lato in the morphology of its supraorbital. The glabella of both specimens is moderate in development

Table 20
Proposed classification for Swartkrans and Drimolen dental specimens

Specimen	Classification
Swartkrans	
SK 27	*Homo habilis*
SKX 267	*Homo* sp. indet.
SKX 268	*Homo habilis*
SKX 339	*Homo* aff. *H. habilis*
SKX 610	*Homo* sp. indet.
Drimolen	
DNH 45	*Homo* aff. *H. habilis*
DNH 70	*Homo habilis*

(Fig. 38). Among early *Homo*, only specimens assigned to *H. habilis* show moderate glabella development, with Plio-Pleistocene *H. sapiens* sensu lato typically exhibiting little prominence of the glabella. However, the supraorbital torus is divided into two parts in both specimens, as is usually found in *H. habilis* and only rarely found in Plio-Pleistocene *H. sapiens* sensu lato (e.g., the condition in KNM-ER 3733 vs. the conditions in KNM-ER 3883 and the Sangiran specimens).

The face is short in Stw 53, but long in SK 847 (Fig. 38; Table 6); however, the range for *H. habilis* (including KNM-ER 1470) incorporates both conditions (e.g., OH 24 short, KNM-ER 1470 long). In contrast, facial length in Plio-Pleistocene *H. sapiens* sensu lato is much less variable, always being long (Table 6). The transverse extent of the supraorbital torus is low in both specimens compared to both *H. habilis* and Plio-Pleistocene *H. sapiens* sensu lato. Superior facial breadth is narrow in Stw 53, being unusually so, but moderate in SK 847 (Fig. 38; Table 6), as in *H. habilis*. The midface is narrow in Stw 53, SK 847 (Fig. 38), and *H. habilis*. Midfacial breadth exceeds superior facial breadth in Stw 53 and SK 847 (Fig. 38), the condition seen in Plio-Pleistocene *H. sapiens* sensu lato. The reverse condition is typical of *H. habilis* (Kimbel and Rak, 1993).

The superior and inferior orbital margins lie in approximately the same plane in Stw 53, as in *H. habilis*, but in SK 847 the superior orbital margin sits anterior to the inferior margin, as in Plio-Pleistocene *H. sapiens* sensu lato. The alveolar height is low in Stw 53, as in *H. habilis*, but moderate in SK 847, which is most similar to Plio-Pleistocene *H. sapiens* sensu lato (Table 6). Nasal (midfacial) projection is low in Stw 53 and moderate in SK 847. Low midfacial projection is the condition seen in *H. habilis*. Of all the morphological features compared in Stw 53 and SK 847, the moderate midfacial projection of the latter specimen (seen as an anterior placement of rhinion relative to the infraorbital plate and curved/concave nasal bones) is one of the most obvious characters that suggests an affinity between SK 847 and Plio-Pleistocene *H. sapiens* sensu lato. Prognathism is low in Stw 53 and SK 847, as seen in Plio-Pleistocene *H. sapiens* sensu lato, while *H. habilis* is characterized by low to moderate projection. The height of the piriform aperture in Stw 53 is low, but moderate in SK 847 (Fig. 38; Table 6). The latter specimen resembles typical members of *H. habilis* in this regard, although there is considerable variation among specimens of Plio-Pleistocene *H. sapiens* sensu lato in this feature.

Maxillo-alveolar length in Stw 53 and SK 847 is moderate, as seen in Plio-Pleistocene *H. sapiens* sensu lato (Table 7). In absolute breadth (interalveolar distances), Stw 53 and SK 847 possess narrow anterior and middle palates, but differ in their posterior palatal breadths. The breadth of the palate, estimated from interalveolar distances, shows Stw 53 and SK 847 to possess a broad anterior palate, relative to the mid-palate (Table 7). However, like Plio-Pleistocene *H. sapiens* sensu lato, but unlike SK 847 and *H. habilis*, Stw 53 is characterized by narrow palatal breadth posteriorly, compared to its middle palatal breadth (Table 7). Additionally, the M^3 is positioned medial to the M^2 in Stw 53, but lateral to it

Table 21
Morphological comparison of Stw 53, SK 847, and early *Homo* taxa

Character	Stw 53	SK 847	*H. habilis* sensu lato	*H. sapiens* sensu lato
1. Minimum frontal breadth (absolute)	Narrow	Narrow	Moderate/broad	Moderate/broad
2. Mastoid length	Long	Short	Short	Long
3. Temporal lines encroach on lateral half of supraorbital rim	Present	Present	Absent	Absent
4. Supraorbital torus	Thin	Moderate	Moderate	Moderate/thick
5. Supratoral sulcus	Slight	Present	Absent/slight	Slight/present
6. Glabella development	Moderate	Moderate	Small/prominent	Small
7. Supraorbital torus divided into two parts	Present	Present	Present	Mostly absent
8. Facial height (absolute)	Short	Long	Short/long	Long
9. Transverse extent of supraorbital torus	Low	Low	Moderate	High
10. Superior facial breadth (absolute)	Narrow	Moderate	Moderate	Broad
11. Midfacial breadth (absolute)	Narrow	Narrow	Narrow	Broad
12. Superior facial breadth exceeds midfacial breadth	Absent	Absent	Variable (typically present)	Absent
13. Superior and inferior orbital margins lie in approximately same plane	Present	Absent	Present	Absent
14. Alveolar height	Low	Moderate	Low	Moderate/high
15. Nasal projection	Low	Moderate	Low	Moderate/high
16. Prognathism	Low	Low	Low/moderate	Low
17. Piriform aperture height	Low	Moderate	Moderate	Moderate/high
18. Maxillo-alveolar length	Moderate	Moderate	Short	Moderate
19. Palate breadth (absolute): anterior	Narrow	Narrow	Moderate	Broad
20. Palate breadth (absolute): mid-palatal	Narrow	Narrow	Broad	Broad/very broad
21. Palate breadth (absolute): posterior	Narrow	Moderate	Broad	Narrow/moderate
22. Palate breadth (relative): middle vs. anterior	Narrow	Narrow	Narrow	Narrow
23. Palate breadth (relative): posterior vs. middle	Broad	Narrow	Narrow	Broad
24. Posterior palatal incurvation (medial placement of M^3 relative to M^2)	Present	Absent	Variable	Present[a]
25. Palatal height	Low	Low	Moderate/high	Moderate/high
26. Anteroposterior length of mandibular fossa	Short	Moderate	Moderate	Long
27. Mediolateral breadth of mandibular fossa	Narrow	Moderate	Moderate	Moderate/broad
28. Mandibular fossa length relative to breadth (length-breadth index)	Short	Short	Short/moderate	Moderate/long
29. Tympanomedian angle	Low	Moderate	High	High
30. Mandibular fossa angle	Moderate	Very low	Moderate	Moderate/high
31. Articular eminence size	Large	Large	Large	Small
32. Postglenoid process size	Reduced	Reduced	Reduced	Enlarged
33. Tympanic merges with postglenoid process	Present	Present	Present	Absent
34. Large petrous crest that merges with anterior mastoid	Present	Present	Present	Absent
35. P^4 root number	3	3	2–3	1[b]
36. M^3 crown size (module)	Large (16.3)	Moderate (13.8)	Moderate (Median = 13.2)	Small (Average = 11.8)
37. M^3 crown shape index value	About 100%	About 80%	Closer to 80%	Closer to 80%

[a] Assessed in only a single specimen.
[b] We suggest that variation in this taxon is likely to be greater than sampled to date. Gabriel (1965), for example, described variation in modern humans as follows: single-rooted is the most common form, while double-rooted is found in 20% of modern humans and triple-rooting does occur, but is uncommon.

in SK 847 (Fig. 25), the former condition being typical of Plio-Pleistocene *H. sapiens* sensu lato, but variable in *H. habilis*. The height of the palate is low in both Stw 53 and SK 847, differing from the conditions in *H. habilis* (moderate–high) and Plio-Pleistocene *H. sapiens* sensu lato (moderate–high) (Table 7).

The mandibular fossa of Stw 53 is short in its anteroposterior length, contrasting with the condition seen in SK 847, *H. habilis*, and Plio-Pleistocene *H. sapiens* sensu lato (Table 3). Mandibular fossa (mediolateral) breadth is low in Stw 53, moderate in SK 847, low to moderate in *H. habilis*, and moderate to broad in Plio-Pleistocene *H. sapiens* sensu lato (Table 3). The mandibular fossa length-breadth index value in SK 847 is identical to the medians for *A. africanus* and *H. habilis*, but slightly below the value in Stw 53 (by 4%; Table 3). The tympanomedian angle in Stw 53 is low, being just below the range for *A. africanus*, but moderate in SK 847. The mandibular fossa angle is low in SK 847, moderate in Stw 53 and *H. habilis*, but low to high in Plio-Pleistocene *H. sapiens* sensu lato (Table 4). The articular eminence is well developed in Stw 53, SK 847, and *H. habilis*, but small in Plio-Pleistocene *H. sapiens* sensu lato. The postglenoid process is reduced and merges with the tympanic in Stw 53, SK 847, and *H. habilis*, but it is moderate to large in size and well separated from the tympanic in Plio-Pleistocene *H. sapiens* sensu lato. The petrous crest is large in all of them, but it merges with the anterior part of the mastoid in Stw 53, SK 847, and *H. habilis* (the mastoid fissure being wide in Plio-Pleistocene *H. sapiens* sensu lato).

The P^4s of Stw 53 and SK 847 are triple-rooted, as in *H. habilis* (2–3 roots), but in contrast with Plio-Pleistocene *H. sapiens* sensu lato (single root). The size of the M^3 crown is large in Stw 53, moderate in SK 847 and *H. habilis*, but much reduced in Plio-Pleistocene *H. sapiens* sensu lato (Tables 11, 12; Fig. 36). However, Stw 53 shows marked MD elongation of the M^3 crown compared to the condition seen in *A. africanus* and *H. habilis*, while SK 847 is most similar in its crown shape index value to the median for *H. habilis* (Tables 11, 12; Fig. 36).

Fig. 38. Casts of Stw 53 (left) and SK 847 (right) in anterior aspect.

Grine (2001) noted three features unique to Stw 53 and SK 847 among the sample of early *Homo* fossils—primitively moderate encroachment of the superior temporal lines on the lateral half or less of the supraorbital rim, a thin supraorbital torus, and a narrow palate—and we have added four features to this list—namely, the low tympanomedian angle, small minimum frontal breadth, low transverse extent of the supraorbital torus, and a shallow palate. We also note that Stw 53 and SK 847 share narrow anterior and middle palates, but differ in the breadth of their posterior palates.

Of even greater bearing on the classification of these specimens, however, is the number of features they share with *H. habilis* or Plio-Pleistocene *H. sapiens* sensu lato. Of the features shown in Table 21, Stw 53 and SK 847 share 11 exclusively with *H. habilis*, one typical of *H. habilis* and rare in Plio-Pleistocene *H. sapiens* sensu lato, and two exclusively with Plio-Pleistocene *H. sapiens* sensu lato. Thus, they have greater phenetic affinity with *H. habilis*, possessing several diagnostic features of this taxon, including: supraorbital torus divided into two parts, a narrow midface (absolute breadth), reduced anteroposterior length of the mandibular fossa, short mandibular fossa relative to breadth, large articular eminence, reduced postglenoid process merged with the tympanic element, large petrous crest that merges with the anterior part of the mastoid process (absence of mastoid fissure), and triple-rooted P^4s. Further, Stw 53 shares with *H. habilis*, to the exclusion of SK 847, the location of the superior and inferior orbital margins in the same plane, low alveolar height, and low nasal (midfacial) projection. Specimen SK 847 shares with *H. habilis*, to the exclusion of Stw 53, short mastoid processes, moderate superior facial breadth, narrow mid-palate relative to posterior palatal breadth, and moderate M^3 crown size. Specimen SK 847 shares with Plio-Pleistocene *H. sapiens* sensu lato a full supratoral sulcus and moderate nasal projection. Specimen Stw 53 and Plio-Pleistocene *H. sapiens* sensu lato share two features to the exclusion of SK 847 and *H. habilis*, i.e., long mastoid processes and medial incurvation of the posterior palate.

We find that the case for SK 847 being most similar to Plio-Pleistocene *H. sapiens* sensu lato has been overstated. Instead, like Stw 53, it is most like *H. habilis* in important aspects of its morphology, and we believe it is best classified in this species (as per Howell, 1978; see also Bilsborough and Wood, 1988). Thus, we agree with Grine (2001) that Stw 53 and SK 847 should be assigned to the same species, and conclude that both can be accommodated within the hypodigm of *H. habilis*.

Conclusions

Owing to its relative completeness, Stw 53 is the most important example of early *Homo* found in southern Africa to date. However, it lacks bone in areas critical to accurate reconstruction of its morphology, especially many neurocranial dimensions, and some existing areas of bone have suffered the effects of post-burial breakage and distortion. The extent of this damage is greater than has been appreciated. We present our new reconstruction as a hypothesis and encourage peer examination and testing, which should ultimately lead to further refinement and improved accuracy.

We have outlined a strong case for the classification of Stw 53 in *H. habilis*, but recognize that ours is not the final word on its systematics. Indeed, we expect that some researchers may criticize our conclusions, especially as it may seem that we have further extended intraspecific variation within the taxon. Some scholars already consider that the claimed hypodigm of *H. habilis* is too variable to accommodate a single species (e.g., Lieberman et al., 1988; Kimbel and Rak, 1993; Rightmire, 1993), but this view has been rebutted (Tobias, 1987, 1991, 2003; Miller, 2000). Other researchers, such as Grine (2001), have argued for classification of Stw 53 along with SK 847 in a new species on account of features they share to the exclusion of eastern African *H. habilis* specimens. However, we have recognized seven such features, and all of them are also found in *A. africanus*, which indicates that they might represent primitive retentions. We find no case for considering

the southern African early *Homo* specimens specifically unique.

Our examination of tooth remains from Sterkfontein Member 5—some of which were recovered by Robinson in the 1950s and others during excavations undertaken since 1973—suggests sympatry of three species in southern Africa during the Plio-Pleistocene: *A. robustus*, *H. habilis*, and *H. sapiens* sensu lato. Thus, this region probably has the same level of diversity as is seen in eastern Africa during the same period.

Acknowledgements

We are grateful to Peter Montja for his skill and patience in the casting of Stw 53, and to Peter Faugust, Paul Halasz, and Dzung Vu for help with photographs. DC thanks Beverley Kramer for providing the facilities of the School of Anatomical Sciences, and the Research Office of the University of the Witwatersrand for financial support, for a nine month postdoctoral fellowship undertaken in 2002. Heather White helped with many aspects of this study and of the postdoctoral fellowship. Our thanks are extended to the University of New South Wales, the Ford Foundation, the Department of Science and Technology of the South African government, the PAST Fund, the Embassy of France in South Africa, and the National Research Foundation, Pretoria. Finally, we are grateful to Terry Harrison, Bill Kimbel, and three anonymous referees whose thoughtful comments greatly helped to improve the manuscript.

References

Ackermann, F., 1941. Une nouvelle théorie à la bas du complexe occluso-articulaire. Schweiz. Monatsschr. Zahnheilkd. 51, 892–898.

Aguirre, E., 1994. *Homo erectus* and *Homo sapiens*: one or more species? Cour. Forsch. Inst. Senckenberg 171, 333–339.

Ahern, J.C.M., 1998. Underestimating intraspecific variation: the problem with excluding Sts 19 from *Australopithecus africanus*. Am. J. Phys. Anthropol. 105, 461–480.

Bilsborough, A., Wood, B.A., 1988. Cranial morphometry of early hominids: facial region. Am. J. Phys. Anthropol. 76, 61–86.

Blumenschine, R.J., Peters, C.R., Masao, F.T., Clarke, R.J., Deino, A.L., Hay, R.L., Swisher, C.C., Stanistreet, I.G., Ashley, G.M., McHenry, L.J., Sikes, N.E., van der Merwe, N.J., Tactikos, J.C., Cushing, A.E., Deocampo, D.M., Njau, J.K., Ebert, J.I., 2003. Late Pliocene *Homo* and hominid land use from western Olduvai Gorge, Tanzania. Science 299, 1217–1221.

Bräuer, G., Mbua, M., 1992. *Homo erectus* features used in cladistics and their variability in Asian and African hominids. J. Hum. Evol. 22, 79–108.

Chamberlain, A.T., 1987. A taxonomic review and phylogenetic analysis of *Homo habilis*. Ph.D. Dissertation, University of Liverpool.

Clarke, R.J., 1977a. The cranium of the Swartkrans hominid SK 847 and its relevance to human origins. Ph.D. Dissertation, University of the Witwatersrand.

Clarke, R.J., 1977b. A juvenile cranium and some adult teeth of early *Homo* from Swartkrans, Transvaal. S. Afr. J. Sci. 73, 46–49.

Clarke, R.J., 1985. *Australopithecus* and early *Homo* in southern Africa. In: Delson, E. (Ed.), Ancestors: The Hard Evidence. Alan R. Liss, New York, pp. 171–177.

Clarke, R.J., Howell, F.C., 1972. Affinities of the Swartkrans 847 hominid cranium. Am. J. Phys. Anthropol. 37, 319–336.

Clarke, R.J., Howell, F.C., Brain, C.K., 1970. More evidence of an advanced hominid at Swartkrans. Nature 225, 1219–1222.

Curnoe, D., 1999. A contribution to the question of early *Homo* in southern Africa. Ph.D. Dissertation, The Australian National University.

Curnoe, D., 2001a. Early *Homo* from southern Africa: a cladistic perspective. S. Afr. J. Sci. 97, 186–190.

Curnoe, D., 2001b. Cranial variability in east African 'robust' hominins. Hum. Evol. 16, 169–198.

Curnoe, D., 2002. Fossil human taxonomic hypotheses examined with topology-dependent permutation tail probability (T-PTP) tests. S. Afr. J. Sci. 98, 310–312.

Curnoe, D., Thorne, A., 2003. Number of ancestral human species: a molecular perspective. Homo 53, 201–224.

Day, M.H., Stringer, C.B., 1982. A reconsideration of the Omo Kibish remains and the erectus-sapiens transition. In: de Lumley, H. (Ed.), L'Homo erectus et la Place de l'Homme de Tautavel Parmi les Hominidés Fossiles, vol. 2. Louis-Jean Scientific and Literary Publications, Nice, pp. 814–846.

Dean, M.C., Wood, B.A., 1982. Basicranial anatomy of Plio-Pleistocene hominids from east and South Africa. Am. J. Phys. Anthropol. 59, 157–174.

Falk, D., 1983. Cerebral cortices of east African early hominids. Science 222, 1072–1074.

FCAT, Federative Committee on Anatomical Terminology, 1998. Terminologia Anatomica. Georg Thieme Verlag, Stuttgart.

Gabriel, A.C., 1965. Anatomy of Teeth and Jaws. University of Sydney, Sydney.

Gabunia, L., Vekua, A., Lordkipanidze, D., Swisher III, C.C., Ferring, R., Justus, A., Nioradze, M., Tvalchrelidze, M., Anton, S.C., Bosinski, G., Joris, O., de Lumley, M-A., Majsuradze, G., Mouskhelishvili, A., 2000. Earliest Pleistocene hominid cranial remains from Dmanisi, Republic of Georgia: taxonomy, geological setting, and age. Science 288, 1019–1025.

Grine, F.E., 1993. Description and preliminary analysis of new hominid craniodental fossils from the Swartkrans formation. In: Brain, C.K. (Ed.), Swartkrans: A Cave's Chronicle of Early Man. Transvaal Museum, Pretoria, pp. 75–116.

Grine, F.E., 2001. Implications of morphological diversity in early *Homo* crania from eastern and southern Africa. In: Tobias, P.V., Raath, M.A., Moggi-Cecchi, J., Doyle, G.A. (Eds.), Humanity from African Naissance to Coming Millennia. Florence University Press, Florence, pp. 107–116.

Grine, F.E., Demes, B., Jungers, W.L., Cole, T.M., 1993. Taxonomic affinity of the early *Homo* cranium from Swartkrans, South Africa. Am. J. Phys. Anthropol. 92, 411–426.

Grine, F.E., Jungers, W.L., Schultz, J., 1996. Phenetic affinities among early *Homo* crania from east and South Africa. J. Hum. Evol. 30, 189–225.

Henneberg, M., Thackeray, J.F., 1995. A single-lineage hypothesis of hominid evolution. Evol. Theory 11, 31–38.

Howell, F.C., 1978. Hominidae. In: Maglio, V.J., Cooke, H.B.S. (Eds.), Evolution of African Mammals. Harvard University Press, Cambridge, pp. 154–248.

Hughes, A.R., Tobias, P.V., 1977. A fossil skull probably of the genus *Homo* from Sterkfontein, Transvaal. Nature 265, 310–312.

Hurme, V.O., 1948. Standards of variation in the eruption of the first six permanent teeth. Child Dev. 19, 213–231.

Hurme, V.O., 1949. Ranges of normalcy in the eruption of permanent teeth. J. Dent. Child 16, 11–15.

Hurme, V.O., 1957. Time and sequence of tooth eruption. J. Forensic Sci. 2, 477–488.

Jacob, T., 1973. Palaeoanthropological discoveries in Indonesia with special reference to the finds of the last two decades. J. Hum. Evol. 2, 473–485.

Jelinek, J., 1981. Was *Homo erectus* already *Homo sapiens*? Colloques Int. CNRS 599, 91–95.

Johanson, D.C., Masao, F.T., Eck, G.G., White, T.D., Walter, R.C., Kimbel, W.H., Asfaw, B., Manega, P., Ndessokia, P., Suwa, G., 1987. New partial skeleton of *Homo habilis* from Olduvai Gorge, Tanzania. Nature 327, 205–209.

Keyser, A.W., 2000. The Drimolen skull: the most complete australopithecine cranium and mandible to date. S. Afr. J. Sci. 96, 189–193.

Keyser, A.W., Menter, C.G., Moggi-Cecchi, J., Rayne Pickering, T.R., Berger, L.R., 2000. Drimolen: a new hominid-bearing site in Gauteng, South Africa. S. Afr. J. Sci. 96, 193–197.

Kimbel, W.H., Johanson, D.C., Rak, Y., 1997. Systematic assessment of a maxilla of *Homo* from Hadar, Ethiopia. Am. J. Phys. Anthropol. 103, 235–262.

Kimbel, W.H., Rak, Y., 1993. The importance of species taxa in paleoanthropology and an argument for the phylogenetic concept of the species category. In: Kimbel, W.H., Martin, L.B. (Eds.), Species, Species Concepts, and Primate Evolution. Plenum Press, New York, pp. 461–484.

Kuman, K., Clarke, R.J., 2000. Stratigraphy, artefacts, industries and hominid associations for Sterkfontein, Member 5. J. Hum. Evol. 38, 827–847.

Leakey, L.S.B., Tobias, P.V., Napier, J.R., 1964. A new species of the genus *Homo* from Olduvai Gorge. Nature 202, 7–9.

Leakey, M.D., Clarke, R.J., Leakey, L.S.B., 1971. New hominid skull from Bed I, Olduvai Gorge, Tanzania. Nature 232, 223–224.

Leakey, R.E.F., 1973. Evidence of an advanced Plio-Pleistocene hominid from East Rudolf, Kenya. Nature 242, 447–450.

Lieberman, D.E., Pilbeam, D.R., Wood, B.A., 1988. A probabilistic approach to the problem of sexual dimorphism in *Homo habilis*: a comparison of KNM-ER 1470 and KNM-ER 1813. J. Hum. Evol. 17, 503–511.

Lockwood, C.A., Tobias, P.V., 1999. A large male hominin cranium from Sterkfontein, South Africa, and the status of *Australopithecus africanus*. J. Hum. Evol. 36, 637–685.

Martin, R., Saller, K., 1957. Lehrbuch der Anthropologie. Gustav-Fischer, Stuttgart.

McCollum, M.A., Grine, F.E., Ward, S.C., Kimbel, W.H., 1993. Subnasal morphological variation in extant hominoids and fossil hominids. J. Hum. Evol. 24, 87–111.

Miller, J.M.A., 2000. Craniofacial variation in *Homo habilis*: an analysis of the evidence for multiple species. Am. J. Phys. Anthropol. 112, 103–128.

Moggi-Cecchi, J., Tobias, P.V., Beynon, A.D., 1998. The mixed dentition and associated skull fragments of a juvenile fossil hominid from Sterkfontein, South Africa. Am. J. Phys. Anthropol. 106, 425–465.

Partridge, T.C., 1978. Re-appraisal of lithostratigraphy of Sterkfontein hominid site. Nature 275, 282–287.

Rak, Y., 1983. The Australopithecine Face. Academic Press, New York.

Rightmire, G.P., 1990. The Evolution of *Homo erectus*. Cambridge University Press, Cambridge.

Rightmire, G.P., 1993. Variation among early *Homo* crania from Olduvai Gorge and the Koobi Fora region. J. Hum. Evol. 90, 1–33.

Robinson, J.T., 1953. *Telanthropus* and its phylogenetic significance. Am. J. Phys. Anthropol. 11, 1–38.

Robinson, J.T., 1958. The Sterkfontein tool-maker. Leech 28, 94–100.

Robinson, J.T., 1962. Australopithecines and artefacts at Sterkfontein: part I: Sterkfontein stratigraphy and the significance of the extension site. S. Afr. Archaeol. Bull. 17, 87–107.

Schwartz, J.H., Tattersall, I., 2003. Craniodental morphology of genus *Homo* (Africa and Asia). In: The Human Fossil Record, vol. 2. Wiley-Liss, New York.

Sherwood, R.J., Ward, S.C., Hill, S., 2002. The taxonomic status of the Chemeron temporal (KNM-BC 1). J. Hum. Evol. 42, 153–184.

Tobias, P.V., 1965. New discoveries in Tanganyika, their bearing on hominid evolution. Curr. Anthropol. 6, 391–399 406–411.

Tobias, P.V., 1978. The earliest Transvaal members of the genus *Homo* with another look at some problems of hominid taxonomy and systematics. Z. Morph. Anthropol. 69, 225–265.

Tobias, P.V., 1985. Single characters and the total morphological pattern redefined: the sorting effected by a selection of morphological features of the early hominids. In: Delson, E. (Ed.), Ancestors: The Hard Evidence. Alan R. Liss, New York, pp. 94–101.

Tobias, P.V., 1987. The brain of *Homo habilis*: a new level of organization in cerebral evolution. J. Hum. Evol. 16, 741–761.

Tobias, P.V., 1991. Olduvai Gorge. In: The Skulls, Endocasts and Teeth of *Homo habilis*, vol. 4. Cambridge University Press, Cambridge.

Tobias, P.V., 1995. The place of *Homo erectus* in nature with a critique of the cladistic approach. In: Bower, J.R.F., Sartono, S. (Eds.), Palaeo-anthropology. Human Evolution in its Ecological Context, vol. 1. Pithecanthropus Centennial Foundation, Leiden, pp. 31–46.

Tobias, P.V., 2003. Encore Olduvai. Science 299, 1193–1194.

Tobias, P.V., Copley, K., Brain, C.K., 1977. Entries for South Africa. In: Oakley, K., Campbell, B., Molleson, T. (Eds.), Catalogue of Fossil Hominids, Part I: Africa, second ed. British Museum (Natural History), London.

Tobias, P.V., Wells, L.H., 1967. Entries for South Africa. In: Oakley, K., Campbell, B. (Eds.), Catalogue of Fossil Hominids. British Museum (Natural History), London, pp. 49–100.

Vekua, A., Lordkipanidze, D., Rightmire, G.P., Agusti, J., Ferring, R., Maisuradze, G., Mouskhelishvili, A., Nioradze, M., de Leon, M.P., Tappen, M., Tvalchrelidze, M., Zollikofer, C., 2002. A new skull of early *Homo* from Dmanisi, Georgia. Science 297, 85–89.

Walker, A., 1981. The Koobi Fora hominids and their bearing on the origins of genus *Homo*. In: Sigmon, B.A., Cybulski, J.S. (Eds.), *Homo erectus*—Papers in Honor of Davidson Black. University of Toronto Press, Toronto, pp. 193–215.

Walker, A., Leakey, R., 1993. The skull. In: Walker, A., Leakey, R. (Eds.), The Nariokotome *Homo erectus* Skeleton. Harvard University Press, Cambridge, pp. 63–94.

Weidenreich, F., 1936. The mandibles of *Sinanthropus pekinensis*: a comparative study. Palaeontol. Sin. 7, 1–162.

Weidenreich, F., 1943. The skull of *Sinanthropus pekinensis*: a comparative study on a primitive hominid. Palaeontol. Sin. D. 10, 1–298.

Wolpoff, M.H., 1996. Human Evolution. Knopf, New York.

Wolpoff, M.H., Thorne, A.G., Jelinek, J., Yinyun, Z., 1994. The case for sinking *Homo erectus*. 100 years of *Pithecanthropus* is enough!. Cour. Forsch. Inst. Senckenberg 171, 341–361.

Wood, B.A., 1991. Koobi Fora Research Project. In: Hominid Cranial Remains, vol. 4. Clarendon Press, Oxford.

Wood, B.A., 1992. Early hominid species and speciation. J. Hum. Evol. 22, 351–365.

Wood, B.A., Collard, M., 1999. The human genus. Science 284, 65–71.

Wu, X.Z., 2004. On the origin of modern humans in China. Quat. Int. 117, 131–140.

Zihlman, A., Bolter, D., Boesch, C., 2004. Wild chimpanzee dentition and its implications for assessing life history in immature hominin fossils. Proc. Natl. Acad. Sci. 101, 10541–10543.